1 Photooxidants from Brown Carbon and Other Chromophores in

2 Illuminated Particle Extracts

- Richie Kaur¹, Jacqueline R. Labins¹, Scarlett S. Helbock¹, Wenging Jiang², Keith J.
- 4 Bein³, Qi Zhang², Cort Anastasio^{1,*}
- ¹Department of Land, Air and Water Resources, University of California-Davis, One Shields Avenue,
- 6 Davis, CA 95616-8627, USA
- ²Department of Environmental Toxicology, University of California-Davis, One Shields Avenue, Davis,
- 8 CA 95616-8627, USA
- ³Center for Health and the Environment, University of California-Davis, One Shields Avenue, Davis, CA
- 10 95616-8627, USA
- 11 Correspondence to: C. Anastasio (canastasio @ucdavis.edu)

12

13

Abstract

14 While photooxidants are important in atmospheric condensed phases, there are very few 15 measurements in particulate matter (PM). Here we measure light absorption and the concentrations of three photooxidants – hydroxyl radical (*OH), singlet molecular oxygen (${}^{1}O_{2}$ *) 16 and oxidizing triplet excited states of organic matter (³C*) – in illuminated aqueous extracts of 17 wintertime particles from Davis, California. ¹O₂* and ³C*, which are formed from 18 19 photoexcitation of brown carbon (BrC), have not been previously measured in PM. In the extracts, mass absorption coefficients for dissolved organic compounds (MAC_{DOC}) at 300 nm 20 range between 13,000–30,000 cm² g–C⁻¹ and are approximately twice as high as previous values 21 in Davis fogs. The average $(\pm 1\sigma)$ OH steady-state concentration in particle extracts is 4.4 $(\pm$ 22 $2.3) \times 10^{-16}$ M, which is very similar to previous values in fog, cloud and rain: although our 23 particle extracts are more concentrated, the resulting enhancement in the rate of 'OH 24 photoproduction is essentially cancelled out by a corresponding enhancement in concentrations 25 of natural sinks for 'OH. In contrast, concentrations of the two oxidants formed primarily from 26 brown carbon (i.e., ¹O₂* and ³C*) are both enhanced in the particle extracts compared to Davis 27 fogs, a result of higher concentrations of dissolved organic carbon and faster rates of light 28 absorption in the extracts. The average ${}^{1}O_{2}^{*}$ concentration in the PM extracts is 1.6 (± 0.5) × 10⁻¹ 29 ¹² M, seven times higher than past fog measurements, while the average concentration of 30 oxidizing triplets is $1.0 (\pm 0.4) \times 10^{-13}$ M, nearly double the average Davis fog value. 31

Additionally, the rates of ${}^{1}O_{2}$ * and ${}^{3}C$ * photoproduction are both well correlated with the rate of sunlight absorption.

Since we cannot experimentally measure photooxidants under ambient particle water conditions, we measured the effect of PM dilution on oxidant concentrations and then extrapolated to ambient particle conditions. As the particle mass concentration in the extracts increases, measured concentrations of 'OH remain relatively unchanged, ¹O₂* increases linearly, and ³C* concentrations increase less than linearly, likely due to quenching by dissolved organics. Based on our measurements, and accounting for additional sources and sinks that should be important under PM conditions, we estimate that [OH] in particles is somewhat lower than in dilute cloud/fog drops, while $[{}^{3}C^{*}]$ is 30 to 2000 times higher in PM than in drops, and $[{}^{1}O_{2}^{*}]$ is enhanced by a factor of roughly 2400 in PM compared to drops. Because of these enhancements in ${}^{1}O_{2}$ * and ${}^{3}C^{*}$ concentrations, the lifetimes of some highly soluble organics appear to be much shorter in particle liquid water than under foggy/cloudy conditions. Based on extrapolating our measured rates of formation in PM extracts, BrC-derived singlet molecular oxygen and triplet excited states are overall the dominant sinks for organic compounds in particle liquid water, with an aggregate rate of reaction for each oxidant that is approximately 200 - 300 times higher than the aggregate rate of reactions for organics with 'OH. For individual, highly soluble reactive organic compounds it appears that ${}^{1}O_{2}^{*}$ is often the major sink in particle water, which is a new finding. Triplet excited states are likely also important in the fate of individual particulate organics, but assessing this requires additional measurements of triplet interactions with dissolved organic carbon in natural samples.

53

54

55

56

57

58

59

60

61

62

63

32

33

34

35

36

37

38

39

40

41

42

43

44

45

46

47

48

49

50

51

52

1 Introduction

Photochemically generated oxidants largely drive atmospheric chemistry, both in the gas phase (Thompson, 1992; Finlayson-Pitts and Pitts Jr, 1999; Seinfeld and Pandis, 2012) and in aqueous drops, where they largely govern the reactions and lifetimes of organic compounds (Lim et al., 2005; Lim et al., 2010; Ervens et al., 2011; He et al., 2013; Herrmann et al., 2015; Blando and Turpin, 2000). Similarly, photooxidants can be important for transformations in water-containing particulate matter (PM): they make new PM mass by functionalizing gaseous volatile organics to oxygenated lower-volatility products, and decrease PM mass by fragmenting large organics into smaller, more volatile species (Jimenez et al., 2009). Oxidants in condensed phases can come from the gas phase (e.g., the mass transport of hydroxyl radical, 'OH) or can be formed

photochemically within the particle or drop (Herrmann et al., 2010b). Our focus in this paper is on the latter pathway.

Of the photooxidants formed in airborne particles, hydroxyl radical (*OH) is the most widely studied. While its concentrations have been measured in cloud/fog drops, rain and dew (Arakaki and Faust, 1998; Arakaki et al., 1999; Anastasio and McGregor, 2001; Kaur and Anastasio, 2017), there are only four known measurements of *OH photoproduction rates, lifetimes, and steady-state concentrations in ambient particles, all from coastal or marine locations (Anastasio and Jordan, 2004; Arakaki et al., 2006; Anastasio and Newberg, 2007; Arakaki et al., 2013). Based on these and other measurements (e.g., Tong et al. (2017)) and complementary modeling work (Herrmann et al., 2010b; Herrmann et al., 2015), the major sources of *OH include photolysis of nitrate, nitrite, and hydrogen peroxide (HOOH) as well as reactions of Fe(II) with HOOH or organic peroxides. The major sinks of *OH are organic molecules since these reactions typically have nearly diffusion-controlled rate constants (Arakaki et al., 2013; Herrmann et al., 2010a; Herrmann et al., 2015).

Photoexcitation of organic chromophores, i.e., light-absorbing brown carbon (BrC), can also form oxidants in particles and drops. For example, sunlight absorption by organic chromophores can promote the molecules from their ground states to reactive triplet excited states (McNeill and Canonica, 2016; Kaur and Anastasio, 2018b). Triplets can both directly oxidize organics via electron transfer reactions and form other photooxidants, including singlet molecular oxygen (${}^{1}O_{2}^{*}$) (Zepp et al., 1985) and hydrogen peroxide (Anastasio et al., 1997). In this work we examine oxidizing triplets, which we refer to as ${}^{3}C^{*}$ or simply "triplets" for simplicity. Such species are important in surface waters, where they rapidly oxidize several classes of compounds including phenols, anilines, phenylurea herbicides, and sulfonamide antibiotics (Canonica et al., 1995; Canonica and Hoigné, 1995; Boreen et al., 2005; Canonica et al., 2006; Bahnmüller et al., 2014).

There has been growing interest in the role and reactivity of triplets formed from particulate brown carbon, especially their role in forming aqueous secondary organic aerosol (SOA(aq))(Smith et al., 2014; 2015; Yu et al., 2014; Yu et al., 2016; Laskin et al., 2015). There is evidence that triplet-forming, light-absorbing species, e.g., imidazoles and pyrazines, are formed in drops and particles (De Haan et al., 2009; 2010; Hawkins et al., 2018) and a few laboratory studies have examined how illuminated imidazole particles can oxidize isoprene or other alkenes to increase PM mass (Aregahegn et al., 2013; Rossignol et al., 2014). But the formation of SOA(aq) from such reactions appears not to be significant under environmentally

relevant conditions where concentrations of triplet precursors are much lower (Tsui et al., 2017). While we recently made the first measurements of triplet concentrations in fog waters (Kaur and Anastasio, 2018b), there are no measurements of ³C* in particles, making it difficult to assess their significance. This is doubly difficult because triplets are not a single oxidant, but rather a suite of species with a wide range of reactivities (McNeill and Canonica, 2016).

Another important photooxidant in atmospheric and surface waters is singlet molecular oxygen ($^{1}O_{2}*$), which is formed by energy transfer from a triplet excited state to dissolved oxygen, and lost via deactivation by water (Zepp et al., 1977; Haag and Hoigné, 1986; Haag and Gassman, 1984; Faust and Allen, 1992). Similar to triplets, singlet oxygen has been studied widely in surface waters (Zepp et al., 1977; Haag and Gassman, 1984; Haag and Hoigné, 1986; Tratnyek and Hoigné, 1994) and reacts rapidly with electron-rich organics such as phenols, polycyclic aromatic hydrocarbons, amino acids, and reduced sulfur species (Wilkinson et al., 1995). However, there are only four measurements of $^{1}O_{2}*$ concentrations in atmospheric waters (Anastasio and McGregor, 2001; Kaur and Anastasio, 2017; Albinet et al., 2010; Faust and Allen, 1992) and none in aqueous particles.

To address this gap, we measured 'OH, ¹O₂*, and ³C* in illuminated aqueous extracts of fine particles collected from the Central Valley of California during winter, a period of heavy residential wood burning. The goals of this study are to: 1) quantify 'OH, ¹O₂*, and ³C* kinetics and concentrations in particle extracts, 2) compare light absorption and photooxidant kinetics with previous measurements made in fog, 3) measure the dependence of oxidant concentrations on particle dilution to predict photooxidant concentrations in ambient particle liquid water, and 4) assess the importance of particle photooxidants in processing organic compounds in the atmosphere.

2 Experimental

2.1 Chemicals

All chemicals were used as received. Furfuryl alcohol (98%), syringol (99%), methyl jasmonate (95%), benzene (≥ 99.9%), 2-methyl-3-buten-2-ol (98%), deuterium oxide (99.9% atom D), and 2-nitrobenzaldehyde (98%) were from Sigma-Aldrich and sulfuric acid (trace metal grade) was from Fisher. All chemical solutions and particulate matter extracts were prepared using purified water (Milli-Q water) from a Milli-Q Advantage A10 system (Millipore; ≥ 18.2

 $M\Omega$ cm) with an upstream Barnstead activated carbon cartridge; total organic carbon concentrations were below 10 ppb C.

2.2 Particle collection and extraction

Wintertime particles were collected in a residential neighborhood in Davis, California, (38.5539° N, 121.7381° W, 16 m above sea level) during December 2015 and January 2016, a period with significant wood burning. PM_{2.5} was collected on 8 × 10 inch Teflon-coated quartz filters (Pall Corporation, EmFabTM filters, type TX40HI20-WW) using a high-volume sampler with a PM₁₀ inlet (Graseby Anderson) followed by two offset, slotted impactor plates (Tisch Environmental, Inc., 230 series) to remove particles greater than 2.5 μm. Due to technical difficulties, the air flow rate was variable and typically ranged between 1130 and 1560 L min⁻¹, corresponding to particle cut points of 2.5 to 1.6 μm. Particles were generally collected over two to three consecutive nights between 5:30 pm and 7:30 am, but one sample (#3) was collected continuously (day and night) for 72 hours (Table S1).

Immediately upon collection, samples were wrapped in aluminum foil (previously baked at 500 °C for 8 h), sealed in ZiplockTM bags and stored at –20 °C. On the day of extraction, several 2 cm × 2 cm pieces were cut (using stainless-steel tools) from the same filter, each was put into a separate pre-cleaned 10 mL amber glass vial, Milli-Q water was added (see below), and the vial was sealed and shaken for 3 hours in the dark. The extracts were filtered (0.22 µm PTFE; Pall), combined, and labeled as Particulate Matter Extract (PME). The standard condition was to use 1.0 mL of Milli-Q to extract each filter square, but in our initial work we used 2.5 mL of Milli-Q per filter square; these latter "dilute extracts" are indicated by an asterisk and footnotes in the figures and tables. We switched from dilute to standard conditions after PME1-3, but we include both results in this work to compare the two types of extracts.

In addition, to study the effect of PM mass concentration, separate portions of filter #3 were extracted using five different extraction volumes between 0.5 and 10 mL (discussed later). Those extracts are labeled as PME3Dx, where "x" is the extraction volume (e.g., PME3D1.3 for filter squares extracted in 1.3 mL of Milli-Q). Upon extraction, each PME was stored in the refrigerator (5 °C) until the day of the illumination experiments. All illumination experiments and analyses on a PME sample were completed within a week of its extraction.

2.3 Sample illumination and chemical analysis

156

174

175

176

177

178

157 For all illumination experiments except 'OH measurements using benzene (discussed in Sect. 2.5.1), on the day of the experiment a 1.0 mL aliquot of an air-saturated particle extract was 158 first acidified to pH 4.2 ± 0.2 using 10 mM sulfuric acid (with sample dilution $\leq 10\%$) to mimic 159 160 the particle water acidity in wintertime PM in California's Central Valley (Parworth et al., 2017). The pH of the sample was measured using a pH microelectrode (MI-414 series, protected tip, 16 161 gauge needle, 6 cm length; Microelectrodes, Inc.). The acidified extract was then spiked with a 162 single photooxidant probe and put into a silicone-plugged, fully-filled GE021 quartz tube (4 mm 163 inner diameter, 6 cm length, 1.0 mL volume) and illuminated with a 1000 W xenon arc lamp 164 filtered with a water filter (to reduce sample heating), an AM 1.0 air mass filter (AM1D-3L, 165 Sciencetech) and 295 nm long-pass filter (20CGA-295, Thorlabs) to mimic tropospheric solar 166 light (Kaur and Anastasio, 2017). Because of the small tube size, samples were not stirred, but 167 the entire sample was illuminated in a chamber held at 20 °C. 100 µL aliquots of illuminated 168 (and parallel dark) samples were periodically removed and analyzed for the concentration of 169 photooxidant probe (see below) using HPLC (Shimadzu LC-10AT pump, ThermoScientific 170 BetaBasic-18 C₁₈ column (250 × 33 mm, 5 μM bead), and Shimadzu-10AT UV-Vis detector). 171 The photon flux in the sample was measured on each experiment day using a 10 µM solution of 172 2-nitrobenzaldehyde (2NB) in the same type of quartz tube as the sample (Galbavy et al., 2010). 173

Major anions and cations in the extracts (Table S2) were quantified using two Metrohm ion chromatographs (881 Compact IC Pro) equipped with conductivity detectors (Ge et al., 2014; Kaur and Anastasio, 2017). Dissolved organic carbon (DOC) in the filtered extracts was measured using a Shimadzu TOC-VCPH analyzer (Yu et al., 2014).

2.4 Light Absorbance

179 Light absorbance was measured immediately after extraction using a Shimadzu UV-

180 2501PC spectrophotometer with 1-cm quartz cuvettes and a baseline of Milli-Q water.

Absorbance (A_{λ}) was converted to light absorption coefficients using

$$182 \alpha_{\lambda} = \frac{A_{\lambda}}{l} (1)$$

where *l* is the pathlength in cm. The rate of sunlight absorption (R_{abs} , mol-photons L⁻¹ s⁻¹) in

each extract was calculated as:

185
$$R_{\text{abs}} = 2.303 \times \frac{10^3}{N_A} \times \sum_{300nm}^{450nm} (\alpha_{\lambda} \times I_{\lambda} \times \Delta \lambda)$$
 (2)

where 2.303 is for base conversion, 10^3 is for units conversion (cm³ L⁻¹), N_A is Avogadro's number, I_{λ} is the Davis winter-solstice actinic flux (photons cm⁻² s⁻¹ nm⁻¹) from the Tropospheric Ultraviolet and Visible (TUV) Radiation Model version 4.1 (Madronich et al.,

189 2002), and $\Delta\lambda$ is the interval between adjacent wavelengths in the TUV output (nm).

Wavelength-dependent mass absorption coefficients for DOC (MAC_{DOC}; cm² g–C⁻¹) were estimated by subtracting the contributions of nitrite and nitrate from the measured absorbance at each wavelength (which were small, $\leq 7\%$ of the total absorbance) and then dividing the remainder by the DOC concentration:

194
$$MAC_{DOC,\lambda} = \frac{\alpha_{DOC,\lambda} \times ln(10) \times 10^3 \times 10^3}{[DOC]}$$
 (3)

where $\alpha_{DOC,\lambda}(cm^{-1})$ is the sample absorbance coefficient at wavelength λ due to DOC (Kaur and Anastasio (2017)); $\ln(10)$ is a base conversion factor; the two 10^3 factors are for unit conversion (cm³ L⁻¹ and mg g⁻¹), and the DOC concentration is in mg-C L⁻¹. Since the average organic matter–to–organic carbon (OM/OC) ratio in California Central Valley particles is approximately 1.7 (Young et al., 2016), the absorption coefficients normalized by OM mass will be approximately 60% of the MAC_{DOC} values.

2.5 Measurement of photooxidants

2.5.1 Hydroxyl radical (OH)

We quantified 'OH kinetics using a benzene probe (Zhou and Mopper, 1990; Anastasio and McGregor, 2001; Kaur and Anastasio, 2017). Briefly, four aliquots of each extract were spiked with varying concentrations of benzene to trap 'OH and form phenol (yield: 73%), which is quantified (Fig. S1). Each benzene stock was made a day before the illumination experiment. Similar to the other photooxidant experiments, all aliquots were air-saturated, acidified to an initial pH of 4.2 (\pm 0.2), capped, and then constantly stirred during illumination in airtight 5.0 mL, 1-cm pathlength, rectangular quartz cuvettes with no initial headspace. For all 'OH measurements where benzene is used as a probe, we used this larger sample volume (5 mL instead of 1 mL) to minimize the headspace in the cuvette and prevent benzene loss due to volatilization. Throughout the illumination period, 100 μ L aliquots were collected through the cap septum and analyzed for phenol using HPLC-UV (eluent of 30% acetonitrile: 70% Milli-Q, flow rate of 0.6 mL/min, detection wavelength of 210 nm and column temperature of 35°C). As described in Kaur and Anastasio (2017), we use these results to determine three experimental

quantities for 'OH: the rate of photoproduction ($P_{OH,EXP}$), the rate constant for 'OH loss due to natural sinks (k'_{OH}), and the steady-state concentration (['OH]_{EXP}). Measured rates of 'OH formation and steady-state concentrations were normalized to values expected under midday, Davis winter-solstice sunlight and were corrected for the small amount of internal light screening due to light absorption by DOM:

$$[{}^{\bullet}OH] = \left(\frac{[{}^{\bullet}OH]_{EXP}}{S_{\lambda} \times j_{2NB,EXP}}\right) \times j_{2NB,WIN}$$
(4)

In this equation, S_{λ} is the internal light screening factor (Table S1), $j_{2NB,WIN}$ is the rate constant for loss of 2-nitrobenzaldehyde at midday near the winter solstice in Davis (solar zenith angle = 62° , $j_{2NB,WIN} = 0.0070 \text{ s}^{-1}$; Anastasio and McGregor, (2001)), and $j_{2NB,EXP}$ is the measured rate constant for loss of 2NB on the day of the experiment. OH results are in Tables S3–S6.

We also measured 'OH steady-state concentrations in squares of particle filter #3 using five different dilutions with water (discussed later). Because these sample volumes were too small to use the benzene technique, we determined the steady-state concentration of 'OH by measuring the loss of 2-methyl-3-buten-2-ol (MBO) (Sect. S1). We then measured $P_{\rm OH}$ in a 1 cm cuvette using a high benzene concentration (1.5 mM) and determined the rate constant for 'OH loss due to natural sinks by dividing the rate of photoproduction by the steady-state concentration, $k'_{\rm OH} = P_{\rm OH} /$ ['OH] (Sect. S1.3). In contrast to the benzene technique, there was some quenching of 'OH by the probe MBO in our PME3 samples; this quenching was most significant in the most dilute extract, PME3D10. We corrected measured 'OH concentrations for quenching by MBO in the PME3 samples (Sect. S1) and the final, corrected values are given in the Tables mentioned above.

2.5.2 Singlet molecular oxygen (¹O₂*)

Singlet oxygen was quantified by measuring the loss of a furfuryl alcohol (FFA) probe and using heavy water (D_2O) as a diagnostic tool (Kaur and Anastasio, 2017; Anastasio and McGregor, 2001). Briefly, each extract was divided into two aliquots, acidified to pH 4.2 (\pm 0.2), and diluted 50:50 using H₂O or D₂O. Both aliquots were spiked to 10 μ M FFA and illuminated in 1 mL quartz tubes. (At this concentration, FFA should decrease the steady-state concentration of 1O_2* in air-saturated solutions by less than 1%.) FFA loss was detected using HPLC-UV (eluent of 10% acetonitrile: 90% Milli-Q water, flow rate of 0.6 mL/min, detection wavelength of 210 nm and column temperature of 35°C). The loss of FFA followed pseudo-first-order kinetics and the slope of the plot of $ln([FFA]_t/[FFA]_0)$ versus time is the negative of the pseudo-

first-order rate constant for loss of FFA (illustrated in Fig. S2). Loss of FFA in the D₂O-diluted 246 aliquot is faster than in H₂O because H₂O is the dominant sink for ¹O₂*, which reacts less 247 quickly with D₂O (Bilski et al., 1997). The differences in the pseudo-first-order rate constants for 248 loss of FFA between the two aliquots of sample were used to calculate the steady-state 249 concentration of ¹O₂* and the rate of singlet oxygen photoproduction (Anastasio and McGregor, 250 2001). These were normalized to values expected in Davis winter-solstice sunlight (i.e., [¹O₂*] 251 and P_{102*}) and corrected for internal light screening using an equation analogous to Eq. (4). ${}^{1}O_{2}*$ 252 253 measurements are in Table S7.

254

255

256

257

258

259

260

261

262

263

2.5.3 Oxidizing triplet excited states of organic matter (³C*)

Triplets were measured using the dual-probe technique we developed recently for fog waters (Kaur and Anastasio, 2018b): two 1.0 mL, pH 4.2 aliquots of each extract were spiked to $10~\mu M$ of either syringol (SYR) or methyl jasmonate (MeJA) and the loss of each probe was measured during illumination in plugged quartz tubes (Sect. 2.3). The measured pseudo-first-order rate constant for probe loss ($k'_{Probe,EXP}$) was determined as the negative of the slope of the plot of $\ln([Probe]/[Probe]_0)$ versus illumination time. Values of $k'_{Probe,EXP}$ were normalized to Davis winter-solstice sunlight and corrected for internal light screening using an analog of Eq. (4); the resulting rate constants are termed k'_{Probe} (s⁻¹) (Tables S8, S9 of the SI). This pseudo-first-order rate constant for loss of probe represents the sum of all loss pathways:

264265

$$266 k'_{\text{Probe}} = k_{\text{Probe+OH}} [\text{OH}] + k_{\text{Probe+IO2}*} [^{1}\text{O}_{2}*] + \sum (k_{\text{Probe+3C}_{i}*} [^{3}\text{C}_{i}*]) + j_{\text{Probe}} + \sum (k_{\text{Probe+Other}} [\text{Other}]) (5)$$

- where the first two terms are the contributions of 'OH and ${}^{1}O_{2}$ * to probe loss; $\Sigma(k_{\text{Probe+3C*}}[{}^{3}\text{C*}])$
- represents the sum of all triplet contributions to probe loss; j_{Probe} is the first-order rate constant
- 269 for direct photodegradation of the probe, which is negligible for our illumination times ($< 4.3 \times$
- $10^{-6}~{\rm s}^{-1}$ and $4.8\times10^{-7}~{\rm s}^{-1}$ for SYR and MeJA, respectively, under Davis winter conditions); and
- $\Sigma(k_{\text{Probe+Other}}[\text{Other}])$ is the sum of contributions from all other oxidants. As described in Sect.
- S3, we estimate that these other oxidants (hydroperoxyl radical / superoxide radical anion, ozone,
- 273 carbonate radical, hydrogen ion / aquated electron) contribute 12 % or less of the average
- measured syringol loss (Sect. S3) and so are ignored. We can then simplify and rearrange Eq. (5)
- 275 to determine the triplet contribution to probe loss:

277
$$k'_{\text{Probe},3C^*} = \sum (k_{\text{Probe}+3Ci^*}[^3C_i^*]) = k'_{\text{Probe}} - (k_{\text{Probe}+OH}[^{\bullet}OH] + k_{\text{Probe}+1O2^*}[^{1}O_2^{*}])$$
 (6)

In other probe techniques, the equivalent of Eq. 6 is rearranged so that $\sum_{i=1}^{3} C_{i}^{*}$ can be determined based on the measured value of $k'_{\text{Probe},3C^*}$ and the literature value of the second-order rate constant $k_{\text{Probe+3Ci}}$. However, because triplets represent a suite of unidentified compounds, there is no one value of $k_{\text{Probe+3Ci}}$. To estimate this second-order rate constant in each sample, we used a combination of rate constants from four model triplets – 2-acetonaphthone (³2AN*), 3'methoxyacetophenone (³3MAP*), 3,4-dimethoxybenzaldehdye (³DMB*), and benzophenone (³BP*) – that roughly span the range of triplet reactivities in natural samples. We first identified the "best match triplets", i.e., the one or two model triplets that match the average oxidizing triplet reactivity in a given extract. To do this, we determined the model triplets whose molefraction-weighted ratio of second-order rate constants (i.e., $k_{SYR+3C^*}/k_{MeJA+3C^*}$) matches the ratio of the measured first-order probe loss rate constants due to triplets $(k'_{SYR.3C^*}/k'_{MeJA.3C^*})$ in each extract (for more details, see Kaur and Anastasio (2018b)). Ratios of the second-order rate constants $(k_{\text{SYR+3C*}} / k_{\text{MeJA+3C*}})$ of the model triplets range from 1.7 for the most reactive species (³BP*) to 100 for the least reactive, ³2AN* (Table S10). For each extract, we calculated two mole-fraction-weighted second-order rate constants for triplets (one for each probe) and used them to estimate the triplet steady-state concentration:

$$\Sigma[^{3}C_{i}^{*}]_{\text{Probe}} = \frac{k \text{ Probe,3C*}}{\chi_{3C1*} \times k \text{Probe+3C1*} + \chi_{3C2*} \times k \text{Probe+3C2*}}$$

$$(7)$$

where χ_{3C1^*} and χ_{3C2^*} are the mole fractions of the two best match triplets (${}^3C_1^*$ and ${}^3C_2^*$), and $k_{\text{Probe+3C1*}}$ and $k_{\text{Probe+3C2*}}$ are the second-order reaction rate constants of the best model triplet matches. Eq. (7) gives us two estimates of the triplet steady-state concentration, one from each probe, i.e., $\sum [{}^3C_i^*]_{\text{SYR}}$ and $\sum [{}^3C_i^*]_{\text{MeJA}}$. We averaged the two to obtain the best value for the triplet steady-state concentration in each extract, $\sum [{}^3C_i^*]$.

300301

302

278

279

280

281

282

283

284

285

286

287

288

289

290

291

292

293

295

296

297

298

299

We next estimated the rate of triplet photoformation (P_{3C^*}) :

303
$$P_{3C^*} = \Sigma[^3C_i^*] \times (k_{3C^*+O2}[O_2] + (k_{rxn} + k_Q)[DOC])$$
 (8)

where k_{3C^*+O2} is the average bimolecular rate constant for quenching of the model triplets by O₂ (= $2.8 \times 10^9 \,\mathrm{M}^{-1} \mathrm{s}^{-1}$: Table S11 and Canonica et al. (2000)), [O₂] is the dissolved oxygen concentration of 284 μ M at 20 °C (USGS, 2018), $k_{\mathrm{rxn}} + k_{\mathrm{Q}}$ is the overall reaction and quenching rate constant for triplets by DOC (9.3 × $10^7 \,\mathrm{L}$ mol-C⁻¹ s⁻¹; see below) and [DOC] values are in Table S2. At the concentrations we used (10 μ M), SYR and MeJA are negligible sinks for triplets. Measurements for triplets are in Tables S12 and S13.

315

311 For all three photooxidants, the quantum yield of formation was calculated as

$$\Phi_{\text{Ox}} = \frac{P_{\text{Ox}}}{R_{abs}} \tag{9}$$

- where P_{OX} is the Davis winter-solstice-normalized rate of oxidant photoproduction and R_{abs} is the
- rate of sunlight absorption by the extract.

2.5.4 PM mass concentration factor (CF)

- Due to the volume required for our probe techniques, we extract particles into Milli-Q water, resulting in extracts that are approximately 1000 times more dilute than ambient particles.
- To examine the impact of dilution on photooxidant concentrations, we extracted sample #3 in
- five different volumes of Milli-Q water (0.5 to 10 mL) and measured 'OH, ¹O₂* and ³C* steady-
- 320 state concentrations in the five extracts. We define the PM mass concentration factor (CF) as the
- ratio of (PM mass) / (water mass) in a given extract relative to the most concentrated extract that
- we can make:

$$323 CF = \frac{V_{MIN}}{V_{EXT} + V_{P}} (10)$$

324

- where V_{MIN} is the minimum experimentally feasible volume of Milli-Q needed for extraction of
- one filter square (0.5 mL), V_{EXT} is the volume of Milli-Q used to extract a given filter square (0.5
- to 10 mL), and V_P is the volume of probe stock solution added (typically 20 μ L). Values of CF
- for the PME3D extracts ranged from 0.05 (least concentrated) to 0.96 (most concentrated) and
- are listed in Table S14.

330

331

334

335

2.5.5 Uncertainties

- In figures, error bars represent \pm 1 standard error (SE) calculated by propagating the
- uncertainties in each term used to calculate the plotted value.

3 Results and discussion

3.1 General extract characteristics

- Similar to Davis fogs collected in 1997-98 (Anastasio and McGregor, 2001) and 2011
- 337 (Kaur and Anastasio, 2017), the most abundant ions in the particle extracts are ammonium
- $(NH_4^+, 280-2600 \,\mu\text{M})$ and nitrate $(NO_3^-, 380-3300 \,\mu\text{M})$ (Table S2). This is expected since

ammonium nitrate is the most significant inorganic component of wintertime particles in the Central Valley (Herner et al., 2006; Heald et al., 2012; Young et al., 2016). The average values of NO_3^- and NH_4^+ are not statistically different (p > 0.5) between the current particle extracts (PME) and previous fogs, although the ranges are much wider in the particle extracts (Table S2). Similar to nitrate, nitrite is another important source of hydroxyl radical in the aqueous phase (Anastasio and McGregor, 2001), with an average concentration of 6.9 (\pm 2.9) μ M in the particle extracts, again statistically similar to the 2011 fog average. On the other hand, the average concentration of potassium – commonly used as a tracer for biomass-burning (Silva et al., 1999; Parworth et al., 2017) – is nearly 40 times higher in the particles than in the 2011 Davis fog samples (p = 0.019), suggesting PME enrichment by residential wintertime wood-burning. This is reflected in the dilute PM extracts as well: even though most characteristics in the dilute extracts are similar to fog, the average K^+ (38 \pm 7 μ M) in the dilute PMEs is 10 times higher than the fog value. Dissolved organic carbon (DOC) in the standard extracts (mean: 3400 (\pm 760) μ M-C) is, on average, three times higher than both the dilute extracts and fog.

We employed two field blanks in this study, one each for dilute and standard extraction conditions. Ions and DOC in both field blanks are lower than 10% of the corresponding PME sample averages, with a few exceptions (Table S2).

3.2 Light absorption in particle extracts

As shown in Fig. 1a and Table S1, the pathlength-normalized absorbance (α , cm⁻¹) declines exponentially with wavelength, with values at 300 nm (α_{300}) between 0.27 and 0.58 cm⁻¹ for the standard extracts PME3–6. The average α_{300} value is nearly five times higher in standard extracts than values in Davis fog samples (Table S1, Fig. S3, data available in Kaur and Anastasio (2018a)), while the "dilute extracts" (PME1*, PME2*, and PME3D2.5*) have absorbances very similar to fog samples. Values of the Absorption Angstrom Exponent (AAE) for all PM extracts range between 6.2 and 7.9 (Table S1), similar to those reported previously for water soluble particulate BrC from biomass burning (Hecobian et al., 2010; Kirchstetter and Thatcher, 2012). For both the fog and PM extracts the calculated rate of sunlight absorption between 300 and 450 nm (R_{abs}) is well-correlated with dissolved organic carbon (DOC) (R^2 = 0.89 and 0.67, respectively; Fig. S4), suggesting that BrC is mainly responsible for light absorption. The R_{abs} values for the standard extracts are high, with an average value of 9.1 (± 4.1) × 10⁻⁶ mol-photons L⁻¹ s⁻¹, five times higher than the dilute extracts and past Davis fogs (Table S1). Similar to fog (Kaur and Anastasio, 2018b), the average rate of sunlight absorbance in the

standard particle extracts is 17 times higher than the total formation rates of the three photooxidants (discussed later), indicating that most of the (photo) energy absorbed is either dissipated via non-reactive pathways or leads to formation of other products.

We next calculated mass absorption coefficients for the organics (MAC_{DOC}) by subtracting the absorbance contributions by nitrite and nitrate from α and dividing by the DOC concentration (Eq. (3)). Across both standard and dilute extracts, the average (\pm σ) MAC_{DOC} value at 300 nm is 2.2 (\pm 0.7) × 10⁴ cm² g–C⁻¹, 1.7 times higher than the fog sample average (Figs. 1b and S3; data available at Kaur and Anastasio (2018a)). Both α and MAC_{DOC} in the PME are generally higher than in fog, especially at shorter sunlight wavelengths (Fig. S5), although AAE values are similar in the extracts and fog (Table S1). Since MAC_{DOC} accounts for dilution (Eq. (3)), the higher values in PM extracts indicates that water-soluble organics in particles are either more strongly light-absorbing (on a per-carbon basis), and/or less diluted with non-absorbing DOC, compared to those in fog. Our PME mass-absorption coefficients at 300 nm are very similar to values reported for the humic–like fraction of biomass-burning aerosols in the Amazon basin (Hoffer et al., 2006) and for the water-soluble organic fractions of rural aerosols (Varga et al., 2001; Sun et al., 2007).

Compared to the samples, light absorption in the field blanks is negligible, representing 0.7% and 3% of the average α_{300} in the standard and dilute extracts, respectively (Table S1).

3.3 Hydroxyl radical

The average Davis winter-solstice-normalized rate of OH photoproduction (P_{OH}) in the standard extracts is $1.2 (\pm 0.5) \times 10^{-9} \,\mathrm{M \ s^{-1}}$ (i.e., $4.2 \pm 1.7 \,\mu\mathrm{M \ h^{-1}}$), 3.3 times faster than the average of previous Davis fogs (Table S3). In Davis fog, the main sources of OH were nitrite and nitrate photolysis, accounting for 70 - 90 % of measured P_{OH} (Anastasio and McGregor, 2001; Kaur and Anastasio, 2017). However, in the standard PM extracts, nitrite and nitrate together account for an average of only (34 ± 14) % of P_{OH} (Table S4), while other, unidentified species account for the remaining (66 ± 14) %. While NO_2^- and NO_3^- concentrations in PME and fog are similar, measured OH photoproduction rates are much higher in the particle extracts. The additional sources of OH likely include photo-Fenton processes (Arakaki and Faust, 1998) and organic peroxides (Tong et al., 2016; Tong et al., 2017; Lim and Turpin, 2015), although there is only a modest correlation between DOC and P_{OH} due to unidentified sources (Fig. S6).

While organic compounds are potentially important sources of 'OH in the particle extracts, they are almost certainly the main 'OH sink, as found previously for atmospheric and surface waters (Brezonik and Fulkerson-Brekken, 1998; Dong et al., 2010; Arakaki et al., 2013). The average ($\pm 1\sigma$) rate constant for 'OH destruction, k'_{OH} , in the standard extracts is 2.5 (± 1.1) × 10^6 s⁻¹, three times higher than in dilute extracts and fog (Table S3); DOC concentrations in the standard PM extracts are similarly enhanced, ranging between 2350 and 4090 μ M-C (Table S2). Based on our calculations, inorganic species together account for no more than 10 % of k'_{OH} in the PM extracts except for PME3D10 which is the most dilute sample and has the largest uncertainty (Tables S5, S6). The rate constant for 'OH destruction due to organics, i.e., $k'_{OH,org}$, obtained by subtracting contributions of the inorganic sinks from k'_{OH} , is well correlated with DOC concentrations ($R^2 = 0.73$) (Fig. S6). Arakaki et al. (2013) showed that the ratio $k'_{OH,org}$ / [DOC] is relatively constant in atmospheric waters, with an average ($\pm 1 \sigma$) value of 3.8 (± 1.9) × 10^8 L (mol–C)⁻¹ s⁻¹. Our average ($\pm 1 \sigma$) measured ratio in all particle extracts is nearly twice as high, 7.1 (± 2.7) × 10^8 L (mol–C)⁻¹ s⁻¹, but not statistically different (Table S3).

Davis winter-solstice-normalized 'OH steady-state concentrations in all extracts are in the range of $(1.7-7.9) \times 10^{-16}$ M, with an average $(\pm 1\sigma)$ value of $5.1 (\pm 2.4) \times 10^{-16}$ M in the standard extracts (Fig. 2a, Table S3). While both the 'OH photoproduction rate and rate constant for 'OH loss are approximately three times higher in the standard PM extracts compared to the dilute extracts and fog, the two enhancements cancel out to give 'OH steady-state concentrations that are similar across all three sample types. This relative consistency of 'OH concentrations has been reported for a wide variety of atmospheric waters (Arakaki et al., 2013); our average concentration is similar to most of these past results (Fig. S7). As we discuss in Sect. 3.6, transport of 'OH from the gas-phase is also an important source to drops and particles, but its importance decreases with decreasing particle size.

We also calculated the quantum yield of hydroxyl radical formation, i.e., the fraction of absorbed photons that result in 'OH formation (Eq. (9)). The average (\pm 1 σ) value of Φ_{OH} in all particle extracts is (0.014 \pm 0.010) %, which is statistically similar to the average fog result (Table S3): while photoformation rates of 'OH increase from fog to standard particle extracts (Table S3), light absorption shows a similar trend (Table S1).

The rate of 'OH photoproduction in the field blanks is negligible, representing 1 % and 6 % of the average rate in standard and dilute extracts, respectively. The rate constants for 'OH destruction (k'_{OH}) in the standard (FB2) and dilute (FB1) field blanks represent 10 % and 43 % of the corresponding PME averages. The latter result is puzzling, since the concentrations of 'OH

sinks measured in FB1 (i.e., DOC and NO₂⁻; Table S2) are much lower relative to the extract.

We discuss measurements of k'_{OH} in the blanks in more detail in Sect. S2. We do not subtract the

field blank results for k'_{OH} from the corresponding PM extract values and thus our sample results

are upper bounds.

3.4 Singlet molecular oxygen

The average (\pm 1 σ) Davis winter solstice-normalized ${}^{1}O_{2}*$ concentration in the dilute extracts (2.4 (\pm 0.7) × 10⁻¹³ M) is very similar to the previous fog average (Fig. 2b). This is likely because brown carbon is the source of ${}^{1}O_{2}*$ (Faust and Allen, 1992; Zepp et al., 1977) and the DOC concentrations in the fog and dilute extracts are very similar (Table S2). On the other hand, the average [${}^{1}O_{2}*$] in the more concentrated, standard PM extracts (PME3–6), is 1.6 (\pm 0.5) × 10⁻¹² M, nearly seven times higher than the averages in Davis fog and dilute extracts (Fig. 2b, Table S7). This is because the standard extracts have higher DOC concentrations but the same major ${}^{1}O_{2}*$ sink, i.e., water. Across all fog and particle extracts, the rate of singlet oxygen formation ($P_{102}*$) is strongly correlated with the rate of sunlight absorption (R_{abs}) (R^{2} = 0.94; Fig. 3a), although this correlation is not evident in only the fog samples (Kaur and Anastasio, 2017).

As seen for 'OH, quantum yields of ${}^{1}O_{2}$ * are similar in the extracts (standard and dilute) and fog (Table S7); the slope of the P_{1O2} * versus R_{abs} correlation line (Fig. 3a) gives an overall quantum yield of ${}^{1}O_{2}$ * of (3.8 ± 0.2) %, i.e., across all samples roughly 4% of the photons absorbed lead to the formation of singlet oxygen. This is nearly 260 times higher than the average quantum yield of 'OH. Our quantum yields for singlet oxygen formation in PM extracts are similar to values previously reported for surface water organics (e.g., 2 – 5% in Zhou et al. (2019).

3.5 Triplet excited states of organic matter (³C*)

We also determined the kinetics and concentrations of oxidizing "triplets", by measuring the loss of two probes, syringol (SYR) and methyl jasmonate (MeJA) (Fig. S8). In the standard extracts, the average ($\pm \sigma$) Davis winter-normalized rate constants for loss of SYR and MeJA (k'_{Probe}) are (4.3 ± 1.7) × 10^{-4} s⁻¹ and (2.6 ± 0.7) × 10^{-5} s⁻¹, which are equivalent to average lifetimes of 0.70 (\pm 0.20) and 11 (\pm 3) h, respectively (Tables S8 and S9). Triplet probe lifetimes in the dilute extracts are approximately three times longer and are very similar to fog values, indicating that the main source of triplet precursors to fog drops is the BrC present in the fog condensation nuclei rather than mass transport from the gas phase.

We correct the loss of triplet probes for oxidation by hydroxyl radical and singlet molecular oxygen (Eq. (6)). In the standard extracts, ${}^{1}O_{2}*$ and ${}^{*}OH$ account for an average of 13 % and 3 % of SYR loss, respectively (Table S8, Fig. S9); for methyl jasmonate, the corresponding contributions are 37 % and 13 %.

Next we use the ratio of the pseudo-first-order rate constants for probe losses by triplets, i.e., $k'_{SYR,3C^*}/k'_{MeJA,3C^*}$, to characterize the average reactivity of the triplet species in each sample: a ratio close to 1 indicates higher reactivity, while a higher ratio indicates lower reactivity. The $k'_{Probe,3C^*}$ ratio (i.e., $k'_{SYR,3C^*}/k'_{MeJA,3C^*}$) in all extracts ranges between 7.9 and 37 (Table S12), which is a narrower range than in Davis fog samples (7.5 to 110) (Kaur and Anastasio, 2018b). Based on the $k'_{Probe,3C^*}$ ratios, triplets in the PM extracts generally have an average reactivity similar to model aromatic triplets 3'-methoxyacetophenone (3 3MAP*) and 3,4-dimethoxybenzaldehyde (3 DMB*) (Fig. 2c, Table S12). The average ($\pm \sigma$) triplet steady-state concentration in the standard extracts is 1.0 (\pm 0.4) × 10⁻¹³ M (Fig. 2c, Table S13), which is nearly twice the fog average, but not statistically significantly different. If we consider only the PM and fog samples that have triplet reactivities similar to 3 3MAP* and 3 DMB* (i.e., the green average lines in Fig. 2c), the average triplet concentration in the standard PM extracts is nearly four times greater than in fog (Table S2), similar to the ratio of DOC concentrations.

In the standard extracts the average concentration of oxidizing triplets is 16 times lower than [${}^{1}O_{2}^{*}$] but nearly 200 times higher than [${}^{\circ}OH$] from *in situ* sources. Our measurements of oxidizing triplet concentrations lie at the higher end of measured and estimated concentrations of total (i.e., oxidizing and energy transfer) triplets in surface waters, 10^{-15} – 10^{-13} M (Zepp et al., 1985; Grebel et al., 2011). The average ($\pm 1 \sigma$) rate of triplet photoformation, P_{3C^*} , is 2.0 (± 1.0) × 10^{-7} M s $^{-1}$ (i.e., 720 (± 360) μ M h $^{-1}$) in the standard extracts (Table S13). Thus the ratios of the average production rates for ${}^{1}O_{2}^{*}$, ${}^{3}C^{*}$, and ${}^{*}OH$ are 290 : 170 : 1. There is a fair correlation between P_{3C^*} and R_{abs} (Fig. 3b), similar to the case for P_{102^*} (Fig. 3a), consistent with BrC as the source of triplets. Sample-to-sample variability in the fraction of the total triplet pool that can oxidize organics likely causes the P_{3C^*} correlation ($R^2 = 0.81$) to be weaker than that of P_{102^*} ($R^2 = 0.94$). The average ($\pm 1\sigma$) oxidizing triplet quantum yield in standard extracts is (2.4 ± 1.0) % (Table S13), approximately two times lower than the value for ${}^{1}O_{2}^{*}$ (Table S7) but 150 times higher than for ${}^{*}OH$ (Table S3). Our triplet quantum yields are within the wide range of values that has been reported for surface waters, approximately 0.4 – 7% (Zepp et al., 1985; Grebel et al., 2011; Zhou et al., 2019).

Triplet excited states have two main reaction pathways: energy transfer (e.g., to make $^{1}O_{2}^{*}$) and electron transfer (e.g., to oxidize a phenol) (Zepp et al., 1985; McNeill and Canonica, 2016; Kaur and Anastasio, 2018b). Essentially all triplets possess enough energy to form $^{1}O_{2}^{*}$ (McNeill and Canonica, 2016), but only a subset of the triplet pool can oxidize organics via electron transfer. Thus the quantum yield of $^{1}O_{2}^{*}$ can be used to estimate the total triplet quantum yield, while our measurements of $\Phi_{3C^{*}}$ constrain the smaller subset of oxidizing triplets (assuming energy transfer from triplets is the only source of $^{1}O_{2}^{*}$). The quantum yield for all triplets can be estimated as $\Phi_{102^{*}}/f_{\Delta}$, where f_{Δ} , the fraction of $^{3}C^{*}$ interactions with dissolved O_{2} that yield $^{1}O_{2}^{*}$, is approximately 0.5 (McNeill and Canonica, 2016; Kaur and Anastasio, 2018b). For our standard extracts, the average value of $\Phi_{102^{*}}/f_{\Delta}$ is 0.078 ± 0.019, i.e., approximately 8 % of the photons absorbed by brown carbon chromophores make a triplet excited state. Next we use the ratio $\Phi_{3C^{*}}/(\Phi_{102^{*}}/f_{\Delta})$ to estimate the fraction of all triplets that can participate in electrontransfer (oxidation) reactions. The average value of this fraction is 0.35 ± 0.12 for all the PM extracts, i.e., on average, approximately a third of all triplets are oxidizing (range = 18–50 %; Table S13).

3.6 Predicting photooxidant concentrations in ambient particle water

Since our particle extracts are approximately 1000 times more dilute than ambient Davis particles during winter, we want to be able to estimate oxidant concentrations under ambient conditions. To do this we first measured photooxidant concentrations as a function of dilution for the same sample and then extrapolated our results to ambient particle conditions. For the first step, we extracted squares of filter #3 using five different volumes of Milli-Q water, from 10 to 0.50 mL (Sect. 2.5.4), corresponding to aqueous PM mass concentration factors (CF) of 0.05 (most dilute) to 0.96 (most concentrated) (Eq. (10)). For this sample, these are equivalent to PM solute mass / water mass ratios typical for dilute to very concentrated cloud or fog drops, i.e., $(0.35-8.4)\times 10^{-4}\,\mu\text{g-PM}\,/\,\mu\text{g-H}_2\text{O}; \text{ in comparison, ambient particles have ratios of approximately 1 $\mu\text{g-PM}\,/\,\mu\text{g-H}_2\text{O}$ and higher (Table S14). The rate of light absorption increases linearly with CF (Fig. 4a), indicating that BrC and other chromophores are efficiently extracted for all Milli-Q volumes employed.$

The change in photooxidant concentration with CF depends on how the ratio of sources and sinks varies with dilution. In the case of hydroxyl radical, P_{OH} and k'_{OH} both increase as extracts get more concentrated (i.e., as CF increases), resulting in an 'OH concentration that is noisy but essentially unchanged over the 20-fold increase in concentration factor (Fig. 4b). This

result is consistent with the relatively constant [OH] in our particle extracts relative to fog (Fig. 3a, black dashed lines) and with prior results showing very similar concentrations for rain, cloud, fog, and marine PM extracts (Fig. S7 and Arakaki et al., 2013).

529

530

531

532

533

534

535

536

537

538539

540

541

542

543

544

545

546

547

548

549

550

551

552

553

554

555

556

557

558

559

560

561

To estimate [OH] in particle liquid water, we use the measured linear dependences of the rate of 'OH photoproduction (P_{OH}) and loss rate constant (k'_{OH}) on concentration factor, which corresponds to a measured PM mass / water mass ratio (Fig. S10). Under a typical wintertime, Central Valley ambient particle water condition (1 μ g-PM / μ g-H₂O), the in situ P_{OH} and k'_{OH} are estimated to be $4.2 \times 10^{-6} \,\mathrm{M \ s^{-1}}$ and $5.5 \times 10^{9} \,\mathrm{s^{-1}}$, respectively (Fig. S10). This extrapolation of only aqueous processes gives an 'OH concentration in particle water of 7.6×10^{-16} M, which is similar to the average of the measurements in Fig. 4b. However, this estimate does not include the contribution of mass transport of gas-phase OH to the particles. As detailed in Sect. S4, we estimate that the rate of 'OH gas-to-particle transport under particle conditions is $4.2 \times 10^{-7} \,\mathrm{M \ s^{-1}}$ 1, which is approximately 10 % of the OH photoformation rate from aqueous sources. Figure 5 shows estimated 'OH steady-state concentrations considering both aqueous reactions and gasphase mass transport across a wide range of drop to particle conditions: [OH] decreases from 5.4 \times 10⁻¹⁵ M under dilute drop conditions (3 \times 10⁻⁵ µg-PM/µg-H₂O) to 8.4 \times 10⁻¹⁶ M under the much more concentrated particle conditions (1 μg-PM/μg-H₂O). The calculated [OH] values (orange line in Figure 5) are higher than our measured values (orange points in Figure 5) because of the gas-phase mass transport source. Changes in this source are also responsible for the slow decrease in calculated [OH] as conditions become more concentrated (i.e., as µg-PM/µg-H₂O increases). In the case of singlet oxygen, steady-state concentrations increase proportionally with PM mass concentration factor (Fig. 4c). Our interpretation of this result is that the concentrations of ${}^{1}O_{2}$ * sources (i.e., BrC) increase proportionally with concentration factor, while the concentration of the main sink for ¹O₂* (i.e., water) is essentially unchanged. At higher PM mass/water mass ratios, we calculate that organic compounds become a significant sink for singlet oxygen (Sect. S4), leading to a plateau in $\lceil {}^{1}O_{2}^{*} \rceil$ under the more concentrated conditions of particles (Fig. 5). This extrapolation for ambient PM conditions (1 µg-PM / µg-H₂O) predicts an ${}^{1}O_{2}$ * concentration in particle water of 1.6 × 10 $^{-10}$ M (Table S15, Fig. 5), which is 2400 times higher than our prediction for dilute fog/cloud drops. While there are no other measurements of ¹O₂* in particles, similar enhancements in ¹O₂* concentrations (up to a factor of roughly 10⁴) have been found in cases where ¹O₂* precursors become highly concentrated, e.g., in liquid-like regions of ice (Bower and Anastasio, 2013) and in regions of hydrophobic CDOM in solution (Latch and McNeill, 2006).

An increase in extract concentration (i.e., CF) also increases the triplet steady-state concentration (Fig. 4d), but there is greater uncertainty in this trend, in part because there is more uncertainty in measurements of $\Sigma[^3C_i^*]$. As described in Sect. S4, we fit the data in Fig. 4d with a hyperbolic regression under two cases: (1) a best fit, where parameters were adjusted to minimize the regression error, and (2) a high estimate fit, where parameters were adjusted so that the regression line passed near the upper portion of the error bar for the CF 0.96 data point. These are the dashed and dotted lines in Fig. 4d, respectively. In both cases the triplet concentration initially rises more quickly with CF but then approaches a plateau at higher CF values. Our interpretation of this behavior is that as CF increases, [DOM] and P_{3C^*} increase linearly but the dominant triplet sink switches from dissolved O₂ at low CF to DOM at high CF. Wenk et al. (2011); (2013) have shown that surface water DOM can guench triplets when DOM concentrations are greater than 20 mg-C L⁻¹; in the PME3D extracts of Fig. 4, DOM ranges from 4.3 to 86 mg-C L⁻¹ (Table S2). Based on our previous work, we believe that phenols from wood combustion are reacting with (and physically quenching) triplets in our PM extracts (Smith et al., 2014; 2015). As described in Sect. S5, by fitting a kinetic model to our triplet dilution data we estimate that the total (reaction and quenching) rate constant for triplets with DOC in the PME3 extracts is $9.3 (\pm 1.3) \times 10^7 \,\text{L mol-C}^{-1} \,\text{s}^{-1}$.

These two extrapolations result in oxidizing triplet concentrations under PM conditions (1 μ g-PM / μ g-H₂O) of 2.3× 10⁻¹³ M (best fit) and 1.3 × 10⁻¹¹ M (high estimate). Taken together with the other oxidant measurements, we estimate that the ratio of ${}^{1}O_{2}*: {}^{3}C*: {}^{*}OH$ concentrations in ambient particle water is approximately 10⁵: 10⁴–10²: 1.

4 Implications

Our dilution experiments suggest that 'OH, ${}^{1}O_{2}*$, and ${}^{3}C*$ behave very differently as the PM/water ratio increases from cloud and fog drop conditions to water-containing particles (Fig. 5). To understand what this implies for the fate of organic compounds, we estimated the gasaqueous partitioning and lifetimes of five model organic compounds for both fog and aqueous aerosol (Fig. 6). We consider reactions with two gas-phase oxidants ('OH, O₃) and four aqueous-phase oxidants ('OH, O₃, ${}^{1}O_{2}*$, ${}^{3}C*$) (Table S16). Our model organics represent two groups in terms of gas-aqueous partitioning: one group with modest Henry's law constants ($K_{\rm H} \sim 10^4$ M atm⁻¹) and one with much higher values ($K_{\rm H} = 10^9 - 10^{11}$ M atm⁻¹) (Fig. 6 and Table S17).

Fig. 6a shows the overall lifetimes of the five model organics and the fraction of each present in fog and PM. For the organics with the lowest $K_{\rm H}$ values, approximately 10–20 % is present in the aqueous-phase under fog conditions, but almost none is present in the particle liquid water. Consequently, gas-phase reactions dominate their overall lifetimes, which are approximately 2 to 3 hours for both fog and PM conditions. In contrast, the compounds with high $K_{\rm H}$ values are partitioned strongly to the aqueous phase for both the fog and PM scenarios (Fig. 6a). But due to the overall higher oxidant concentrations in PM, the lifetimes of these organics are predicted to be shorter – sometimes by large factors – in PM than in fog (Fig. 6a, Table S17). Additionally, their main sinks change from fog to PM, shifting from aqueous 'OH, O₃, and $^{1}O_{2}$ * in fog to being generally dominated by $^{1}O_{2}$ * in PM water (Fig. 6b). For example, for tyrosine (compound 3), the predominant sink changes from aqueous O₃ in fog to $^{1}O_{2}$ * in water-containing particles, while its lifetime decreases from 1.6 h to 0.04 h (Fig. 6b and Table S17).

While triplets are negligible oxidants for individual organics in particles under the conditions of Fig. 6, the picture changes if we move from the Fig. 6 triplet concentration of 2.3×10^{-13} M to the high estimate concentration $(1.3 \times 10^{-11} \,\mathrm{M}; \,\mathrm{Fig.}\,5)$. Under this condition aqueous oxidation still dominates the loss of the high- $K_{\rm H}$ compounds, but ${}^{3}\mathrm{C}^{*}$ becomes a much more important oxidant in PM and organic lifetimes get shorter by factors of 3 to 180 compared to fog (Fig. S11). While there is large uncertainty in the triplet concentrations in PM, Figs. 6 and S11 both indicate that aqueous oxidants can control the fate of highly soluble species in aerosols and that organic lifetimes can be shorter in PM because of an enhancement in oxidant concentrations.

Finally, despite the uncertainty in triplet concentration under particle conditions, the formation rate of ${}^3C^*$ is fast enough – and the fraction of triplets lost via reaction with organics is high enough – that triplets represent, in aggregate, a significant sink for organic compounds in particles. While these two ideas might seem contradictory, we propose that the suite of reactive organic compounds is suppressing the triplet concentrations enough that ${}^3C^*$ are small sinks for individual organic compounds, but are significant sinks when integrated over all of the reactive organics. As described in Sect. 3.5, the formation rates for ${}^1O_2^*$, ${}^3C^*$, and 4OH have a ratio of 290 : 170 : 1, respectively, in the PM extracts; based on our dilution experiments (Fig. 4), we expect similar ratios in ambient particle liquid water. Since organic compounds appear to be the major sinks for all three oxidants under ambient particle conditions, and since each oxidant is at steady-state, the ratio of formation rates is approximately the same as the ratio of total rates of organic compound oxidation by each oxidant. Thus, while the steady-state concentration of ${}^3C^*$ might be significantly lower than that of ${}^1O_2^*$ in particle water, both oxidants appear to be

similarly important in the overall processing of particulate organics. In contrast, the total rate of oxidation of organics by 'OH appears to be 200–300 times slower, although 'OH will be relatively more important for less reactive organics. This comparison suggests that both singlet molecular oxygen and triplet excited states are important for the processing of organic compounds in particle liquid water.

Conclusions and Uncertainties

We have made the first measurements of singlet molecular oxygen and oxidizing triplet states in aqueous extracts of particles, in addition to measuring hydroxyl radical. Under our standard condition, the particle extracts are approximately three times more concentrated than wintertime Davis fog waters. The extracts contain significant amounts of brown carbon, with DOC-normalized mass absorption coefficients between roughly 15,000 and 30,000 cm² g-C⁻¹ and Absorption Angstrom Exponents of 6.2 to 7.9. Upon absorbing light, BrC and other chromophores in the samples form significant amounts of 'OH, ¹O₂*, and ³C*. While concentrations of 'OH in the PM extracts are in the same range as found in fog waters, concentrations of the oxidants derived primarily from BrC – i.e., ¹O₂* and ³C* – are higher in the extracts compared to in fog by factors of approximately seven and two, respectively.

Dilution experiments indicate that the 'OH concentration is essentially independent of the PM mass concentration in solution, consistent with previous results, while ${}^{1}O_{2}*$ and ${}^{3}C^{*}$ increase with increasing aqueous PM concentration. Extrapolating our findings to the much more concentrated conditions expected in ambient particle water suggests that hydroxyl radical concentrations in particles will be somewhat lower than values in fog and cloud drops, a result of size-dependent changes in mass transport from the gas phase. In contrast, oxidants formed from illumination of brown carbon will be enhanced in particles: moving from very dilute drops ($3 \times 10^{-5} \,\mu g\text{-PM/}\mu g\text{-H}_2\text{O}$) to concentrated particles ($1 \,\mu g\text{-PM/}\mu g\text{-H}_2\text{O}$) we predict that the concentration of ${}^{1}O_{2}*$ will increase by approximately a factor of 2400, while concentrations of oxidizing triplets will increase between a factor of 30 and 2000. The higher ${}^{1}O_{2}*$ concentrations predicted in particles lead to a large decrease in the lifetimes of highly water-soluble organic compounds compared to foggy conditions, even though the liquid water content of the particles is roughly 10^{4} times lower than the fog. It appears that triplets are also more significant oxidants for individual organic compounds in PM than in fog, but there is too much uncertainty in our data to properly assess this increase. In contrast, 'OH is important for the oxidation of organics

that react only slowly with ${}^{1}O_{2}^{*}$ and ${}^{3}C^{*}$, but is otherwise a minor oxidant for the organics we considered since the particulate ${}^{*}OH$ concentration is quite low.

While our results suggest that oxidants derived from brown carbon are very significant in water-containing particles, there are several large uncertainties. Most significantly, because of experimental limitations on the maximum PM concentration in our extracts, we need to extrapolate oxidant measurements over a very large range (approximately a factor of 1000) to predict oxidant levels in ambient water-containing particles. This results in very large uncertainties. As part of this uncertainty, it is difficult to assess how reactions in the particles might suppress concentrations of ¹O₂* and ³C*. Secondly, while calculations suggest that unaccounted oxidants are minor sinks for our triplet probes, if these species are important our triplet concentrations would be biased high. Finally, it is unclear how widely our results, which are for one season and one location, can be applied to other particles containing brown carbon. However, PME3, our one sample collected during both daytime (with little biomass burning) and night (with significant biomass burning) had similar reactivity to the other samples, which were collected only at night. Regardless, since these are the first measurements of ¹O₂* and ³C* in particles, strengthening and improving our findings requires more measurements, especially for other seasons and locations. Measurements under much higher particle mass/water mass ratios, ideally under ambient conditions, are also needed.

Despite the uncertainties, our results indicate that BrC-derived photooxidants such as singlet molecular oxygen and organic triplet excited states can be important oxidants in atmospheric particles. Currently these oxidants are not included in atmospheric models, although our calculations suggest that ${}^{1}O_{2}$ * and ${}^{3}C$ * can dominate the processing of highly soluble organic molecules in aerosol particles.

Competing Interests

658

659

660

661

662

663

664

665

666

667

668

669

670

671

672

673

674

675

676

677

678

679

680

681

682

683

684

685

686

687

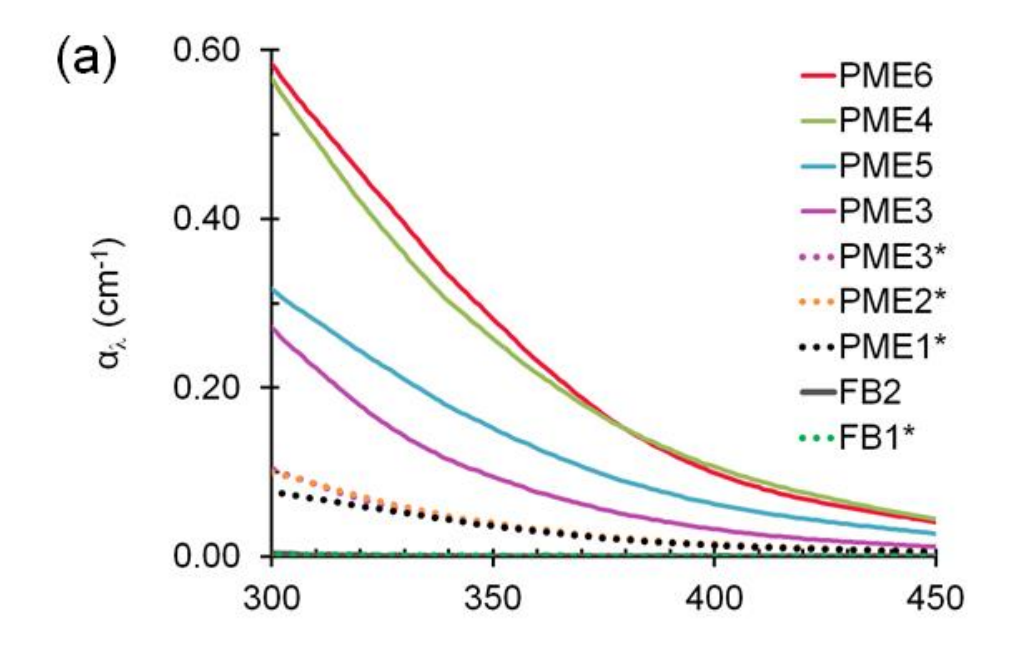
The authors declare that they have no conflict of interest.

Author Contribution

CA and RK developed the research goals and designed the experiments. KB lent and set up the sampler, while RK, CA, and WJ collected samples. RK, JL, and SH performed the photochemistry experiments while WJ analyzed ions and OC. RK analyzed the data and prepared the manuscript with contributions from all co-authors. CA reviewed, wrote portions of, and

edited the manuscript. CA and QZ provided supervision and oversight during the experiments 688 689 and writing. 690 **Data Availability** Light absorption data have been submitted to the data repository Pangaea, cited in the text and 691 are available at https://doi.pangaea.de/10.1594/PANGAEA.896418. Other data are available 692 693 upon request. 694 Acknowledgments 695 We thank Ann Dillner, Alexandra Boris, and April Chaney (UC Davis, Air Quality Research Center) for use of a microbalance and an anonymous reviewer for extensive and helpful 696 697 comments. Funding was provided by the National Science Foundation (AGS-1649212), California Agricultural Experiment Station (Project CA-D-LAW-6403-RR), a UC Guru Gobind 698 Singh Fellowship, a Donald G. Crosby Graduate Fellowship, and a James and Rita Seiber 699 700 International Student Support Award.

701 Figures



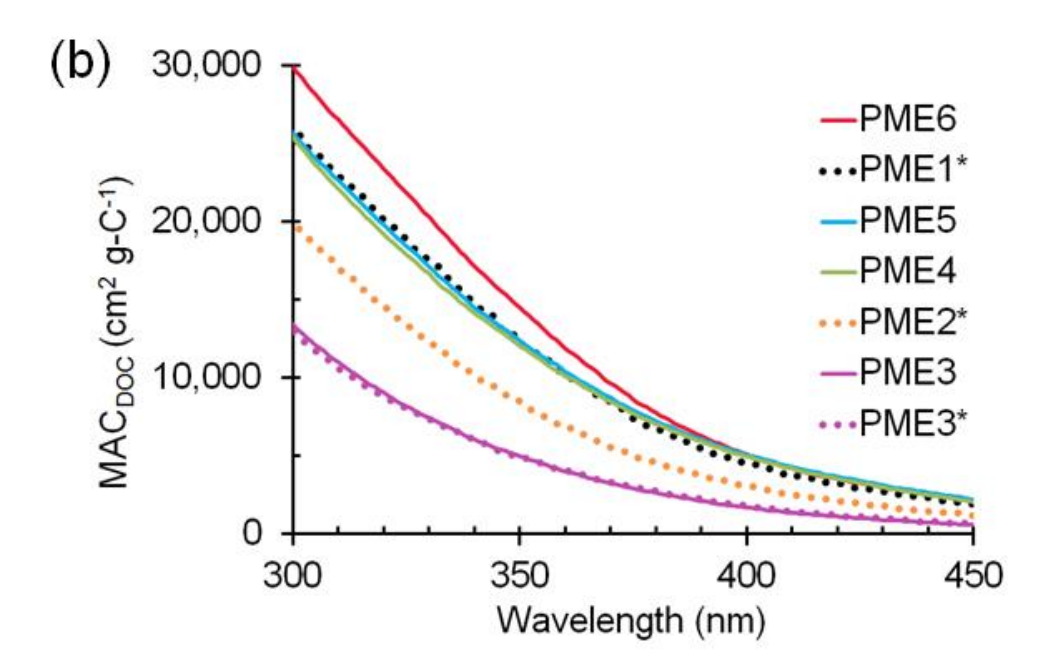


Figure 1. (a) Light absorption coefficients, α_{λ} , in particulate matter extracts (PME) (Eq. (1)) and field blanks (FB). The legend shows the sample identities, arranged from the highest absorbing (top) to lowest absorbing (bottom) at 300 nm. Solid and dotted lines represent standard and dilute extracts, respectively (with the latter indicated with an asterisk; Sect. 2.2). (b) Mass absorption coefficients of DOC in the particle extracts (Eq. (3)).

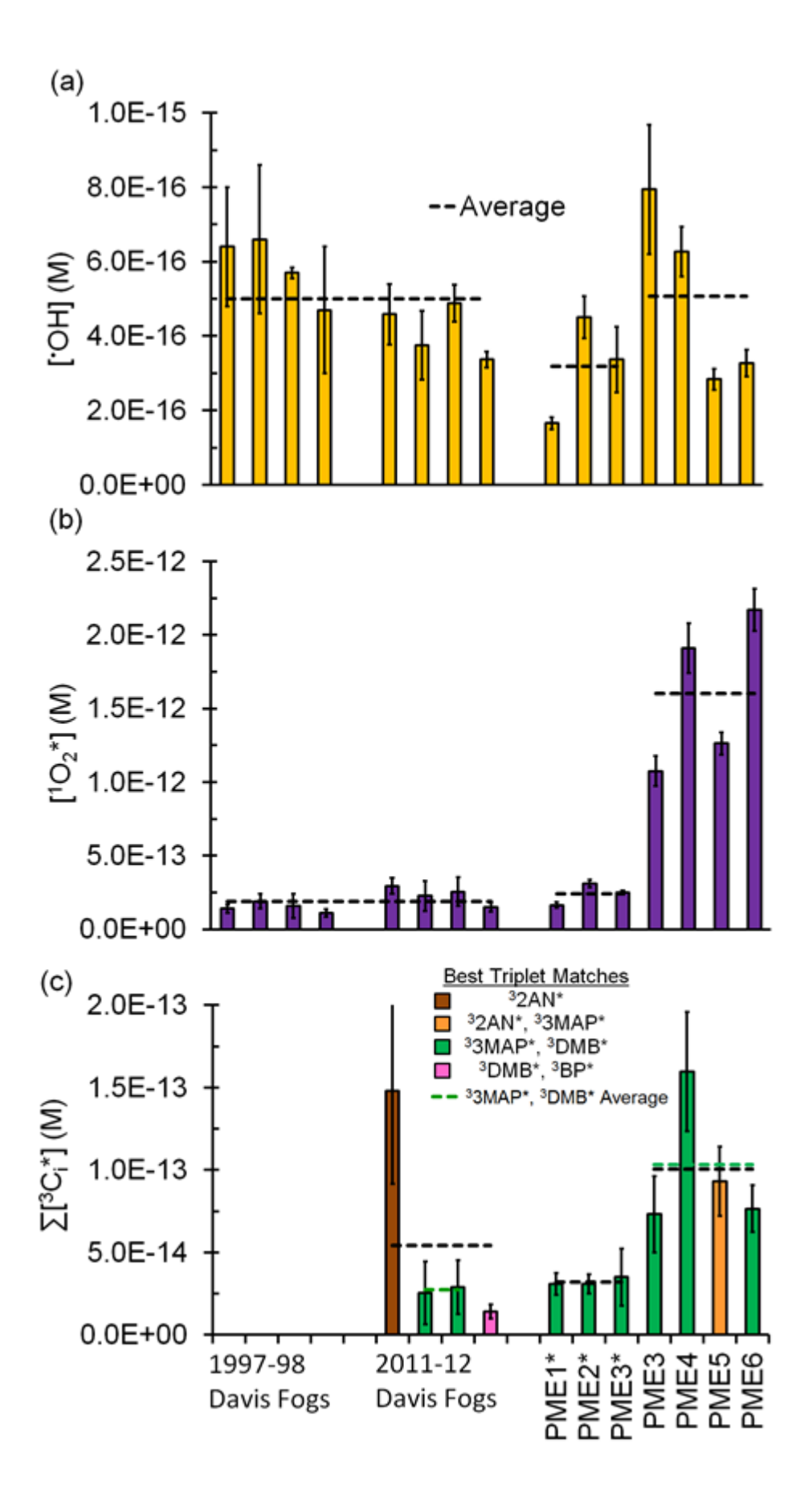


Figure 2. Measured steady-state concentrations of (a) hydroxyl radical, (b) singlet molecular oxygen and, (c) oxidizing triplet excited states of organic matter in particle extracts, along with previous measurements made in Davis fogs collected between 1997-98 and 2011-12 (Anastasio and McGregor, 2001; Kaur and Anastasio, 2017; Kaur and Anastasio, 2018b). All concentrations are normalized to Davis midday, winter solstice sunlight. Dilute particle extracts are indicated with an asterisk. Dashed lines represent sample averages.

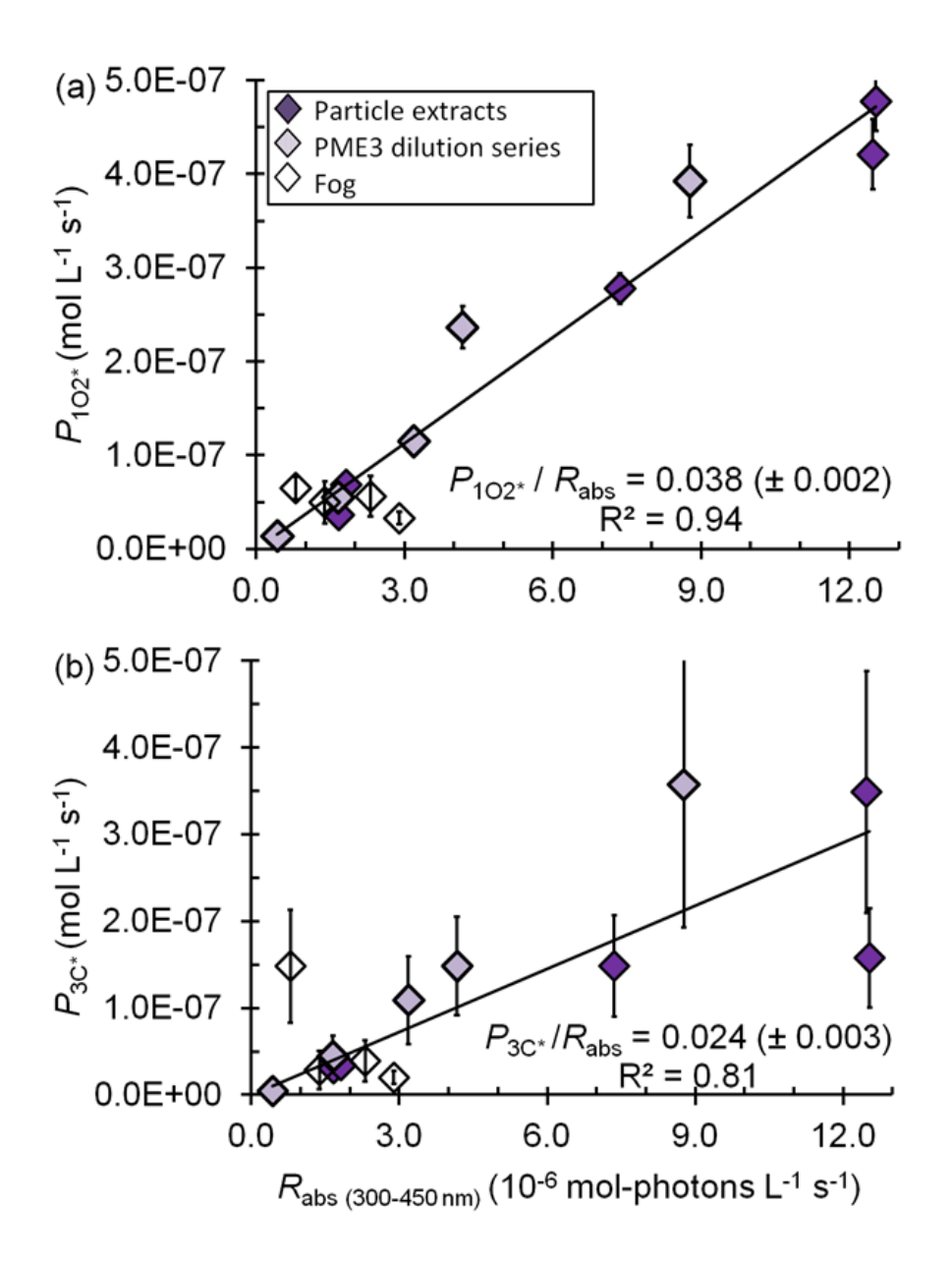


Figure 3. Correlations between (a) the rate of singlet oxygen photoproduction normalized to Davis winter solstice sunlight (P_{1O2^*}) , (b) the rate of triplet photoproduction normalized to Davis winter solstice sunlight (P_{3C^*}) and the rate of light absorption (Rabs) between 300 to 450 nm. Triplet rates for the fog samples were adjusted to account for the small DOC sink for triplets; Eq. (8). The P/R_{abs} ratios (\pm 1 SE) listed are unitless and represent the quantum yields.

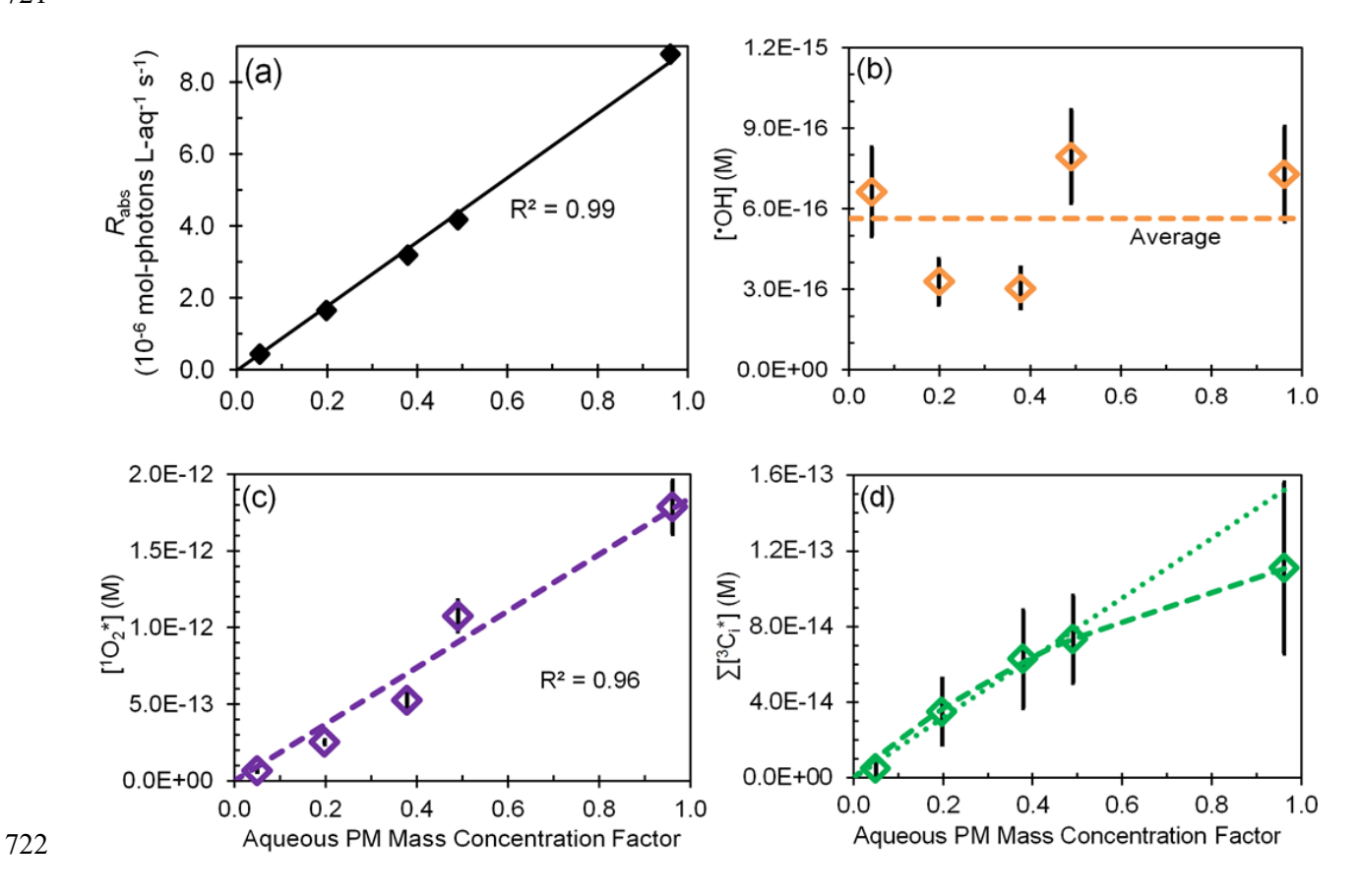


Figure 4. Effect of change in aqueous particle mass concentration (i.e., sample dilution) for sample PME3 on (a) rate of light absorption and the steady-state concentrations of (b) hydroxyl radical, (c) singlet molecular oxygen and, (d) oxidizing triplet excited states of organic matter. The last panel shows both linear (dotted) and hyperbolic (dashed) fits to the data. In each plot the x-axis is a measure of sample dilution, with higher concentration factors corresponding to more concentrated particle extracts (Eq. (10)).

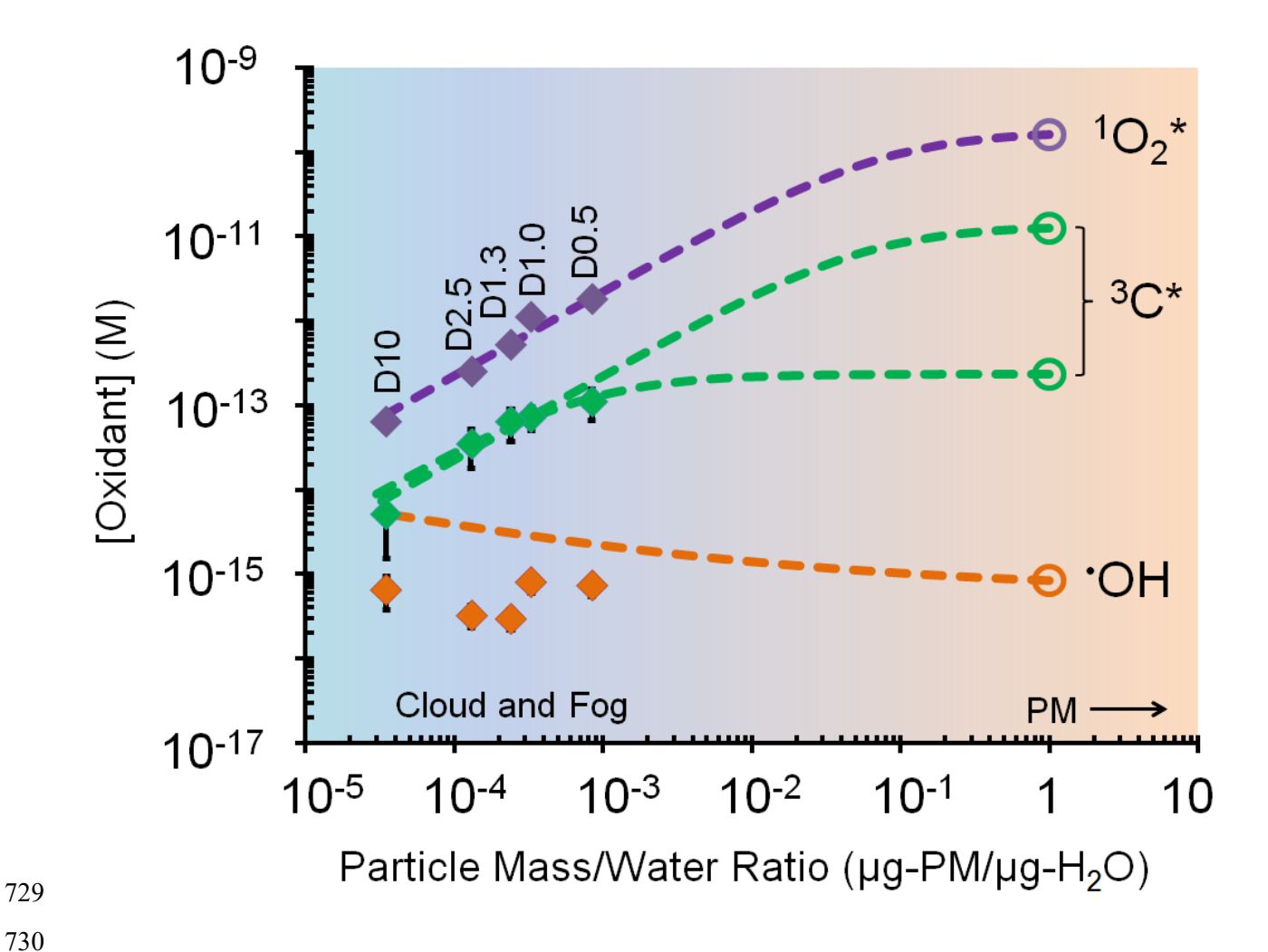


Figure 5. Dependence of photooxidant concentrations on particle mass / water mass ratio (i.e., aqueous particle concentration) in extracts of sample PME3. Solid diamonds are measured values under experimental dilution conditions (typical for clouds or fogs), while the open circles are values expected in more concentrated particle liquid water based on the dashed line extrapolations. For the solid symbols, error bars (\pm 1 σ) are often smaller than the symbols. Data labels on the diamonds (e.g., D10) represent the water volume used to extract the PME3 filter square (Sect. 2.5.4). The dashed line extrapolations include the contributions from both aqueous processes and interactions with the gas phase (Sect. S4). For oxidizing triplets, two extrapolation scenarios are shown: a best estimate (lower line) and a high estimate (upper line), as described in Sect. S4 and Table S15.

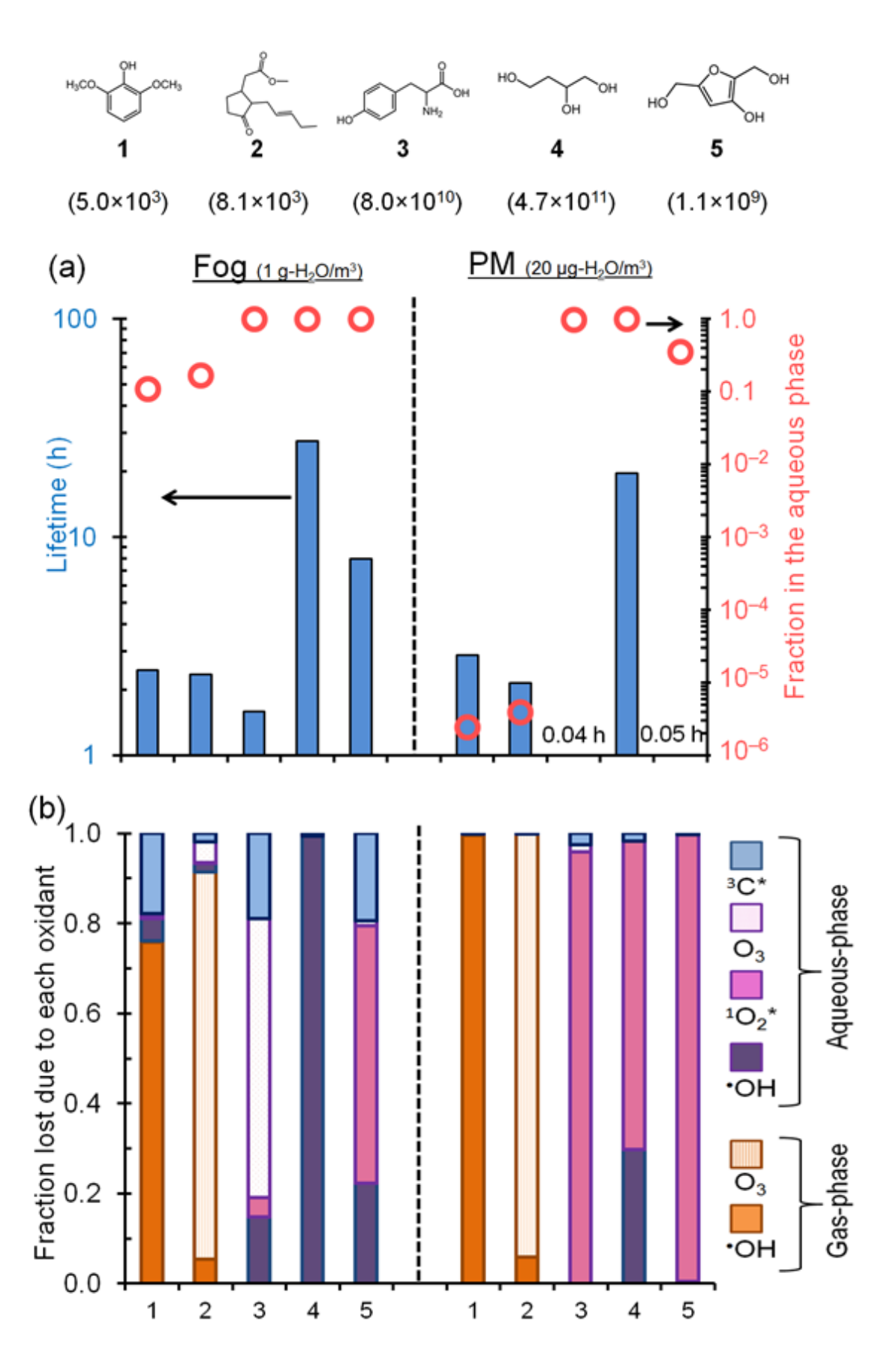


Figure 6. Fate of five model organic compounds – (1) syringol, (2) methyl jasmonate, (3) tyrosine, (4) 1,2,4-butanetriol and (5) 3-hydroxy-2,5-bis(hydroxymethyl)furan – under liquid water content conditions for fog (left of vertical dashed line; 1 g-H₂O / m³-air) and PM (right of line; 20 μ g-H₂O / m³-air). Estimated Henry's law constants for the compounds (in units of M atm⁻¹) are in parentheses beneath each structure. In panel (a) the columns represent overall lifetimes of the organics and the open circles represent the fractions in the aqueous phase. Panel

- 748 (b) shows the fraction of each compound lost via various gas and aqueous pathways. The triplet
- contribution in PM is estimated using the lower-bound triplet concentration extrapolation i.e., 1.3
- 750 \times 10⁻¹³ M (Fig. 5). Oxidant concentrations and rate constants are in Tables S16 and S17.

- Albinet, A., Minero, C., and Vione, D.: Photochemical generation of reactive species upon irradiation of rainwater: Negligible photoactivity of dissolved organic matter, Sci. Total Environ., 408, 3367-3373, 2010.
- Anastasio, C., Faust, B. C., and Rao, C. J.: Aromatic carbonyl compounds as aqueous-phase photochemical sources of hydrogen peroxide in acidic sulfate aerosols, fogs, and clouds .1. Non-phenolic methoxybenzaldehydes and methoxyacetophenones with reductants (phenols), Environ. Sci. Technol., 31, 218-232, 1997.
 - Anastasio, C., and McGregor, K. G.: Chemistry of fog waters in California's central valley: 1. In situ photoformation of hydroxyl radical and singlet molecular oxygen, Atmospheric Environment, 35, 1079-1089, 2001.
 - Anastasio, C., and Jordan, A. L.: Photoformation of hydroxyl radical and hydrogen peroxide in aerosol particles from Alert, Nunavut: Implications for aerosol and snowpack chemistry in the Arctic, Atmos. Environ., 38, 1153-1166, 2004.
 - Anastasio, C., and Newberg, J. T.: Sources and sinks of hydroxyl radical in sea-salt particles, J. Geophys. Res., 112, D10306, https://doi.org/10.1029/2006JD008061, 2007.
 - Arakaki, T., and Faust, B. C.: Sources, sinks, and mechanisms of hydroxyl radical (*OH) photoproduction and consumption in authentic acidic continental cloud waters from Whiteface Mountain, New York: The role of the Fe (R)(R= II, III) photochemical cycle, J. Geophys. Res. Atmos., 103, 3487-3504, 1998.
 - Arakaki, T., Miyake, T., Shibata, M., and Sakugawa, H.: Photochemical formation and scavenging of hydroxyl radical in rain and dew waters, Nippon Kagaku Kaishi, 5, 335-340, 1999.
 - Arakaki, T., Kuroki, Y., Okada, K., Nakama, Y., Ikota, H., Kinjo, M., Higuchi, T., Uehara, M., and Tanahara, A.: Chemical composition and photochemical formation of hydroxyl radicals in aqueous extracts of aerosol particles collected in Okinawa, Japan, Atmos. Environ., 40, 4764-4774, 2006.
 - Arakaki, T., Anastasio, C., Kuroki, Y., Nakajima, H., Okada, K., Kotani, Y., Handa, D., Azechi, S., Kimura, T., Tsuhako, A., and Miyagi, Y.: A general scavenging rate constant for reaction of hydroxyl radical with organic carbon in atmospheric waters, Environ. Sci. Technol., 47, 8196-8203, 2013.
 - Aregahegn, K. Z., Nozière, B., and George, C.: Organic aerosol formation photo-enhanced by the formation of secondary photosensitizers in aerosols, Faraday Discuss., 165, 123-134, 2013.
 - Bahnmüller, S., von Gunten, U., and Canonica, S.: Sunlight-induced transformation of sulfadiazine and sulfamethoxazole in surface waters and wastewater effluents, Water Res., 57, 183-192, 2014.
 - Bilski, P., Holt, R. N., and Chignell, C. F.: Properties of singlet molecular oxygen O₂ (1Δg) in binary solvent mixtures of different polarity and proticity, J. Photochem. Photobiol., A, 109, 243-249, 1997.
- Blando, J. D., and Turpin, B. J.: Secondary organic aerosol formation in cloud and fog droplets:
 A literature evaluation of plausibility, Atmos. Environ., 34, 1623-1632, 2000.
- Boreen, A. L., Arnold, W. A., and McNeill, K.: Triplet-sensitized photodegradation of sulfa
 drugs containing six-membered heterocyclic groups: Identification of an SO₂ extrusion
 photoproduct, Environ. Sci. Technol., 39, 3630-3638, 2005.

Bower, J. P., and Anastasio, C.: Measuring a 10,000-fold enhancement of singlet molecular oxygen (1 O 2*) concentration on illuminated ice relative to the corresponding liquid solution, Atmos. Environ., 75, 188-195, 2013.

802

803 804

805 806

807

808

809

819

- Brezonik, P. L., and Fulkerson-Brekken, J.: Nitrate-induced photolysis in natural waters:
 Controls on concentrations of hydroxyl radical photo-intermediates by natural scavenging agents, Environ. Sci. Technol., 32, 3004-3010, 1998.
 - Canonica, S., and Hoigné, J.: Enhanced oxidation of methoxy phenols at micromolar concentration photosensitized by dissolved natural organic material, Chemosphere, 30, 2365-2374, 1995.
 - Canonica, S., Jans, U., Stemmler, K., and Hoigne, J.: Transformation kinetics of phenols in water: Photosensitization by dissolved natural organic material and aromatic ketones, Environ. Sci. Technol., 29, 1822-1831, 1995.
 - Canonica, S., Hellrung, B., and Wirz, J.: Oxidation of phenols by triplet aromatic ketones in aqueous solution, J. Phys. Chem. A, 104, 1226-1232, 2000.
- Canonica, S., Hellrung, B., Müller, P., and Wirz, J.: Aqueous oxidation of phenylurea herbicides by triplet aromatic ketones, Environ. Sci. Technol., 40, 6636-6641, 2006.
- De Haan, D. O., Corrigan, A. L., Smith, K. W., Stroik, D. R., Turley, J. J., Lee, F. E., Tolbert, M. A., Jimenez, J. L., Cordova, K. E., and Ferrell, G. R.: Secondary organic aerosol-forming reactions of glyoxal with amino acids, Environ. Sci. Technol., 43, 2818-2824, 2009.
- De Haan, D. O., Hawkins, L. N., Kononenko, J. A., Turley, J. J., Corrigan, A. L., Tolbert, M. A., and Jimenez, J. L.: Formation of nitrogen-containing oligomers by methylglyoxal and amines in simulated evaporating cloud droplets, Environ. Sci. Technol., 45, 984-991, 2010.
 - Dong, M. M., Mezyk, S. P., and Rosario-Ortiz, F. L.: Reactivity of effluent organic matter (EFOM) with hydroxyl radical as a function of molecular weight, Environ. Sci. Technol., 44, 5714-5720, 2010.
- Ervens, B., Turpin, B., and Weber, R.: Secondary organic aerosol formation in cloud droplets and aqueous particles (aqSOA): a review of laboratory, field and model studies, Atmos. Chem. Phys., 11, 11069-11102, 2011.
- Faust, B. C., and Allen, J. M.: Aqueous-phase photochemical sources of peroxyl radicals and singlet molecular oxygen in clouds and fog, J. Geophys. Res. Atmos., 97, 12913-12926, 1992.
- Finlayson-Pitts, B. J., and Pitts Jr, J. N.: Chemistry of the upper and lower atmosphere: theory, experiments, and applications, Academic Press, San Diego,, 1999.
- Galbavy, E. S., Ram, K., and Anastasio, C.: 2-Nitrobenzaldehyde as a chemical actinometer for solution and ice photochemistry, J. Photochem. Photobiol., A, 209, 186-192, 2010.
- Ge, X., Shaw, S. L., and Zhang, Q.: Toward understanding amines and their degradation products from postcombustion CO₂ capture processes with aerosol mass spectrometry, Environmental Science & Technology, 48, 5066-5075, 2014.
- Grebel, J. E., Pignatello, J. J., and Mitch, W. A.: Sorbic acid as a quantitative probe for the formation, scavenging and steady-state concentrations of the triplet-excited state of organic compounds, Water Res., 45, 6535-6544, 2011.
- Haag, W. R., and Gassman, E.: Singlet oxygen in surface waters—Part I: Furfuryl alcohol as a trapping agent, Chemosphere, 13, 631-640, 1984.
- Haag, W. R., and Hoigné, J.: Singlet oxygen in surface waters .3. Photochemical formation and steady-state concentrations in various types of waters, Environ. Sci. Technol., 20, 341-348, 1986.

- Hawkins, L. N., Welsh, H. G., and Alexander, M. V.: Evidence for pyrazine-based chromophores in cloud water mimics containing methylglyoxal and ammonium sulfate, Atmospheric Chemistry & Physics, 18, 12413-12431, 2018.
- He, C., Liu, J., Carlton, A., Fan, S., Horowitz, L., Levy, I., and Tao, S.: Evaluation of factors
 controlling global secondary organic aerosol production from cloud processes, Atmos.
 Chem. Phys., 13, 1913-1926, 2013.
- Heald, C. L., Collett Jr, J., Lee, T., Benedict, K., Schwandner, F., Li, Y., Clarisse, L., Hurtmans,
 D., Van Damme, M., and Clerbaux, C.: Atmospheric ammonia and particulate inorganic
 nitrogen over the United States, Atmos. Chem. Phys., 12, 10295-10312, 2012.
- Hecobian, A., Zhang, X., Zheng, M., Frank, N., Edgerton, E. S., and Weber, R. J.: Water-Soluble
 Organic Aerosol material and the light-absorption characteristics of aqueous extracts
 measured over the Southeastern United States, Atmos. Chem. Phys., 10, 5965-5977,
 2010.
- Herner, J. D., Ying, Q., Aw, J., Gao, O., Chang, D. P., and Kleeman, M. J.: Dominant mechanisms that shape the airborne particle size and composition distribution in central California, Aerosol Sci. Technol., 40, 827-844, 2006.
 - Herrmann, H., Hoffmann, D., Schaefer, T., Brauer, P., and Tilgner, A.: Tropospheric aqueousphase free-radical chemistry: Radical sources, spectra, reaction kinetics and prediction tools, ChemPhysChem, 11, 3796-3822, 2010a.

860

861 862

863

864865

866

867 868

869870

871

- Herrmann, H., Hoffmann, D., Schaefer, T., Bräuer, P., and Tilgner, A.: Tropospheric aqueousphase free-radical chemistry: Radical sources, spectra, reaction kinetics and prediction tools, ChemPhysChem, 11, 3796-3822, 2010b.
- Herrmann, H., Schaefer, T., Tilgner, A., Styler, S. A., Weller, C., Teich, M., and Otto, T.: Tropospheric aqueous-phase chemistry: Kinetics, mechanisms, and its coupling to a changing gas phase, Chem. Rev., 115, 4259-4334, 2015.
- Hoffer, A., Gelencsér, A., Guyon, P., Kiss, G., Schmid, O., Frank, G., Artaxo, P., and Andreae, M.: Optical properties of humic-like substances (HULIS) in biomass-burning aerosols, Atmos. Chem. Phys., 6, 3563-3570, 2006.
- Jimenez, J., Canagaratna, M., Donahue, N., Prevot, A., Zhang, Q., Kroll, J. H., DeCarlo, P. F., Allan, J. D., Coe, H., and Ng, N.: Evolution of organic aerosols in the atmosphere, Science, 326, 1525-1529, 2009.
- Kaur, R., and Anastasio, C.: Light absorption and the photoformation of hydroxyl radical and singlet oxygen in fog waters, Atmos. Environ., 164, 387-397, 2017.
- Kaur, R., and Anastasio, C.: Light absorption coefficients of aqueous extracts of wintertime PM collected in Davis, CA, USA., PANGAEA, DOI:

 https://doi.pangaea.de/10.1594/PANGAEA.896422, 2018a.
- Kaur, R., and Anastasio, C.: First measurements of organic triplet excited states in atmospheric waters, Environ. Sci. Technol., 52, 5218-5226, 2018b.
- Kirchstetter, T., and Thatcher, T.: Contribution of organic carbon to wood smoke particulate matter absorption of solar radiation, Atmos. Chem. Phys., 12, 6067-6072, 2012.
- Laskin, A., Laskin, J., and Nizkorodov, S. A.: Chemistry of atmospheric brown carbon, Chem. Rev., 115, 4335-4382, 2015.
- Latch, D. E., and McNeill, K.: Microheterogeneity of singlet oxygen distributions in irradiated humic acid solutions, Science, 311, 1743-1747, 2006.
- Lim, H.-J., Carlton, A. G., and Turpin, B. J.: Isoprene forms secondary organic aerosol through cloud processing: Model simulations, Environ. Sci. Technol., 39, 4441-4446, 2005.

- Lim, Y., Tan, Y., Perri, M., Seitzinger, S., and Turpin, B.: Aqueous chemistry and its role in secondary organic aerosol (SOA) formation, Atmos. Chem. Phys., 10, 10521-10539, 2010.
- Lim, Y., and Turpin, B.: Organic peroxide and OH formation in aerosol and cloud water: laboratory evidence for this aqueous chemistry, Atmospheric Chemistry & Physics Discussions, 15, 12867-12877, 2015.
- Tropospheric ultraviolet-visible model (TUV) version 4.1 http://cprm.acom.ucar.edu/Models/TUV/Interactive TUV/, 2002

904

905

906

- McNeill, K., and Canonica, S.: Triplet state dissolved organic matter in aquatic photochemistry:
 Reaction mechanisms, substrate scope, and photophysical properties, Environ. Sci.
 Process. Impact., 18, 1381-1399, 2016.
- Parworth, C. L., Young, D. E., Kim, H., Zhang, X., Cappa, C. D., Collier, S., and Zhang, Q.:
 Wintertime water-soluble aerosol composition and particle water content in Fresno,
 California, J. Geophys. Res. Atmos., 122, 3155-3170, 2017.
 - Rossignol, S. p., Aregahegn, K. Z., Tinel, L., Fine, L., Noz e, B., and George, C.: Glyoxal induced atmospheric photosensitized chemistry leading to organic aerosol growth, Environ. Sci. Technol., 48, 3218-3227, 2014.
 - Seinfeld, J. H., and Pandis, S. N.: Atmospheric chemistry and physics: from air pollution to climate change, John Wiley & Sons, Hoboken, New Jersey, 2012.
- 908 Silva, P. J., Liu, D.-Y., Noble, C. A., and Prather, K. A.: Size and chemical characterization of 909 individual particles resulting from biomass burning of local Southern California species, 910 Environ. Sci. Technol., 33, 3068-3076, 1999.
- 911 Smith, J. D., Sio, V., Yu, L., Zhang, Q., and Anastasio, C.: Secondary organic aerosol production 912 from aqueous reactions of atmospheric phenols with an organic triplet excited state, 913 Environ. Sci. Technol., 48, 1049-1057, 2014.
- 914 Smith, J. D., Kinney, H., and Anastasio, C.: Aqueous benzene-diols react with an organic triplet 915 excited state and hydroxyl radical to form secondary organic aerosol, Phys. Chem. Chem. 916 Phys., 17, 10227-10237, 2015.
- 917 Sun, H. L., Biedermann, L., and Bond, T. C.: Color of brown carbon: A model for ultraviolet and visible light absorption by organic carbon aerosol, Geophys. Res. Lett., 34, L17813, 2007.
- Thompson, A. M.: The oxidizing capacity of the Earth's atmosphere: Probable past and future changes, Science, 256, 1157-1165, 1992.
- Tong, H., Arangio, A. M., Lakey, P. S., Berkemeier, T., Liu, F., Kampf, C. J., Brune, W. H., Pöschl, U., and Shiraiwa, M.: Hydroxyl radicals from secondary organic aerosol decomposition in water, Atmos. Chem. Phys., 16, 1761-1771, 2016.
- Tong, H., Lakey, P. S., Arangio, A. M., Socorro, J., Kampf, C. J., Berkemeier, T., Brune, W. H., Pöschl, U., and Shiraiwa, M.: Reactive oxygen species formed in aqueous mixtures of secondary organic aerosols and mineral dust influencing cloud chemistry and public health in the Anthropocene, Faraday Discuss., 200, 251-270, 2017.
- Tratnyek, P. G., and Hoigné, J.: Photo-oxidation of 2,4,6-trimethylphenol in aqueous laboratory solutions and natural waters: Kinetics of reaction with singlet oxygen, J. Photochem. Photobiol., A, 84, 153-160, 1994.
- Tsui, W. G., Rao, Y., Dai, H.-L., and McNeill, V. F.: Modeling photosensitized secondary organic aerosol formation in laboratory and ambient aerosols, Environ. Sci. Technol., 51, 7496-7501, 2017.
- 935 USGS: U.S. Geological Survey. Water Properties Dissolved Oxygen. Available at 936 https://water.usgs.gov/edu/dissolvedoxygen.html [last accessed: January 23, 2018], 2018.

- Varga, B., Kiss, G., Ganszky, I., Gelencsér, A., and Krivacsy, Z.: Isolation of water-soluble organic matter from atmospheric aerosol, Talanta, 55, 561-572, 2001.
- Wenk, J., Von Gunten, U., and Canonica, S.: Effect of dissolved organic matter on the
 transformation of contaminants induced by excited triplet states and the hydroxyl radical,
 Environ. Sci. Technol., 45, 1334-1340, 2011.
- Wenk, J., Eustis, S. N., McNeill, K., and Canonica, S.: Quenching of excited triplet states by
 dissolved natural organic matter, Environ. Sci. Technol., 47, 12802-12810, 2013.

948 949

950

955 956

957

- Wilkinson, F., Helman, W. P., and Ross, A. B.: Rate constants for the decay and reactions of the
 lowest electronically excited singlet-state of molecular-oxygen in solution an expanded
 and revised compilation, J. Phys. Chem. Ref. Data, 24, 663-1021, 1995.
 - Young, D. E., Kim, H., Parworth, C., Zhou, S., Zhang, X., Cappa, C. D., Seco, R., Kim, S., and Zhang, Q.: Influences of emission sources and meteorology on aerosol chemistry in a polluted urban environment: results from DISCOVER-AQ California, Atmos. Chem. Phys., 16, 5427-5451, 2016.
- Yu, L., Smith, J., Laskin, A., Anastasio, C., Laskin, J., and Zhang, Q.: Chemical characterization
 of SOA formed from aqueous-phase reactions of phenols with the triplet excited state of
 carbonyl and hydroxyl radical, Atmos. Chem. Phys., 14, 13801-13816, 2014.
 Yu, L., Smith, J., Laskin, A., George, K. M., Anastasio, C., Laskin, J., Dillner, A. M., and
 - Yu, L., Smith, J., Laskin, A., George, K. M., Anastasio, C., Laskin, J., Dillner, A. M., and Zhang, Q.: Molecular transformations of phenolic SOA during photochemical aging in the aqueous phase: competition among oligomerization, functionalization, and fragmentation, Atmos. Chem. Phys., 16, 4511-4527, 2016.
- Zepp, R. G., Wolfe, N. L., Baughman, G. L., and Hollis, R. C.: Singlet oxygen in natural waters, Nature, 267, 421-423, 1977.
- Zepp, R. G., Schlotzhauer, P. F., and Sink, R. M.: Photosensitized transformations involving
 electronic energy transfer in natural waters: role of humic substances, Environ. Sci.
 Technol., 19, 74-81, 1985.
- Zhou, H., Yan, S., Lian, L., and Song, W.: Triplet-state Photochemistry of Dissolved Organic
 Matter: Triplet-state Energy Distribution and Surface Electric Charge Conditions,
 Environ. Sci. Technol., 53, 2482–2490, 2019.
- Zhou, X., and Mopper, K.: Determination of photochemically produced hydroxyl radicals in seawater and freshwater, Mar. Chem., 30, 71-88, 1990.

Supporting Information for:

2	Photooxidants from Brown Carbon and Other Chromophores in
3	Illuminated Particle Extracts
4	Richie Kaur ¹ , Jacqueline R. Labins ¹ , Scarlett S. Helbock ¹ , Wenqing Jiang ² , Keith J
5	Bein ³ , Qi Zhang ² , Cort Anastasio ^{1,*}
6	¹ Department of Land, Air and Water Resources, University of California-Davis, One Shields Avenue,
7	Davis, CA 95616-8627, USA
8	² Department of Environmental Toxicology, University of California-Davis, One Shields Avenue, Davis,
9	CA 95616-8627, USA
10	³ Center for Health and the Environment, University of California-Davis, One Shields Avenue, Davis, CA
11	95616-8627, USA
12	
13	Correspondence to: C. Anastasio (<u>canastasio@ucdavis.edu</u>)
14	
15	Originally Submitted to Atmospheric Chemistry and Physics, 2 December 2018
16	Revised and Submitted on 23 April 2019

18 19	1. Text Sections	
20	S1. Hydroxyl radical measurements in PME3 and PME3D extracts	35
21	S2. OH sink measurements (k'_{OH}) in field blanks FB1 and FB2	
22	S3. Other oxidants in PM extracts	
23 24	S4. Impacts of mass transport and increasing organic concentration on estimates of aqueous photooxidant concentrations in ambien particles	
25	S5. Estimating triplet characteristics in particle extract PME3	50
26	S6. References	53
27		
28	2. Tables and Figures	
29	Table S1. Sample collection details and light absorption of particle extracts	4
30	Table S2. Chemical characteristics of particle extracts	
31	Table S3. Hydroxyl radical measurements	7
32	Table S4. Contributions of nitrite, nitrate and other sources to 'OH photoproduction	9
33	Table S5. Determination of chloride as an 'OH sink, following procedure of Anastasio and Newberg (2007)	10
34	Table S6. Contributions of nitrite, chloride and organics to k'_{OH}	11
35	Table S7. Singlet oxygen measurements	12
36	Table S8. Syringol loss kinetics	13
37	Table S9. Methyl jasmonate loss kinetics	14
38	Table S10. Second-order rate constants for reactions of syringol and methyl jasmonate with hydroxyl radical, singlet oxygen, and	
39	triplet excited states	
40	Table S11. Characteristics of model triplet species	
41	Table S12. Best triplet matches and best estimate triplet steady-state concentrations	17
42	Table S13. Measurements of triplet excited states of organic matter	
43	Table S14. Particle mass to water mass ratios in the PME3 extracts, typical fog drops, and particles	
44	Table S15. Photooxidant concentrations (formed <i>in situ</i>) in PME3D extracts and expected values in ambient particles	
45	Table S16. Gas- and aqueous-phase reaction rate constants for selected organic compounds with the major oxidants	
46	Table S17. Fate of selected organic compounds in fog and particles	
47	Figure S1. OH measurement in extract PME5.	
48	Figure S2. Singlet oxygen kinetic measurements in extract PME5 diluted 1:1 (volume : volume) with H ₂ O or D ₂ O	25
49	Figure S3. Top panel: Light absorbance by fog samples collected during 2011-12 in Davis, CA. Bottom panel: Mass absorption	
50	coefficient of DOC in the Davis fog samples.	26
51	Figure S4. Correlation between the rate of sunlight absorption (R_{abs}) in the 300-450 nm wavelength range and dissolved organic	27
52	carbon (DOC) for the fog samples and particle extracts (PME)	21

53	Figure S5. (Top) Ratio of pathlength-normalized absorbance for PME and fog samples with highest (black) and median (grey)
54	absorbances. (Bottom): Ratio of mass absorption coefficients of DOC in PME and fog samples with highest (black) and median (grey)
55	absorbances
56	Figure S6. (Top) Correlation between the rate of 'OH photoproduction due to sources other than nitrite and nitrate and the
57	concentration of dissolved organic carbon (DOC). (Bottom) Correlation between apparent pseudo-first order rate constant for loss of
58	OH due to organic sinks (obtained by subtracting inorganic contributions from the measured k'_{OH}) and DOC
59	Figure S7. Comparison of hydroxyl radical steady-state concentrations formed <i>in situ</i> in various atmospheric waters
60	Figure S8. Loss of probes for measuring triplet excited states: syringol (SYR) and methyl jasmonate (MeJA) in extract PME5 31
61	Figure S9. Winter-solstice-normalized pseudo-first-order rate constants (k'_{Probe}) for loss of syringol (top panel) and methyl jasmonate
62	
63	Figure S10. Dependence of rate of 'OH photoproduction (P_{OH} ; red circles, left y-axis) and rate constant for loss of 'OH due to natural
64	sinks (k' _{OH} ; blue squares, right y-axis) with PM mass/water mass ratio in three PME3D samples
65	Figure S11. Fate of five model organic compounds – syringol, methyl jasmonate, tyrosine, 1,2,4-butanetriol and 3-hydroxy-2,5-
66	bis(hydroxymethyl)furan – under fog (left of vertical dashed line) and PM (right of dashed line) conditions using an upper-bound
67	estimate for triplet concentrations in PM
68	Table S18. Determination of hydroxyl radical steady-state concentrations, [*OH], from results of the MBO experiments
69	Figure S12. Measured pseudo-first-order rate constant for loss of OH due to natural sinks (k'_{OH}) in various solutions using sodium
70	benzoate/benzoic acid and benzene as 'OH probes
71	Table S 19. Estimates of the organic sink of ${}^{1}O_{2}^{*}$ in aqueous particles at 1 μ g-PM/ μ g-H ₂ O
72	Figure S13. Change in triplet steady-state concentration with dissolved organic carbon concentration in the PME3D extracts 52
73	

Table S1. Sample collection details and light absorption of particle extracts

74

76

80

Sample ID	Collection Dates	Collection Times ^d	Average hourly PM _{2.5} concentration e (µg/m ³ -air)	α_{300}^{f} (cm ⁻¹)	Average Mass of PM extracted ^g	$R_{\rm abs}$ (300-450nm) h (10 ⁻⁶ mol-photons L ⁻¹ s ⁻¹)	$f_{ m Rabs~IN}$ $^{ m i}$	MAC _{DOC} (300 nm) ^j (10 ⁴ cm ² g ⁻¹ -C)	AAE ^k	Light Screening Factor ¹
Particle Extracts				•						
PME1*a	01/06/16 - 01/08/16	17:30 - 07:30 (N)	5.8 (2.1)	0.077	105 (16)	1.7	0.00080	2.6	6.8	0.98
PME2*a	12/18/15 - 12/20/15	17:30 - 07:30 (N)	15 (10)	0.100	269 (30)	1.8	0.0059	2.0	7.2	0.97
PME3 ^b	01/26/16 - 01/29/16	10:20 - 09:45 (C)	16 (11)	0.272	328 (19)	4.2	0.0076	1.3	7.9	0.93
PME4 ^b	12/16/15 - 12/18/15	17:30 - 07:30 (N)	20 (8)	0.567	350 (14)	12	0.0031	2.6	6.4	0.85
PME5 b	01/10/16 - 01/12/16	17:30 - 07:30 (N)	5.9 (3.4)	0.317	132 (11)	7.4	0.00080	2.6	6.2	0.91
PME6 b	01/23/16 - 01/26/16	17:30 - 07:30 (N)	6.8 (2.9)	0.584	174 (14)	13	0.00058	3.0	6.9	0.84
D1 5000 0 7 C				0.555	200 (04)					
PME3D0.5 °				0.556	323 (21)	8.8	0.0051	1.2	7.7	0.87
PME3D1.3 °				0.199	315 (23)	3.2	0.0071	1.3	7.6	0.95
PME3D2.5* a				0.103	331 (15)	1.7	0.0092	1.3	7.6	0.97
PME3D10 °				0.0263	347	0.42	0.0062	1.3	7.6	0.99
Averages (±σ)										
"Standard" (PME3-6)				0.44 (0.16)		9.1 (4.1)	0.0030 (0.0033)	2.4 (0.7)	6.8 (0.7)	
"Dilute" (PME1*- 2*,3D2.5*)				0.093 (0.014)		1.7 (0.1)	0.0053 (0.0042)	2.0 (0.6)	7.2 (0.4)	
Davis Fog ^m				0.094 (0.047)		1.8 (0.9)	0.0082 (0.0031)	1.3 (0.1)	6.6 (0.5)	
Test statistic ⁿ				0.021		0.035	0.061	0.013	0.56	
Field Blanks										
FB1 ^a	12/18/15	09:38 - 09:40		0.0025	17.8 (7.6)	0.024				
FB2 ^b	01/20/16	10:08 - 10:10		0.0037	24.9 (9.1)	0.022				

^a Samples extracted in 2.5 mL/filter square and referred to as the "dilute" extracts in the main text.

^b PME3-6 were extracted as 1 mL/filter square and are referred to as "standard" extracts in the main text.

c PME3D0.5, PME3D1.3 and PME3D10 are extracts of sample PME3 using varying extraction volumes per filter square, namely 0.5, 1.3 and 10 mL, respectively.
 d N = Night-time samples, collected from 17:30 on one day until 07:30 AM the next day; this was done for consecutive days on the same filter. C

^d N = Night-time samples, collected from 17:30 on one day until 07:30 AM the next day; this was done for consecutive days on the same filter. C = Continuous collection for the indicated number of days.

 ⁸¹ e Average (± 1σ) hourly PM_{2.5} concentration for each sampling period measured at the UC Davis sampling site by the California Air Resources
 82 Board as reported on the *i*ADAM online database (California Air Resources Board, 2018).

^{83 &}lt;sup>f</sup> Base-10 absorbance of the extract (in cm⁻¹) at 300 nm.

⁸⁴ g Average ($\pm 1\sigma$) mass of PM extracted from each filter square for a given sample.

h Rate of sunlight absorption by each extract in the 300 – 450 nm wavelength range (Eq. (2), main text).

Fraction of calculated sunlight absorption due to inorganic nitrogen (nitrite and nitrate) in each sample. Equations are in Kaur and Anastasio (2017).

⁸⁸ Mass absorption coefficient of dissolved organic species at 300 nm for each sample (Eq. (3), main text) in units of 10⁴ cm⁻² g⁻¹-C.

k Absorption Angstrom Exponent (AAE), calculated as the negative of the slope of a linear regression of the extract absorbance data between 300 and 450 nm versus the log of the wavelength: log(Abs_λ) = log(Abs₃₀₀)–AAE × log(λ), where λ is the wavelength and Abs_λ and Abs₃₀₀ are the absorbance values at λ and 300 nm, respectively.

92 Light-absorption-weighted internal screening factor, calculated as $S_{\lambda} = \frac{\sum[(1-10^{-\alpha}\lambda^l)\times I'_{\lambda}]}{\sum[(2.303\times\alpha_{\lambda}l)\times I'_{\lambda}]}$. In this equation, α_{λ} is the pathlength-normalized

absorbance of the extract at each wavelength, summed for the wavelength range in which light absorption by the extracts was the highest (280-350 nm); l is the pathlength of the quartz tube used for illuminating the extracts (0.4 cm); l'_{λ} is the actinic flux (mol-photons L⁻¹ s⁻¹) of the illumination system, calculated using the photon count of the illumination system measured using a TIDAS Photo Diode Array Spectrometer and the measured pseudo-first-order rate constant for loss of our chemical actinometer, 2-nitrobenzaldehyde. The numerator represents the actual rate of light absorption by all chromophores in the extract while the denominator is the estimated rate of light absorption in the extract assuming it is low light-absorbing. A value of 1.0 indicates no light screening (Smith et al., 2014; Rehorek and Seidel, 1989).

^m Average values previously measured in Davis fog samples (n = 4) (Kaur and Anastasio, 2017).

ⁿ Test statistic for comparison of standard PME and Davis fog averages: *p*-value for a two-tailed *t*-test for samples of unequal variance. Values below 0.05 are in bold.

Table S2. Chemical characteristics of particle extracts

Sample ID	DOC	$[NO_2^-]$	$[NO_3^-]$	$[SO_4^{2-}]$	[Cl ⁻]	[HCOO ⁻]	$[\mathrm{NH_4}^+]$	$[Na^{+}]$	$[K^{+}]$	[Ca ²⁺]	$[Mg^{2+}]$
	μM-C	μM	μΜ	μM	μM	μM	μΜ	μM	μΜ	μM	μM
Particle											
Extracts											
PME1*a	562	0.29	113	12.5	15.7	2.1	55.3	82.3	29.9	2.5	0.0
PME2*a	900	2.8	884	31.3	19.8	4.1	751	78.9	43.0	8.3	2.3
PME3 ^b	3610	10.2	2520	302	66.3	13.0	2580	343	171	22.1	3.3
PME4 ^b	4090	8.3	3290	91.1	69.6	21.4	2010	317	197	44.1	11.3
PME5 b	2350	3.8	375	22.9	36.7	10.9	287	287	76.7	9.8	2.2
PME6 b	3720	5.4	432	65.6	77.7	4.9	276	362	97.2	13.0	7.4
PME3D0.5 °	7132	18	4820	533	127	27	5052	681	342	53	6.4
PME3D1.3	2760	6.4	1830	216	48.2	10.5	1600	233	105	20.0	1.6
PME3D2.5 a	1400	4.1	1250	195	27.3	5.1	816	118	42.6	4.7	1.3
PME3D10	356	1.2	183	28.1	6.9	1.0	177	24.3	11.9	0.0	0.0
Averages (±σ)											
"Standard"	2440 (760)	(0(20)	1650	120 (124)	(2 ((17 0)	12.5	1290	227 (22)	126 (59)	22.2	(1 (4 1)
(PME3-6)	3440 (760)	6.9 (2.9)	(1480)	120 (124)	62.6 (17.9)	(6.8)	(1190)	327 (33)	136 (58)	(15.5)	6.1 (4.1)
"Dilute"											
(PME1*-	953 (419)	2.4 (1.9)	749 (580)	80 (101)	20.9 (5.9)	3.8 (1.5)	541 (420)	93.2 (21.9)	38.5 (7.4)	5.2 (2.9)	1.2 (1.1)
2*,3D2.5*)											
Davis Fog	1240 (560)	3.4 (6.1)	1080 (630)	120 (84)	22.9 (13.0)	5.1 (2.6)	1070 (550)	_ d	3.5 (1.9)	4.2 (1.1)	1.4 (0.4)
Test statistic ^e	0.0042	0.35	0.51	0.98	0.013	0.11	0.75	ı	0.019	0.10	0.11
Field Blanks											
FB1 ^a	78.9	0	4.5	0.8	9.0	1.1	3.1	63.8	8.3	1.4	0.0
FB2 ^b	244	0	1.1	0.4	6.1	9.0	12.3	143.5	10.9	3.4	0.0
MQ	< DT	< DT	< DT	< DL	< DL	< DL	< DL	1.8	< DL	< DL	< DL

^a Samples extracted in 2.5 mL/filter square and referred to as the "dilute" extracts in the main text.

b Samples extracted in 1mL/filter square and are referred to as "standard" extracts in the main text.

^c DOC and IC values for sample PME3D0.5 were not measured due to a shortage of sample; instead, they were estimated by extrapolating the linear trends between these values and concentration factors for the other PME3 samples, namely, PME3, PME3D1.3, PME3D2.5 and PME3D10.

¹⁰⁸ description of Sodium could not be measured in the 2011 Davis fog samples due to high background sodium content .

^e Test statistic for comparison of standard PME and Davis fog averages: *p*-value for a two-tailed *t*-test for samples of unequal variance. Values below 0.05 are in bold.

Table S3. Hydroxyl radical measurements

111

Sample ID	$P_{\rm OH}^{\ a}$ $10^{-10}{\rm M~s^{-1}}$	$P_{ m OH}^{^a}$ $\mu{ m M~h}^{-1}$	$\frac{k'_{ m OH}}{10^6}^{ m b}$	τ _{OH} ^c μs	[*OH] ^d 10 ⁻¹⁶ M	$10^4 \times \Phi_{ m OH}^{ m f}$	$k'_{\rm OH,org} / [{ m DOC}]^{ m g}$ 10 ⁸ L (mol-C) ⁻¹ s ⁻¹
Particle Extracts		,		•			
PME1*	1.0 (0.1)	0.37 (0.04)	0.63 (0.01)	1.6 (0.1)	1.7 (0.2)	0.62 (0.06)	11.1 (0.2)
PME2*	2.0 (0.2)	0.71 (0.07)	0.44 (0.04)	2.3 (0.2)	4.5 (0.6)	1.1 (0.1)	4.6 (0.4)
PME3	14.7 (0.3)	5.3 (0.1)	1.9 (0.4)	0.54 (0.13)	7.9 (1.9) ^e	3.5 (0.1)	4.9 (1.2)
PME4	14 (2)	5.2 (0.6)	2.3 (0.2)	0.43 (0.03)	6.3 (0.6)	1.2 (0.1)	5.4 (0.4)
PME5	4.6 (0.5)	1.7 (0.2)	1.6 (0.1)	0.62 (0.03)	2.8 (0.3)	0.63 (0.07)	6.8 (0.4)
PME6	13 (3)	4.8 (1.0)	4.0 (0.8)	0.25 (0.05)	3.3 (0.3)	1.1 (0.2)	11 (2)
PME3D0.5					7.3 (1.8) ^e		
PME3D1.3					3.0 (0.8) ^e		
PME3D2.5*	3.1 (0.1)	1.1 (0.02)	0.94 (0.29)	1.1 (0.3)	3.3 (1.0) ^e	1.86 (0.03)	6.4 (2.0)
PME3D10	0.47 (0.04)	0.17 (0.01)	0.071(0.031)	14 (6)	6.6 (2.8) ^e	1.1 (0.1)	1.7 (0.7)
Averages (±σ)							
"Standard" (PME3-6)	12 (5)	4.2 (1.7)	2.5 (1.1)	0.46 (0.16)	5.1 (2.4)	1.6 (1.3)	6.9 (2.6)
"Dilute" (PME1*- 2*,3D2.5*)	2.0 (1.0)	0.73 (0.37)	0.67 (0.63)	1.6 (0.6)	3.2 (1.4)	1.2 (0.6)	7.4 (3.4)
Davis Fog	3.5 (1.0)	1.3 (0.3)	0.87 (0.31)	1.2 (0.4)	4.2 (0.7)	2.4 (1.7)	7.5 (3.2)
Test statistic h	0.039	0.039	0.058	0.019	0.51	0.47	0.79
				·			
Field Blanks i							
FB1 (dilute)	≤ 0.012	≤ 0.045	0.34 (0.04)	3.0 (0.4)			
FB2 (standard)	≤ 0.012	≤ 0.042	0.27 (0.01)	3.8 (0.2)			

Listed uncertainties (in parentheses) are ± 1 standard error from the errors in inverse plot $(1/R_p^*)$ vs. 1/[Benzene]) parameters, except for the averages ($\pm 1\sigma$)

All equations used for these calculations are discussed in Kaur and Anastasio (2017) unless otherwise stated.

* Samples extracted in 2.5 mL/filter square and referred to as the "dilute" extracts in the main text.

116 ^a Davis winter solstice-normalized rate of OH photoproduction.

b Apparent pseudo-first rate constant for destruction of OH due to natural sinks.

118 ° Lifetime of 'OH, calculated as $1/k'_{OH}$.

d Winter solstice-normalized steady-state concentration of 'OH.

COH concentrations in PME3 and PME3D extracts were measured using MBO as a probe, corrected for loss due to quenching by MBO (discussed in Sect. S1). k OH for these samples was calculated as POH / [OH].

122 f Apparent quantum yield of OH during simulated sunlight illumination, calculated as $\Phi_{OH} = P_{OH} / R_{abs.}$

123 g Ratio of $k'_{OH,org}$ (rate constant for loss of OH due to organics only; Table S6) to the DOC concentration.

- 124 h Test statistic for comparison of standard PME and Davis fog averages: *p*-value for a two-tailed *t*-test for samples of unequal variance. Values below 0.05 are in bold.
- Blanks were analyzed by adding 1.5 mM benzene to an aliquot of the blank. Very little phenol formation was observed after 200 minutes of illumination in both blanks, which was used to calculate the upper limit P_{OH}.

Table S4. Contributions of nitrite, nitrate and other sources to 'OH photoproduction

Sample ID	$f_{ m POH,NO2}$ — $^{ m a}$	f _{РОН,NО3} − ^b	$f_{ m POH,Other}^{ m \ c}$
Particle Extracts			
PME1*	0.072 (0.010)	0.15 (0.02)	0.78 (0.02)
PME2*	0.36 (0.05)	0.63 (0.09)	0.011 (0.010)
PME3	0.18 (0.02)	0.24 (0.02)	0.58 (0.03)
PME4	0.15 (0.02)	0.32 (0.05)	0.53 (0.05)
PME5	0.21 (0.03)	0.11 (0.02)	0.67 (0.04)
PME6	0.11 (0.03)	0.046 (0.011)	0.85 (0.03)
PME3D0.5		-	-
PME3D1.3	-	-	-
PME3D2.5*	0.35 (0.04)	0.57 (0.06)	0.084 (0.068)
PME3D10	0.67 (0.08)	0.55 (0.07)	-0.22 (0.11) ^d
Averages (±σ)			
"Standard" (PME3-6)	0.16 (0.05)	0.18 (0.12)	0.66 (0.14)
"Dilute" (PME1*- 2*,3D2.5*)	0.26 (0.16)	0.45 (0.26)	0.29 (0.42)
Davis Fog	0.24 (0.40)	0.46 (0.29)	0.41 (0.41)

Listed uncertainties (in parentheses) are ± 1 standard error calculated from propagating errors in individual terms, except for the averages ($\pm 1\sigma$).

^{*} Samples extracted in 2.5 mL/filter square and referred to as the "dilute" extracts in the main text.

^a Fraction of OH photoproduction rate attributable to nitrite. Calculated as $(j_{\text{NO2}\rightarrow\text{OH}}\times[\text{NO}_2^-])/P_{\text{OH}}$ where the numerator is the rate of OH photoproduction due to nitrite $(P_{\text{OH},\text{NO2}})$, and is the product of the aqueous photolysis rate constant under Davis winter-solstice sunlight, $j_{\text{NO2}^-\rightarrow\text{OH}}=2.6\times10^{-5}\text{ s}^{-1}$ (Anastasio and McGregor, 2001), and the molar concentration of NO_2^- in each sample.

^b Fraction OH photoproduction rate attributable to nitrate. Calculated using an equation analogous to $f_{POH,NO2-}$, using aqueous nitrate photolysis rate constant, $j_{NO3^- \to OH} = 1.4 \times 10^{-7} \text{ s}^{-1}$ (Anastasio and McGregor, 2001) and molar concentration of NO_3^- in each sample.

^c Fraction of OH photoproduction due to non-nitrite and –nitrate sources; calculated as $(P_{OH} - P_{OH,NO2} - P_{OH,NO3}) / P_{OH}$.

^d f_{POH,other} is negative for PME3D10 indicating that the total rate of ^oOH photoproduction is over-predicted using the measured molar NO₂⁻ and NO₃⁻ concentrations.

Table S5. Determination of chloride as an 'OH sink, following procedure of Anastasio and Newberg (2007)

Sample ID	Measured k'_{OH}^{c} s ⁻¹	[Cl ⁻] ^d M	[H ⁺] ^e M	$f_{ ext{Cl-re-formed}}^{ ext{ f}}$	k' _{OH,Cl} - ^g s ⁻¹	$f_{ m kOH,Cl}$ h
PME1*a	6.3E+05	1.6E-05	6.31E-05	0.9997828	1.5E+01	2.3E-05
PME2* a	4.4E+05	2.0E-05	6.31E-05	0.99978	1.8E+01	4.2E-05
PME3	1.9E+06	6.6E-05	6.31E-05	0.99978	6.2E+01	3.3E-05
PME4	2.3E+06	7.0E-05	6.31E-05	0.99978	6.5E+01	2.8E-05
PME5	1.6E+06	3.7E-05	6.31E-05	0.999783	3.4E+01	2.1E-05
PME6	4.0E+06	7.8E-05	6.31E-05	0.99978	7.3E+01	1.8E-05
PME3D2.5* a	9.4E+05	2.7E-05	6.31E-05	0.99978	2.5E+01	2.7E-05
PME3D10 ^b	7.1E+04	6.9E-06	6.31E-05	0.999783	6.4E+00	9.0E-05

^a Samples PME1*, PME2*, PME3D2.5 were extracted in 2.5 mL Milli-Q per filter square, and are referred to as "dilute extracts" in the main text.

150 (1) ${}^{\bullet}OH + Cl^{-} \rightarrow HOCl^{\bullet-} k_1 = 4.3E + 09 M^{-1} s^{-1}$

139

141

143

144

- 151 (2) $HOCl^{\bullet-} + Cl^{-} \rightarrow {}^{\bullet}Cl_{2}^{-} + OH^{-}, k_{2} = 1.0E + 04 M^{-1}s^{-1}$
- 152 (3) $HOCl^{\bullet-} + H^{+} \rightarrow Cl^{\bullet} + H_{2}O, k_{3} = 2.1E+10 \text{ M}^{-1}\text{s}^{-1}$
- 153 (4) HOCl^{•-} \rightarrow Cl⁻ + •OH, $k_4 = 6.4$ E+09 M⁻¹s⁻¹

^b PME3D10 was extracted in 10 mL Milli-Q per filter square.

^c Measured pseudo-first order rate constant for loss of OH.

^d Measured chloride concentrations in the extracts.

^e Hydrogen ion concentration. Since the extracts were acidified to pH 4.2, this value is constant across all extracts.

¹⁴⁵ Fraction of Cl⁻ reacting with OH that ends up back as Cl⁻ and OH. Values are calculated based on the reactions 1-4 below and the equation f_{Cl}
146 f_{Cl}
147 re-formed = f_{Cl}
148 f_{Cl}
149 re-formed = f_{Cl}
149 f_{Cl}
140 f_{Cl}
150 f_{Cl}
160 f_{Cl}
170 $f_$

¹⁴⁷ Rate constant for loss of OH due to Cl based on the fraction of reformed Cl, calculated as $k'_{OH,Cl} = (1 - f_{Cl re-formed}) \times k_1$

^h Fraction of measured *k*'_{OH} due to chloride.

Table S6. Contributions of nitrite, chloride and organics to k'_{OH}

Sample ID	Measured k'_{OH}^{c}	$k'_{\text{OH,NO2}}$ - d s ⁻¹	$k'_{\text{OH,CI}}$ $\stackrel{\text{e}}{\overset{\text{o}}}{\overset{\text{o}}{\overset{\text{o}}{\overset{\text{o}}{\overset{\text{o}}{\overset{\text{o}}{\overset{\text{o}}{\overset{\text{o}}}{\overset{\text{o}}{\overset{\text{o}}{\overset{\text{o}}{\overset{\text{o}}{\overset{\text{o}}{\overset{\text{o}}{\overset{\text{o}}{\overset{\text{o}}{\overset{\text{o}}{\overset{\text{o}}}{\overset{\text{o}}{\overset{\text{o}}{\overset{\text{o}}}{\overset{\text{o}}{\overset{\text{o}}}{\overset{\text{o}}}{\overset{\text{o}}}{\overset{\text{o}}}{\overset{\text{o}}}{\overset{\text{o}}}{\overset{\text{o}}}{\overset{\text{o}}}{\overset{\text{o}}}}}}{\overset{\text{o}}{\overset{\text{o}}{\overset{\text{o}}{\overset{\text{o}}{\overset{\text{o}}{\overset{\text{o}}{\overset{\text{o}}{\overset{\text{o}}{\overset{\text{o}}{\overset{\text{o}}{\overset{\text{o}}}{\overset{\text{o}}}{\overset{\text{o}}}{\overset{\text{o}}}}}}}{\overset{\text{o}}{\overset{\text{o}}{\overset{\text{o}}{\overset{\text{o}}{\overset{\text{o}}}{\overset{\text{o}}}{\overset{\text{o}}}}}}{\overset{\text{o}}}}}{\overset{\overset{\text{o}}}{\overset{\text{o}}}}}}{\overset{\overset{\text{o}}}{\overset{\text{o}}}}}}{\overset{\overset{\text{o}}{\overset{\text{o}}}{\overset{\text{o}}}}}}{\overset{\overset{o}}{\overset{\text{o}}}}{\overset{\overset{o}}{\overset{o}}}}}}}}}}$	$k_{\mathrm{OH,org}}^{\mathrm{rot}}$ s	$f_{ m kOH,NO2}$ – $^{ m g}$	$f_{ m kOH,org}$
PME1* a	6.3E+05	2.9E+03	1.5E+01	6.2E+05	0.0046	1.0
PME2* a	4.4E+05	2.7E+04	1.8E+01	4.1E+05	0.063	0.94
PME3	1.9E+06	1.0E+05	6.2E+01	1.8E+06	0.055	0.95
PME4	2.3E+06	8.3E+04	6.5E+01	2.2E+06	0.036	0.96
PME5	1.6E+06	3.8E+04	3.4E+01	1.6E+06	0.023	0.98
PME6	4.0E+06	5.4E+04	7.3E+01	4.0E+06	0.013	0.99
PME3D2.5* a	9.4E+05	4.1E+04	2.5E+01	9.0E+05	0.044	0.96
PME3D10 ^b	7.1E+04	1.2E+04	6.4E+00	5.9E+04	0.16	0.83

^a Samples PME1*, PME2*, and PME3D2.5* were extracted in 2.5 mL Milli-Q per filter square, and are referred to as "dilute extracts" in the main text.

154

160

161

162

163

164

165

166

167

168

169

170

171

172

173

174

- (1) $CO_2 \leftrightarrow CO_2$. H_2O (aq), $K_{H^*} = 3.4E-02$ M atm⁻¹ (Physical Henry's law constant)
- (2) $CO_2.H_2O$ (aq) $\leftrightarrow H^+ + HCO_3^-, K_{a1} = 4.3E-07 M (pKa1 = 6.3)$
- (3) $HCO_3^- \leftrightarrow H^+ + CO_3^{2-}, K_{a2} = 4.7E-11 \text{ M } (pKa2 = 10.3)$
- Thus, the contributions of HCO_3^- and CO_3^{2-} to measured k'_{OH} in all PME samples should be negligible.

b PME3D10 was extracted in 10 mL Milli-Q per filter square. All other extracts were extracted in 1.0 mL Milli-Q per filter square (standard extracts).

^c Measured pseudo-first order rate constant for loss of *OH (Table S3).

^d Pseudo-first order rate constant for loss of OH due to nitrite. Value is calculated as $k'_{\text{OH,NO2}}$ = $(k_{\text{OH+NO2-}} \times [\text{NO}_2^-])$ where $k_{\text{OH+NO2-}} = 1.1 \times 10^{10} \text{ M}^- 1 \text{ s}^{-1}$ (Barker et al., 1970).

^e Pseudo-first order rate constant for loss of ^oOH due to chloride. Value is calculated using the reaction between ^oOH and Cl⁻ corrected for the fraction of the initial product HOCl⁻ that fragments to reform ^oOH and Cl⁻, as discussed in Table S5 and Anastasio and Newberg (2007).

^f Calculated pseudo-first-order rate constant for loss of ^oOH due to organics, determined by subtracting the contribution of nitrite from the measured k'_{OH} . Contributions to k'_{OH} from common inorganic ions, including sulfate, nitrate, chloride, bicarbonate/carbonate (see footnote h below), and ammonium are negligible.

^g Fraction of measured *k*'_{OH} due to nitrite.

^h Fraction of measured OH sink due to organic species, estimated by subtracting the contributions due to nitrite from the measured value of k'_{OH} .

¹ The upper bound of the fraction of the measured k'_{OH} due to bicarbonate (HCO₃⁻) and carbonate (CO₃²⁻) was calculated to be 1.1×10^{-6} based on using the sample pH of 4.2 and assuming equilibrium with 400 ppm of atmospheric CO₂. This fraction was calculated based on the CO₂ equilibria 1-3 below (Seinfeld and Pandis, 2012), $k_{OH+HCO3}=1 \times 10^7 \text{ M}^{-1}\text{s}^{-1}$, and $k_{OH+CO3}=4 \times 10^8 \text{ M}^{-1}\text{s}^{-1}$ (Buxton et al., 1988b).

177 **Table S7.** Singlet oxygen measurements

Sample ID	P_{1O2*}^{a}	$P_{102*}^{\ a}$	$[{}^{1}O_{2}^{*}]^{b}$	f _{FFA,1O2} c	$10^2 \times \Phi_{102*}{}^{d}$
•	10^{-7} M s^{-1}	$\mu \mathrm{M} \; \mathrm{h}^{-1}$	$10^{-12} \mathrm{M}$,	
Particle Extracts		·			
PME1*	0.36 (0.04)	131 (15)	0.16 (0.02)	0.51 (0.08)	2.2 (0.2)
PME2*	0.68 (0.06)	246 (20)	0.31 (0.03)	0.72 (0.07)	3.8 (0.3)
PME3	2.4 (0.2)	851 (81)	1.1 (0.1)	1.1 (0.1)	5.7 (0.5)
PME4	4.2 (0.4)	1515 (135)	1.9 (0.2)	1.0 (0.1)	3.4 (0.3)
PME5	2.8 (0.2)	1000 (59)	1.3 (0.1)	1.2 (0.1)	3.8 (0.2)
PME6	4.8 (0.3)	1719 (114)	2.2 (0.1)	1.1 (0.1)	3.8 (0.3)
PME3D0.5	3.9 (0.4)	1413 (138)	1.8 (0.2)	0.79 (0.10)	4.5 (0.4)
PME3D1.3	1.1 (0.1)	414 (40)	0.52 (0.05)	0.68 (0.07)	3.6 (0.3)
PME3D2.5*	0.55 (0.03	198 (11)	0.25 (0.01)	0.61 (0.04)	3.3 (0.2)
PME3D10	0.14 (0.02)	50.8 (6.0)	0.064 (0.008)	0.59 (0.09)	3.3 (0.4)
Average (±σ)					
"Standard" (PME3-6)	3.5 (1.1)	1271 (412)	1.6 (0.5)	1.1 (0.1)	4.2 (1.0)
"Dilute" (PME1*-2*,3D2.5*)	0.53 (0.16)	192 (58)	0.24 (0.07)	0.61 (0.11)	3.1 (0.8)
Davis Fog	0.51 (0.14)	183 (49)	0.23 (0.06)	1.4 (0.8)	3.8 (3.1)
Test statistic ^f	0.0064	0.0064	0.0064		0.98
Field Blanks ^e					
FB1 (dilute)	≤ 0.076	≤ 27	≤ 0.0034		
FB2 (standard)	≤ 0.069	<u>≤</u> 25	<u>≤</u> 0.0031		

Listed uncertainties are ± 1 standard error unless otherwise stated.

184

All equations involved in the technique are discussed in Kaur and Anastasio (2017).

^{*} Samples extracted in 2.5 mL/filter square and referred to as the "dilute" extracts in the main text.

^a Davis winter solstice-normalized rate of ¹O₂* formation.

b Davis winter solstice-normalized steady-state concentration of ${}^{1}O_{2}^{*}$.

^c Fraction of probe FFA lost due to ¹O₂*.

d Apparent quantum yield of ${}^{1}O_{2}$ *, calculated as Φ_{1O2} * = P_{1O2} / $R_{abs.}$

e Blanks were analyzed by measuring FFA loss in undiluted blanks. This is an upper bound determined by ascribing all FFA loss to ${}^{1}O_{2}^{*}$.

186 Test statistic for comparison of standard PME and Davis fog averages: *p*-value for a two-tailed *t*-test for samples of unequal variance. Variance.

f Test statistic for comparison of standard PME and Davis fog averages: *p*-value for a two-tailed *t*-test for samples of unequal variance. Values below 0.05 are in bold.

Table S8. Syringol loss kinetics

188

192

194

195

198 199

Sample ID	k' _{SYR} a	$ au_{ m SYR}^{\;\; m b}$	k' _{SYR,OH} c	k' _{SYR,1O2} d	k' _{SYR,3C*} e	$f_{\rm SYR,3C^*}{}^{\rm f}$
	$10^{-5} \mathrm{s}^{-1}$	h	$10^{-5} \mathrm{s}^{-1}$	$10^{-5} \mathrm{s}^{-1}$	$10^{-5} \mathrm{s}^{-1}$	
Particle Extracts						
PME1*	12 (1)	2.3 (0.3)	0.43 (0.04)	0.59 (0.07)	11 (1)	0.92 (0.15)
PME2*	14 (2)	2.0 (0.3)	1.2 (0.1)	1.1 (0.09)	11 (2)	0.83 (0.17)
PME3	33 (1)	0.85 (0.03)	2.1 (0.5)	3.9 (0.4)	27 (1)	0.82 (0.06)
PME4	69 (8)	0.40 (0.04)	1.6 (0.2)	6.9 (0.6)	61 (8)	0.88 (0.15)
PME5	35 (2)	0.80 (0.04)	0.74 (0.07)	4.5 (0.3)	29 (2)	0.85 (0.06)
PME6	37 (3)	0.74 (0.05)	0.85 (0.09)	7.8 (0.5)	24 (3)	0.77 (0.09)
PME3D0.5	48 (3)	0.58 (0.04)	1.9 (0.5)	6.4 (0.6)	40 (3)	0.83 (0.08)
PME3D1.3	26 (2)	1.1 (0.1)	0.78 (0.21)	1.9 (0.2)	24 (2)	0.90 (0.11)
PME3D2.5*	15 (2)	1.9 (0.3)	0.86 (0.26)	0.90 (0.05)	13 (2)	0.88 (0.19)
PME3D10	3.6 (0.4)	7.7 (0.8)	1.7 (0.7)	0.23 (0.03)	1.6 (0.8)	0.46 (0.24)
Average (±σ)						
"Standard" (PME3-6)	43 (17)	0.70 (0.20)	1.3 (0.7)	5.8 (1.9)	36 (16)	0.83 (0.05)
"Dilute" (PME1*-						
2*,3D2.5*)	14 (1)	2.0 (0.2)	0.82 (0.37)	0.87 (0.26)	12(1)	0.88 (0.04)
Davis Fog	16 (11)	2.4 (1.4)	1.1 (0.2)	0.83 (0.22)	14 (11)	0.85 (0.06)
Test statistic ^g	0.040					
Field Blanks						
FB1 (dilute)	1.3 (0.2)	22 (3)	·		·	
FB2 (standard)	0.95 (0.07)	29 (2)	<u>-</u>		·	

Listed uncertainties are ± 1 standard error unless otherwise stated.

Bimolecular rate constants are given in Table S10.

193 b Lifetime of syringol, calculated as $1/k'_{SYR}$.

^{*} Samples extracted in 2.5 mL/filter square and referred to as the "dilute" extracts in the main text.

^a Davis winter-solstice-normalized value of the measured pseudo-first-order rate constant for loss of syringol (SYR).

^c Pseudo-first-order rate constant for loss of SYR due to hydroxyl radical, calculated as $k'_{\text{SYR,OH}} = k_{\text{SYR+OH}} \times [\text{OH}]$.

^d Pseudo-first-order rate constant for loss of SYR due to singlet oxygen, calculated as $k'_{SYR,102} = k_{SYR+102} \times [^{1}O_{2}*]$.

e Pseudo-first-order rate constant for loss of SYR due to triplet excited states, calculated as $k'_{SYR,3C^*} = k'_{SYR} - (k'_{SYR,0H} + k'_{SYR,102})$.

¹⁹⁷ Fraction of SYR loss due to triplets, calculated as $k'_{SYR,3C^*} / k'_{SYR}$.

^g Test statistic for comparison of standard PME and Davis fog averages: *p*-value for a two-tailed *t*-test for samples of unequal variance. Values below 0.05 are in bold.

Table S9. Methyl jasmonate loss kinetics

200

202

203

206

207

211

Sample ID	k' _{MeJA} a	$ au_{ m MeJA}^{ m \ b}$	k' _{MeJA,OH} c	k' _{MeJA,1O2} d	k' _{MeJA,3C*} e	$f_{ m MeJA,3C^*}{}^{ m f}$
	$10^{-5} \mathrm{s}^{-1}$	h	$10^{-5} \mathrm{s}^{-1}$	$10^{-5} \mathrm{s}^{-1}$	$10^{-5} \mathrm{s}^{-1}$	
Particle Extracts						
PME1*	0.98 (0.13)	28 (4)	0.11 (0.01)	0.099 (0.010)	0.77 (0.13)	0.79 (0.17)
PME2*	1.1 (0.1)	26 (1)	0.30 (0.04)	0.19 (0.02)	0.59 (0.07)	0.55 (0.07)
PME3	2.4 (0.2)	12 (1)	0.53 (0.13)	0.64 (0.06)	1.2 (0.2)	0.51 (0.10)
PME4	3.5 (0.4)	7.9 (0.8)	0.42 (0.04)	1.1 (0.1)	2.0 (0.4)	0.56 (0.12)
PME5	1.7 (0.2)	16 (2)	0.19 (0.02)	0.76 (0.04)	0.79 (0.18)	0.45 (0.11)
PME6	2.7 (0.2)	10(1)	0.22 (0.02)	1.3 (0.1)	1.2 (0.2)	0.44 (0.08)
PME3D0.5	4.7 (0.5)	5.9 (0.7)	0.49 (0.12)	1.1 (0.1)	3.1 (0.6)	0.67 (0.14)
PME3D1.3	2.6 (0.2)	11 (1)	0.20 (0.05)	0.31 (0.03)	2.1 (0.3)	0.80 (0.12)
PME3D2.5*	1.8 (0.2)	16 (2)	0.22 (0.07)	0.15 (0.01)	1.4 (0.2)	0.79 (0.15)
PME3D10	0.67(0.09)	42 (5)	0.44 (0.19)	0.038 (0.005)	0.19 (0.21)	0.28 (0.31)
Average $(\pm \sigma)$						
"Standard" (PME3-6)	2.6 (0.7)	11 (3)	0.34 (0.16)	0.96 (0.31)	1.3 (0.5)	0.49 (0.05)
"Dilute" (PME1*-						
2*,3D2.5*)	1.3 (0.4)	23 (7)	0.21 (0.10)	0.15 (0.04)	0.92 (0.42)	0.71 (0.14)
Davis Fog	0.90 (0.12)	31 (4)	0.28 (0.05)	0.14 (0.04)	0.48 (0.17)	0.53 (0.13)
Test statistic ^g	0.018					
Field Blanks						
FB1 (dilute)	0.17 (0.2)	160 (18)				
FB2 (standard)	0.27 (0.08)	104 (31)				

Listed uncertainties are ± 1 standard error unless otherwise stated.

Bimolecular rate constants are given in Table S10.

^{*} Samples extracted in 2.5 mL/filter square and referred to as the "dilute" extracts in the main text.

^a Davis winter-solstice-normalized measured pseudo-first-order rate constant for loss of methyl jasmonate (MeJA).

 ^a Davis winter-solstice-normalized measured pseudo-fi
 ^b Lifetime of methyl jasmonate, calculated as 1/k'_{MeJA}.

^c Pseudo-first-order rate constant for loss of MeJA due to hydroxyl radical, calculated as $k'_{\text{MeJA,OH}} = k_{\text{MeJA+OH}} \times [\text{OH}]$.

^d Pseudo-first-order rate constant for loss of MeJA due to singlet oxygen, calculated as $k'_{\text{MeJA},102} = k_{\text{MeJA}+102} \times [\bar{^{1}}O_{2}*]$.

e Pseudo-first-order rate constant for loss of MeJA due to triplet excited states, calculated as $k'_{\text{MeJA},3C^*} = k'_{\text{MeJA}} - (k'_{\text{MeJA},OH} + k'_{\text{MeJA},1O2})$.

 ²⁰⁹ fraction of MeJA loss due to triplets, calculated as k'_{MeJA,3C*} / k'_{MeJA}.
 210 g Test statistic for comparison of standard PME and Davis fog average

g Test statistic for comparison of standard PME and Davis fog averages: p-value for a two-tailed t-test for samples of unequal variance. Values below 0.05 are in bold.

Table S10. Second-order rate constants for reactions of syringol and methyl jasmonate with hydroxyl radical, singlet oxygen, and triplet excited states

Oxidants	$k_{ m SYR+Oxidant}$ $10^9~{ m M}^{-1}~{ m s}^{-1}$	Reference	$k_{ m MeJA+Oxidant} \ 10^8 { m M}^{-1} { m s}^{-1}$	Reference	
•он	26	O'Neill and Steenken (1977)	67 (± 3)	Richards-Henderson et al. (2014a)	
¹ O ₂ *	0.0036	Tratnyek and Hoigne (1991a)	$0.0060 \ (\pm 0.0007)$	Richards-Henderson et al. (2014b)	
Model Triplets (³ C*)					$k_{ m SYR+3C}*/k_{ m MeJA+3C}*$
³ 2AN*	1.9 (± 0.1)	Kaur and Anastasio (2018)	0.19 (± 0.07)	Kaur and Anastasio (2018)	100 (± 37)
³ 3MAP*	3.8 (± 0.6)	Kaur and Anastasio (2018)	1.2 (± 0.3)	Richards-Henderson et al. (2014b)	32 (± 9)
³DMB*	3.5 (± 0.8)	Smith et al. (2015)	4.1 (± 1.6)	Richards-Henderson et al. (2014b)	8.5 (± 3.8)
³ BP*	8.5 (± 1.6)	Kaur and Anastasio (2018)	51 (± 9)	Kaur and Anastasio (2018)	1.7 (± 0.4)

Listed uncertainties are ± 1 standard error.

^a Ratio of the bimolecular rate constants for reaction of a given model triplet with syringol (SYR) and methyl jasmonate (MeJA).

Table S11. Characteristics of model triplet species

Model Triplet	E _T ^a (kJ mol ⁻¹)	E ⁰ *(³ C*/C*-) b (V)	$k_{\rm O2+3C*}^{\rm c}$ (10 ⁹) $M^{-1}s^{-1}$	$f_{\Delta}^{}$ d
³ 2AN*	249	1.10	2.5	0.81 (C ₆ H ₆)
³ 3MAP*	303	1.64	3.3	$0.33 (C_6H_6)$
³ DMB*	298 (estimated) ^e	-	-	< 0.61 (MeOH) (estimated) ^e
³ BP*	288	1.67	2.6	0.35 (C ₆ H ₆)

- All values from Canonica et al. (Canonica et al., 2000) and Wilkinson et. al. (Wilkinson et al., 1993)
- 218 a Triplet state energy $(T_1 \rightarrow S_0)$.

216

217

220221

222

223

224225

- 219 b One-electron reduction potential for the triplet/triplet radical anion pair.
 - ^c Bimolecular rate constant for quenching of triplet by molecular O_2 . To calculate rates of triplet photoformation (described in the main text), an average value of $2.8 (\pm 0.4) \times 10^9 \, \text{M}^{-1} \text{s}^{-1}$ is used.
 - ^d Yield of singlet oxygen from quenching of model triplet species by O_2 . The solvent used in the determination is indicated in parentheses. Including the upper-bound value of 0.61 for ³DMB* (discussed in footnote *e*), the average value of f_{Δ} for the model triplets is 0.53 (± 0.23).
 - ^e Since the E_T and f_{Δ} values for ³DMB* are not available, values for benzaldehyde (Hunter, 1970; Wilkinson et al., 1993) are used as estimates. The f_{Δ} value is an upper-bound estimate.

Table S12. Best triplet matches and best estimate triplet steady-state concentrations

		Mole-fra	actions of Be	est Triplet M	atches b	Bimolecular	Bimolecular rate constants (M ⁻¹ s ⁻¹)			Triplet Steady-State Concentration			
		111010 111	ections of Be	st Implet ivi	accines	$\chi_{3C1^*} \times k_{Prob}$	_{e+3C1*} + χ _{3C2*} >	$\times k_{\text{Probe+3C2*}}^{\text{c}}$	$(10^{-14} \mathrm{M})$				
Sample ID	k' _{SYR,3C*} / k' _{MeJA,3C*} a	³ 2AN*	³ 3MAP*	³ DMB*	³ BP*	SYR	MeJA	SYR/MeJA Ratio	$\sum [^{3}C_{i}^{*}]_{SYR}^{d}$	$\sum [^3C_i^*]_{MeJA}^e$	$\sum [{}^{3}C_{i}^{*}]$ (± 1S.E.) Best Estimate f,g		
PME1*	15 (3)		0.55	0.45		3.7E+09	2.5E+08	15	3.1	3.1	3.1 (1.2)		
PME2*	20 (4)		0.76	0.24		3.7E+09	1.9E+08	20	3.1	3.1	3.1 (1.0)		
PME3	20 (4)		0.77	0.23		3.7E+09	1.9E+08	20	7.3	7.3	7.3 (2.3)		
PME4	30 (7)		0.98	0.02		3.8E+09	1.3E+08	30	16	16	16 (5)		
PME5	37 (8)	0.34	0.66			3.2E+09	8.5E+07	37	9.3	9.3	9.3 (3.1)		
PME6	24 (4)		0.86	0.14		3.8E+09	1.6E+08	24	7.7	7.7	7.7 (2.2)		
PME3D0.5	12 (2)		0.41	0.59		3.6E+09	2.9E+08	12	11	11	11 (5)		
PME3D1.3	12 (2)		0.38	0.62		3.6E+09	3.0E+08	12	6.3	6.3	6.3 (2.6)		
PME3D2.5*	10 (3)		0.22	0.78		3.6E+09	3.5E+08	10	3.5	3.5	3.5 (1.7)		
PME3D10	7.9 (7.6)			0.99	0.01	3.5E+09	4.5E+08	7.9	0.51	0.51	0.51 (0.36)		

²²⁸ Uncertainties in parentheses are ± 1 standard error.

227

²²⁹ Details of the technique are discussed in Kaur and Anastasio (2018).

^{*} Samples extracted in 2.5 mL/filter square and referred to as the "dilute" extracts in the main text. 230

^a Ratio of measured values of $k'_{\text{Probe},3C^*}$ in a given particle extract 231

²³² ^b Mole fractions of model triplets whose $k_{\text{Probe+3C*Model}}$ ratio lies closest to the $k'_{\text{Probe,3C*}}$ ratio in each sample.

^c Mole-fraction-weighted bimolecular rate constants for both probes. 233

^d Triplet steady-state concentration calculated from syringol loss as $k'_{SYR,3C^*}/(\chi_{3C1^*} k_{SYR+3C1^*} + \chi_{3C2^*} \times k_{SYR+3C2^*})$

^e Triplet steady-state concentration calculated from methyl jasmonate loss as $k'_{\text{MeJA},3C^*/}(\chi_{3C1^*} \times k_{\text{MeJA}+3C1^*} + \chi_{3C2^*} \times k_{\text{MeJA}+3C2^*})$ 235 236

^f Best estimate steady-state concentration calculated as the average of the $\Sigma[^3C_i^*]_{SYR}$ and $\Sigma[^3C_i^*]_{MeJA}$.

g Uncertainties in parentheses are ± 1 SE propagated from the errors of $k'_{SYR,3C^*}$ and $k'_{MeJA,3C^*}$ and the mole-fraction-weighted bimolecular rate constants. Values are 237 238 shown in Tables S8 and S9.

Table S13. Measurements of triplet excited states of organic matter

Sample ID	$\begin{array}{c} \sum[^3C_i*]\\ \text{Best Estimate }^a\\ 10^{-14}\text{M} \end{array}$	$P_{3C^*}^{\ b}$ $10^{-7} \mathrm{M \ s^{-1}}$	${P_{3{ m C}^*}}^{ m b} \ { m \mu M} \ { m h}^{-1}$	$10^2 \times \Phi_{3C^*}{}^c$	$\frac{\Phi_{3C^*}}{(\Phi_{102^{*/}f\Delta})} d$	$\frac{\Sigma[^3C_i^{\ *}]}{2^{10}C_i^{\ *}]} e$
Particle Extracts						
PME1*	3.1 (1.2)	0.30 (0.13)	109 (48)	1.8 (0.8)	0.44 (0.20)	0.19 (0.07)
PME2*	3.1 (1.0)	0.34 (0.13)	122 (47)	1.9 (0.7)	0.26 (0.10)	0.10 (0.03)
PME3	7.3 (2.3)	1.5 (0.6)	534 (204)	3.6 (1.4)	0.33 (0.13)	0.068 (0.022)
PME4	16 (5)	3.5 (1.4)	1260 (501)	2.8 (1.1)	0.44 (0.18)	0.083 (0.029)
PME5	9.3 (3.1)	1.5 (0.6)	534 (211)	2.0 (0.8)	0.28 (0.11)	0.074 (0.025)
PME6	7.7 (2.2)	1.6 (0.6)	568 (206)	1.3 (0.5)	0.18 (0.06)	0.035 (0.011)
PME3D0.5	11 (5)	3.6 (1.6)	1286 (593)	4.1 (1.9)	0.48 (0.23)	0.062 (0.026)
PME3D1.3	6.3 (2.6)	1.1 (0.5)	393 (182)	3.4 (1.6)	0.50 (0.24)	0.12 (0.05)
PME3D2.5*	3.5 (1.7)	0.44 (0.24)	160 (86)	2.7 (1.5)	0.43 (0.23)	0.14 (0.07)
PME3D10	0.51 (0.36)	0.0047 (0.0034)	17 (12)	1.1 (0.8)	0.18 (0.13)	0.079 (0.057)
Averages (±σ)						
"Standard" (PME3-6)	10 (4)	2.0 (1.0)	723 (355)	2.4 (1.0)	0.31 (0.11)	0.065 (0.021)
"Dilute" (PME1*- 2*,3D2.5*)	3.2 (0.2)	0.36 (0.01)	130 (26)	2.1 (0.5)	0.38 (0.10)	0.14 (0.04)
Davis Fog	5.4 (6.3)	0.59 (0.60)	212 (216)	5.8 (8.6)	0.55 (0.44)	0.21 (0.20)
Test statistic ^f	0.27	0.059	0.059	0.49	0.35	0.25

Listed uncertainties are ± 1 standard error.

239

240

241

242

243

244

245

246247

^{*} Samples extracted in 2.5 mL/filter square and referred to as the "dilute" extracts in the main text.

^a Best estimate of oxidizing triplets steady-state concentration, calculated as the average of the $\Sigma[^3C_i^*]_{SYR}$ and $\Sigma[^3C_i^*]_{MeJA}$ values, as shown in Table S12.

^b Davis winter solstice-normalized rate of triplet photoproduction, calculated as $P_{3C^*} = \Sigma[^3C_i^*] \times (k_{3C^*+O2} \times [O_2] + (k_{rxn} + k_Q)[DOC])$ (Eq. (8), main text).

^c Quantum yield for formation of oxidizing organic triplet excited states, calculated as $\Phi_{3C^*} = P_{3C^*}/R_{abs}$.

^d Fraction of the total triplet pool that can oxidize our probes, i.e., that are "oxidizing triplets". This is estimated as the ratio of the quantum yields for oxidizing triplets and singlet oxygen (Table S7) divided by the average yield of ${}^{1}O_{2}*(f_{\Delta}=0.53; \text{ Table S11})$ from ${}^{3}C*$ via energy transfer. The denominator, Φ_{102}/f_{Δ} , is an estimate of the quantum yield for formation of energy-transfer triplets that can make singlet molecular oxygen, a pool that likely includes essentially all organic triplet states.

- 249
- ^e Ratio of the Davis-winter-normalized steady-state triplet and singlet oxygen concentrations.

 ^f Test statistic for comparison of standard PME and Davis fog averages: *p*-value for a two-tailed *t*-test for samples of unequal variance. Values below 0.05 are in 250 251 bold.

Table S14. Particle mass to water mass ratios in the PME3 extracts, typical fog drops, and particles

Sample ID	Number of filter squares extracted	Volume of Milli-Q water per filter square (mL) ^a	Aqueous PM mass concentration factor (CF) ^b	Average PM mass extracted per filter square	Total PM mass extracted (μg)	Total volume of extract (mL) ^e	PM mass / water mass $(\mu g\text{-PM} / \mu g\text{-H}_2O)^f$
				(μg) ^c			
PME3D10	1	10	0.05	347	347	10	3.5E-05
PME3D2.5	12	2.5	0.20	331 (15)	3977	30	1.3E-04
PME3D1.3	8	1.3	0.38	315 (23)	2520	10	2.4E-04
PME3D1 or "PME3"	12	1.0	0.49	328 (19)	3932	12	3.3E-04
PME3D0.5	26	0.5	0.96	323 (21)	10979	13	8.4E-04
Cloud/Fog drop			_				$(1-5)E-04^g$
Particles			_				≥ 1 ^h

^a Volume of water used to extract each 2 × 2 cm square piece of the filter sheet.

252

256

257

258

259

260

261262263

b PM mass concentration factor in the extract (Eq. (10), main text).

^c Average ($\pm 1\sigma$) mass extracted from the filter squares for each dilution.

d Total mass extracted per extract. For each extract, the filter pieces used in the extraction were weighed pre- and post-extraction using a Mettler Toledo XP2U ultramicrobalance (error ± 2 μg). The PM mass extracted is the difference between pre- and post-extraction weights.

^e Total volume of extract = number of filter pieces extracted × water volume per filter square.

f PM mass-to-water mass ratio, calculated as total solute mass extracted / total volume of extract.

g For fog drops, we estimate that PM mass/water mass ratios are in the range of $(1-5) \times 10^{-4}$ μg-PM/μg-H₂O based on a typical PM mass of 31 μg m³-air in California's Central Valley, as measured by Young et al. (2016), and assuming a range for the liquid water content (LWC) of 0.06 to 0.3 g-H₂O m⁻³-air (Hess et al., 1998).

h Based on measurements of particle mass concentration (Young et al. (2016)) and estimated particle water (Parworth et al., 2017) in California's Central Valley during winter, the calculated range of PM mass to water mass ratios is 0.79 – 50. From this range, we use a value of 1 to represent typical PM conditions.

Table S15. Photooxidant concentrations (formed *in situ*) in PME3D extracts and expected values in ambient particles

Sample ID	Aqueous PM Mass Concentration Factor (CF) ^a	PM Mass /Water Mass (μg-PM/μg-H ₂ O) ^b	['OH] (M)	[¹O ₂ *] (M)	$\frac{\sum[^{3}C_{i}^{*}]}{(M)}$
PME3D10	0.05	3.5E-05	6.7E-16	6.4E-14	5.1E-15
PME3D2.5*	0.20	1.3E-04	3.4E-16	2.5E-13	3.5E-14
PME3D1.3	0.38	2.4E-04	3.2E-16	5.2E-13	6.3E-14
PME3D1	0.49	3.3E-04	8.5E-16	1.1E-12	7.3E-14
PME3D0.5	0.96	8.4E-04	8.3E-16	1.8E-12	1.1E-13
Ambient Particles		1.0	8.4E-16 °	1.6E-10 ^d	2.3E-13 ^e
					1.3E-11 ^f

^a Aqueous PM mass concentration factor (Eq. (10), main text).

^b PM mass/water mass ratio (Table S14).

^c Expected *in situ* [OH] concentration in ambient PM (in the absence of partitioning of OH from the gas phase), determined as the average of the five measurements in PME3D extracts and corrected for quenching by probe MBO (Sect. S1.1). Including mass transport of OH(g) to the drops will increase the aqueous concentration by approximately 30%, as discussed in the text.

^d Expected [¹O₂*] concentration in ambient PM; see section S4..

e Best estimate for the Σ [3C_i*] concentration in ambient PM, obtained by plotting Σ [3C_i*] against the PM mass/water mass ratio, fitting the data to the equation y = ax/(1+bx); parameters $a = 3.08 \times 10^{-10}$ M and $b = 1.31 \times 10^3$ were obtained using Excel. The curve was then extrapolated to a PM mass/water mass ratio of 1.0 μg-PM/μg-H₂O.

High estimate for the $\sum [^3C_i^*]$ concentration in ambient PM, obtained by fitting $\sum [^3C_i^*]$ against PM mass/water mass ratio with the equation y = ax/(1+bx); parameters $a = 2.26 \times 10^{-10}$ M and b = 17.0 were obtained using Excel. The curve was then extrapolated to a PM mass/water mass ratio of 1.0 μ g-PM/ μ g-H₂O.

Table S16. Gas- and aqueous-phase reaction rate constants for selected organic compounds with the major oxidants

#	Organic Compound Gas-phase rate constant, $k_{ORG+Ox(g)}$ (cm ³ mlc ⁻¹ s ⁻¹)					Aqueous-phase rate constants, $k_{ORG+Ox(aq)}$ (M ⁻¹ s ⁻¹)							
	Compound	*OH(g)	Ref.	O ₃ (g)	Ref.	*OH(aq)	Ref.	¹ O ₂ *(aq)	Ref.	O ₃ (aq)	Ref.	³ C*(aq) ^a	Ref.
1	Syringol	9.6E-11	(Lauraguais et al., 2012)	4.0E-19	(Zein et al., 2015)	2.6E+10	(O'Neill and Steenken, 1977)	3.6E+07	(Tratnyek and Hoigne, 1991b)	1.3E+04	(Hoigné and Bader, 1983)	3.7E+09	(Kaur and Anastasio, 2018), (Smith et al., 2015)
2	Methyl jasmonate	7.8E-12	(Meylan and Howard, 1993)	1.7E-16	(Meylan and Howard, 1993)	6.7E+09	(Richards- Henderson et al., 2014a)	6.0E+06	(Richards- Henderson et al., 2014b)	1.0E+05 e	(Richards- Henderson et al., 2014b)	2.7E+08	(Kaur and Anastasio, 2018)
3	Tyrosine	2.8E-11	(Rinke and Zetzsch, 1984)	4.7E-19	(Atkinson et al., 1982)	1.3E+10	(Solar et al., 1984)	3.8E+07	(Bertolotti et al., 1991)	3.3E+05 (pH 4.2)	(McGregor and Anastasio, 2001)	6.6E+08	(Canonica et al., 2000)
4	1,2,4-Butanetriol	8.5E-12	(Atkinson et al., 2006)	1.0E-20 j	(Atkinson et al., 2006)	5.0E+09	(Anbar et al., 1966)	6.0E+04 ¹	(Wilkinson et al., 1995)	2 ^m	(Hoigné and Bader, 1983)	1.1E+06	(Tetreau et al., 1972)
5	3-Hydroxy-2,5- bis(hydroxymeth yl) furan	4.0E-11	(Atkinson et al., 1983)	2.4E-18	(Atkinson et al., 1983)	3.9E+09	(Lilie, 1971)	1.0E+08 ^q	(Wilkinson et al., 1995)	1.2E+03	(Andreev, 2012)	1.4E+08	(Kaur and Anastasio, 2018)

References for the measured rate constants are indicated. Values indicated are at 298 K wherever available. In cases where no measurements were found, rate constants for structurally similar compounds are used as proxies; references for those are provided, and discussed in the following footnotes.

^a For triplets, we use an average of rate constants for ³3MAP* and ³DMB*.

277

278

279

280

281

282 283

284 285

286

287

288 289

292 293

294

295

^b Second-order rate constant for the gas-phase reaction of O₃ with guaiacol (2-methoxyphenol).

^c Second-order rate constant for the aqueous reaction of O₃with phenol is used as a proxy, with a ten-fold enhancement based on the measured ratio of phenol and syringol rate constants for reaction with ³DMB* (discussed in the SI of Kaur and Anastasio (2018)).

^d Average of cis- and trans-methyl jasmonate rate constants with hydroxyl radical and ozone.

^e Estimated by Richards-Henderson et al. (2014b) using a structurally similar compound.

^f Second-order rate constant for the aqueous-phase reaction of O₃ with phenol.

^g Second-order rate constant for the aqueous-phase reaction of O₃ with 3-methylphenol.

^h Second-order rate constant for aqueous-phase reaction of tyrosine with 3'-methoxyacetophenone.

ⁱ Second-order rate constant for gas-phase reaction of OH with 1-butanol.

290 Second-order rate constant for gas-phase reaction of O₃ with pinonaldehyde.

291 * Second-order rate constant for aqueous-phase reaction of *OH with 1,6-hexanediol.

Second-order rate constant for aqueous-phase reaction of ${}^{1}O_{2}$ * with 2-butanol.

^m Second-order rate constant for aqueous-phase reaction of O₃ with 2-propanol.

ⁿ Second-order rate constant for aqueous-phase reaction of ³DMB* with 2-propanol.

^o Second-order rate constant for gas-phase reaction of ^oOH and O₃ with furan.

^p Second-order rate constant for aqueous-phase reaction of OH with furan.

^q Second-order rate constant for aqueous-phase reaction of ¹O₂* with furan, adjusted by multiplying with 0.5 based on effect of changing substituents.

^r Second-order rate constant for aqueous-phase reaction of O₃ with furan in glacial acetic acid.

s Average of the second-order rate constant for aqueous-phase reaction of ³3MAP* and ³DMB* with methyl jasmonate is used a proxy, adjusted by multiplying with 0.5 based on effect of changing substituents observed for rate constant of furan with ¹O₂*.

Table S17. Fate of selected organic compounds in fog and particles

		V a		Ov	erall		Perce	nt of loss due	to each oxid	lant ^e	
#	Organic Compound	$K_{\rm H}^{a}$ (M atm ⁻¹)	$f_{ m aq}^{ m b}$	$k'_{\mathrm{ORG}}^{\mathrm{c}}$ (s^{-1})	$ au_{\mathrm{ORG}}^{}}}$ (h)	•OH(g)	$O_3(g)$	•OH(aq)	¹ O ₂ *(aq)	O ₃ (aq)	³ C*(aq)
Fog											
1	Syringol	5.0E+03	0.11	1.1E-04	2.5	76	0	5	1	0	18
2	Methyl jasmonate	8.1E+03	0.17	1.2E-04	2.3	5	86	2	0	5	2
3	Tyrosine	8.0E+10	1.0	1.8E-04	1.6	0	0	15	4	62	19
4	1,2,4-Butanetriol	4.7E+11	1.0	1.0E-05	28	0	0	99	0	0	0
5	3-Hydroxy-2,5- bis(hydroxymethyl) furan	1.1E+09	1.0	3.5E-05	7.9	0	0	22	57	1	19
PM (B	PM (Best-fit 3C* scenario)										
1	Syringol	5.0E+03	2.4E-06	9.6E-05	2.9	100	0	0	0	0	0
2	Methyl jasmonate	8.1E+03	4.0E-06	1.3E-04	2.1	6	94	0	0	0	0
3	Tyrosine	8.0E+10	0.98	6.3E-03	0.044	0	0	0	96	2	2
4	1,2,4-Butanetriol	4.7E+11	1.0	1.4E-05	20	0	0	30	68	0	2
5	3-Hydroxy-2,5- bis(hydroxymethyl) furan	1.1E+09	0.35	5.7E-03	0.049	0.5	0	0	99	0.0	0.2
PM (F	ligh estimate [³ C*] scenario)										
1	Syringol	5.0E+03	2.4E-06	9.6E-05	2.9	98	0	0	0	0	1
2	Methyl jasmonate	8.1E+03	4.0E-06	1.3E-04	2.1	6	94	0	0	0	0
3	Tyrosine	8.0E+10	0.98	1.4E-02	0.020	0	0	0	42	1	57
4	1,2,4-Butanetriol	4.7E+11	1.0	2.6E-05	10.5	0	0	16	37	0	47
5	3-Hydroxy-2,5- bis(hydroxymethyl) furan	1.1E+09	0.35	6.3E-03	0.044	0.4	0	0	90	0	9

For fog, a liquid water content of 1×10^{-6} L-aq / L-air is assumed.

For PM, a liquid water content of 2×10^{-11} L-ag / L-air is assumed, based on typical wintertime Central Valley conditions (Parworth et al., 2017).

^a Henry's law constant estimated using EPISuite version 4.11(USEPA, 2012). For methyl jasmonate, measured value from Vempati (2014).

^b Fraction of organic compound present in the aqueous-phase, calculated as $f_{aq} = 1/(1+1/(K_H \times L \times R \times T))$, where K_H is the Henry's law constant, L is the liquid water content, R is the gas constant (0.082 L atm K⁻¹ mol⁻¹), and T = 298 K.

Total pseudo-first order rate constant for loss of organic compound, calculated as $k'_{ORG} = \Sigma(f_{aq} \times k'_{ORG,Ox(aq)} + (1-f_{aq}) \times k'_{ORG,Ox(g)})$. $k'_{ORG,Ox(g)}$ and $k'_{ORG,Ox(aq)}$ are by calculated by multiplying the bimolecular reaction rate constant (Table S16) with the corresponding steady-state concentration of oxidant: [${}^{\bullet}$ OH(g)] = 1 × 10⁶ molecules cm⁻³, [O₃(g)] = 30 ppbv = 7.4 × 10¹¹ molecules cm⁻³, [${}^{\bullet}$ OH(aq)] = 2 × 10⁻¹⁵ M (includes gas-to-aqueous partitioning; Kaur and Assatisio (2017) and this study), [O₃(aq)] = 3.3 × 10⁻¹⁰ M (based on equilibrium with 30 ppbv O₃(g) and $K_H = 1.1 \times 10^{-2}$ M atm⁻¹; Seinfeld and Pandis (2012)), [1 O₂*(aq)] = 2 × 10⁻¹³ M in fog (average in Davis fog; Kaur and Anastasio (2017)), and 1.5 × 10⁻¹⁰ M in PM (estimate in PM after accounting for evaporative loss and loss due to organic sinks at higher DOC concentrations; Sect. S5). In case of the triplets, in fog [3 C*(aq)] = 5 × 10⁻¹⁴ M (average in Davis fog; Kaur and Anastasio (2018)); in PM both the best-fit and high-estimate concentrations obtained via extrapolation (Table S15) are considered, i.e., [3 C*(aq)] = 2.3 × 10⁻¹³ M and 1.3 × 10⁻¹¹ M, respectively.

^d Overall lifetime of organic compound, calculated as $1/k'_{ORG}$.

^e Percent of organic compound lost due to each pathway, calculated as $(f_{aq} \times k'_{ORG,Ox(aq)})/k'_{ORG}$ for aqueous pathways and $((1-f_{aq}) \times k'_{ORG,Ox(g)})/k'_{ORG}$ for gas-phase processes. The sum of all pathways for a given compound is sometimes not equal to 100% because of rounding.

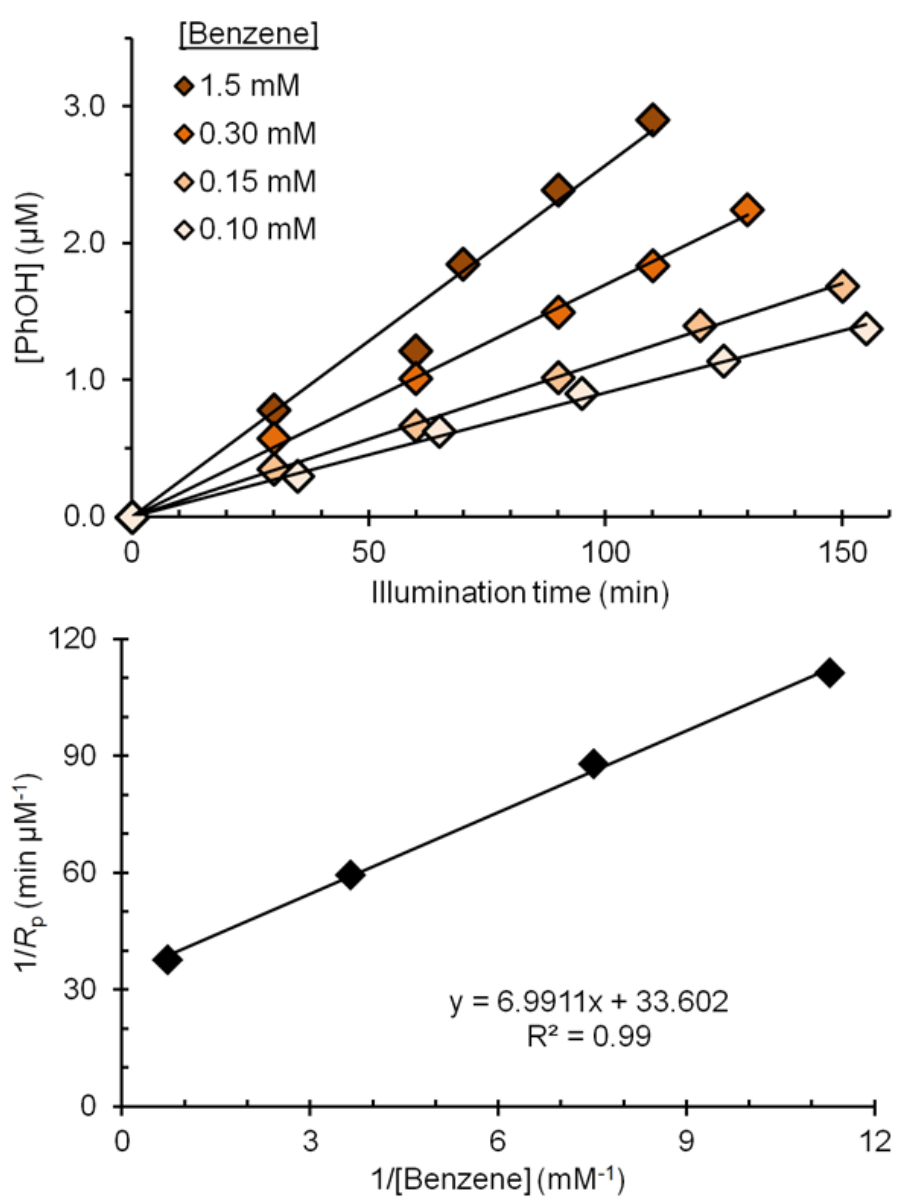


Figure S1. OH measurement in extract PME5. Top Panel: Photoformation of phenol in four aliquots of the extract spiked with varying benzene concentrations (0.10 to 1.5 mM). The rates of phenol formation, R_p , were determined as the slopes of the linear fits for each of the four data sets. Bottom: "Inverse" plot, i.e., the inverse of R_p vs. the inverse of the benzene concentration. The slope and y-intercept from this plot are used to calculate P_{OH} , [OH], and k'_{OH} using equations described in Kaur and Anastasio (2017). OH results for all particle extracts are tabulated in Table S3.

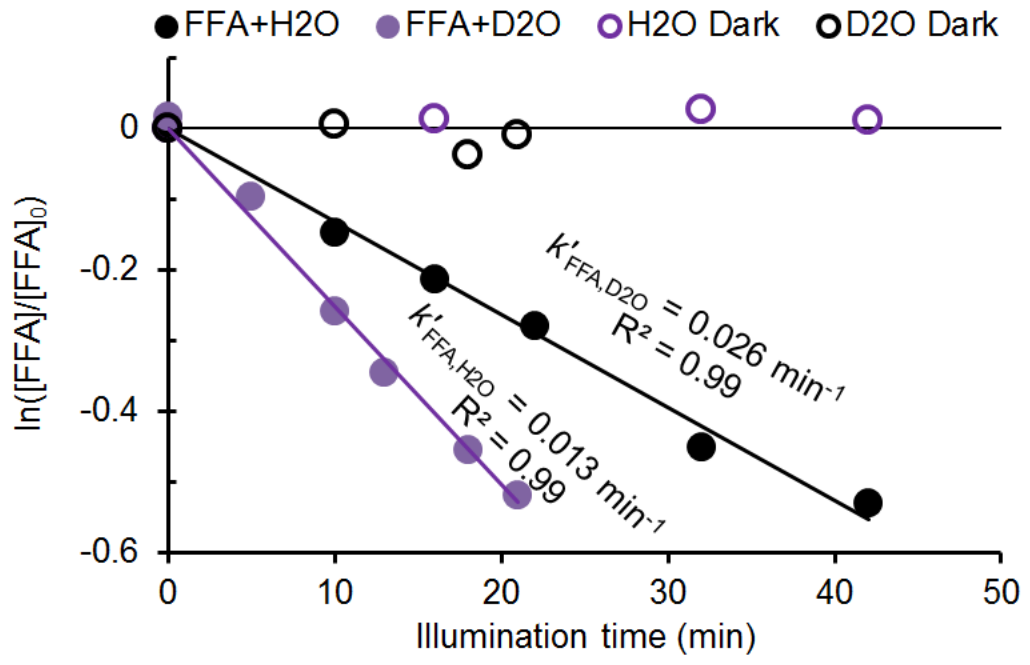


Figure S2. Singlet oxygen kinetic measurements in extract PME5 diluted 1:1 (volume : volume) with H_2O or D_2O . Data show the change in probe concentration (furfuryl alcohol, FFA) with illumination time. Closed symbols are illuminated samples while open symbols represent dark controls. Equations for calculating 1O_2* steady-state concentrations and rates of photoproduction are described in Kaur and Anastasio (2017).



337

338

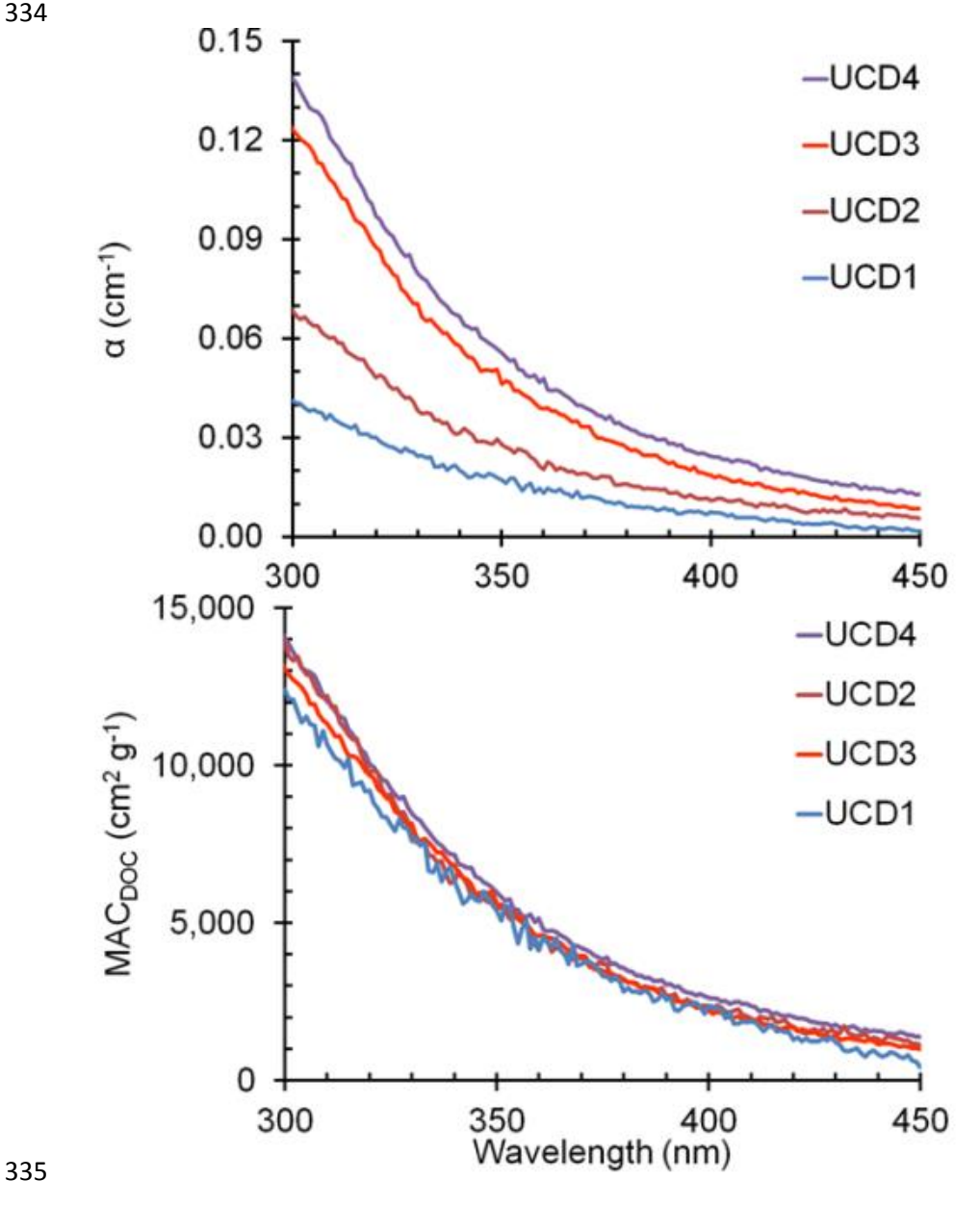


Figure S3. Top panel: Light absorbance by fog samples collected during 2011-12 in Davis, CA. The legend shows the sample identities, arranged from the highest absorbing (top) to lowest absorbing (bottom) at 300 nm. Bottom panel: Mass absorption coefficient of DOC in the Davis fog samples. All data from Kaur and Anastasio (2017).

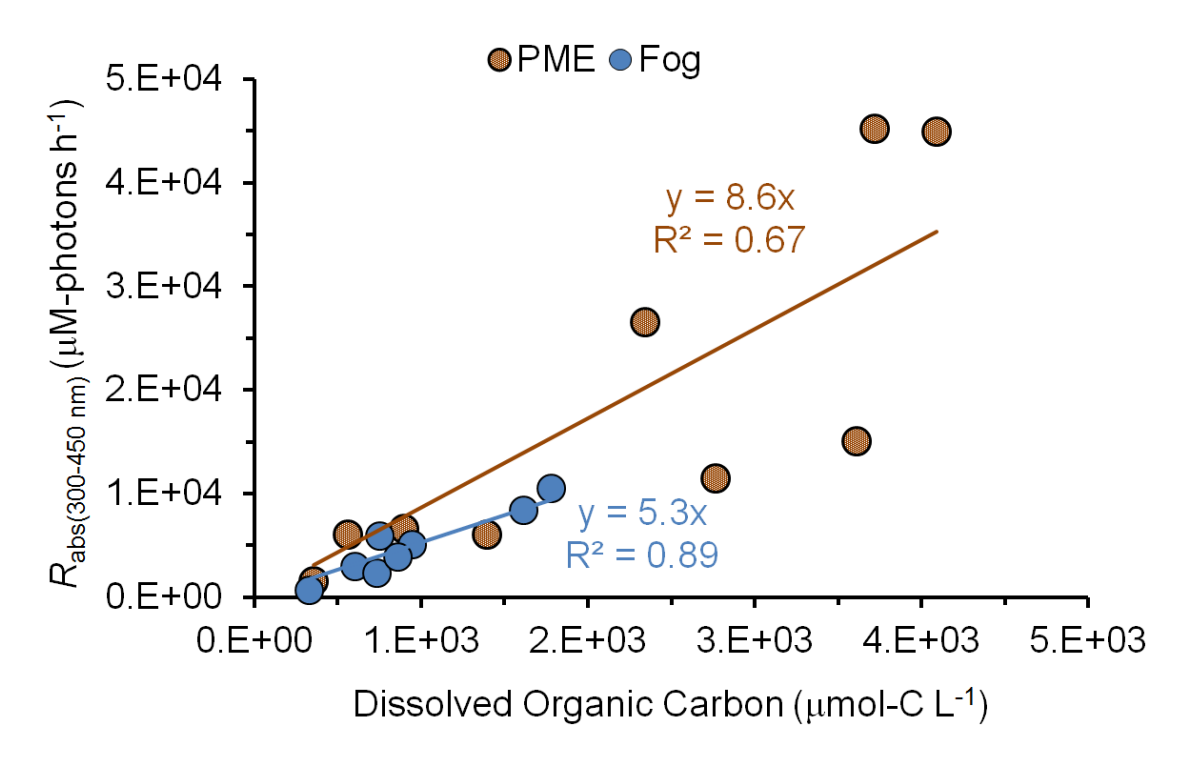


Figure S4. Correlation between the rate of sunlight absorption (R_{abs}) in the 300-450 nm wavelength range and dissolved organic carbon (DOC) for the fog samples (data from Kaur and Anastasio (2017)) and particle extracts (PME) (this work). Values for PME in this plot are summarized in Table S1.

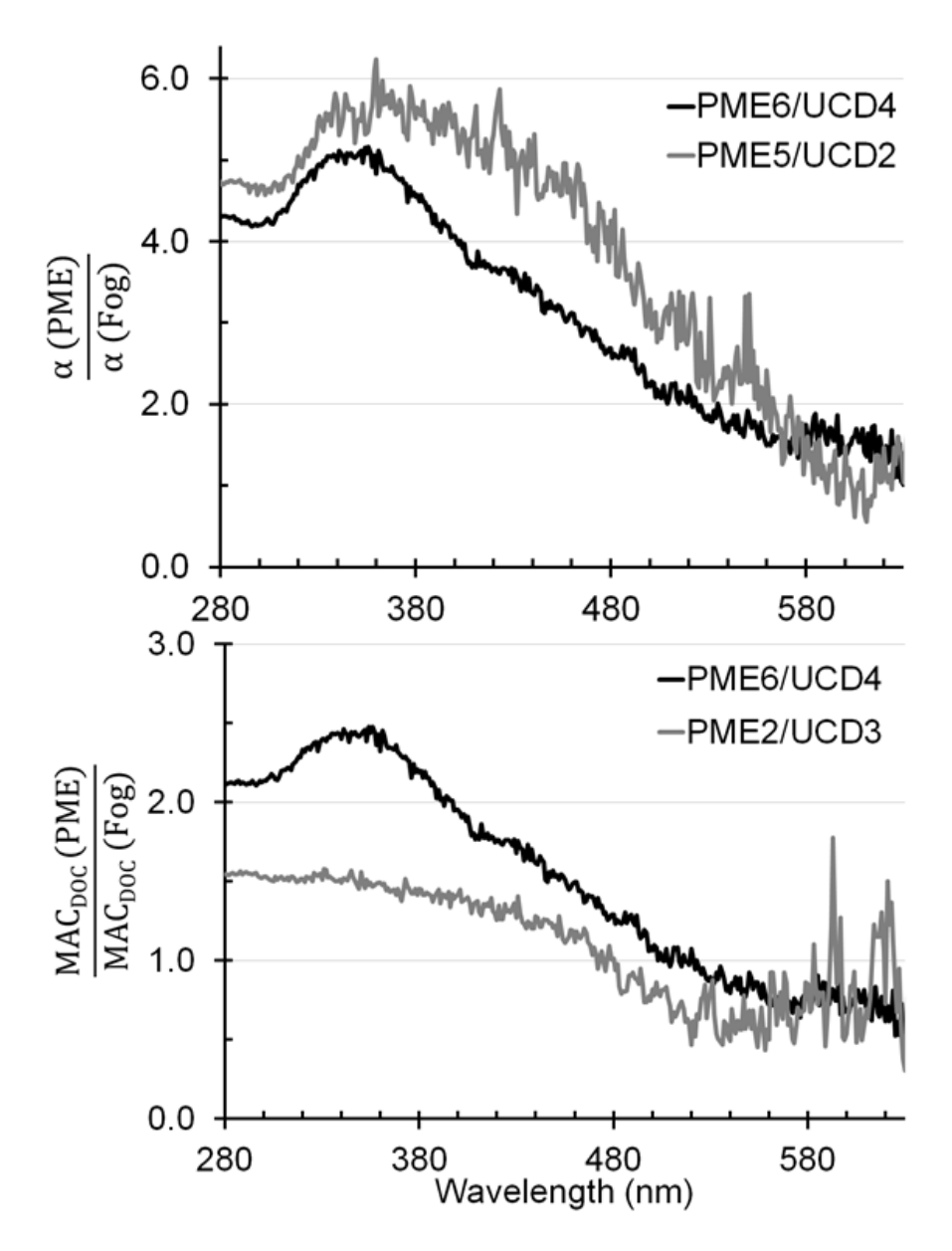


Figure S5. (Top) Ratio of pathlength-normalized absorbance for PME and fog samples with highest (black) and median (grey) absorbances. (Bottom): Ratio of mass absorption coefficients of DOC in PME and fog samples with highest (black) and median (grey) absorbances.

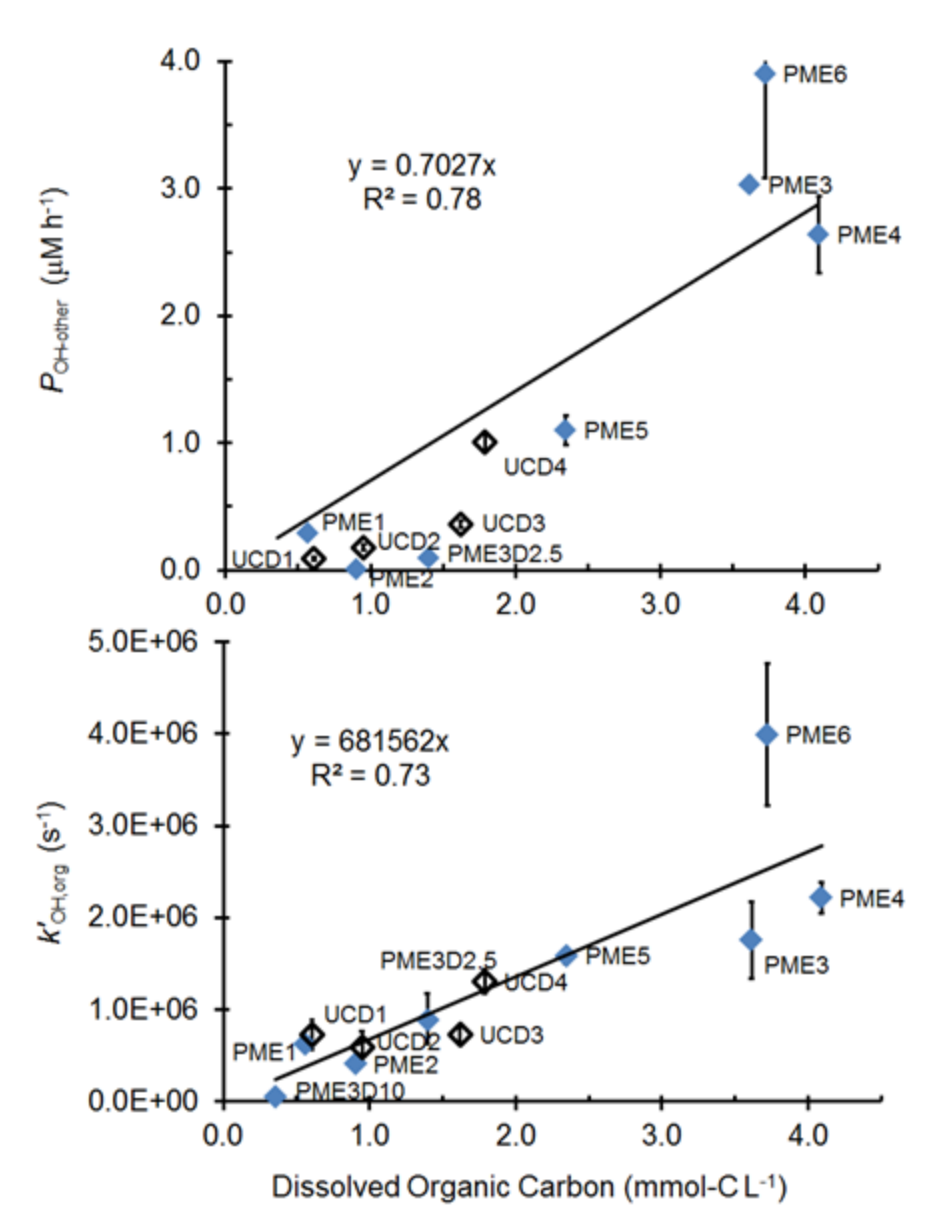


Figure S6. (Top) Correlation between the rate of 'OH photoproduction due to sources other than nitrite and nitrate and the concentration of dissolved organic carbon (DOC). While the R^2 value for this correlation is relatively high, this is largely driven by the highest three points: most of the data are poorly fit by the regression line. (Bottom) Correlation between apparent pseudo-first order rate constant for loss of 'OH due to organic sinks (obtained by subtracting inorganic contributions from the measured k'_{OH}) and DOC. Data include measurements in particle extracts (measured in this work) and in Davis fogs (Kaur and Anastasio, 2017).

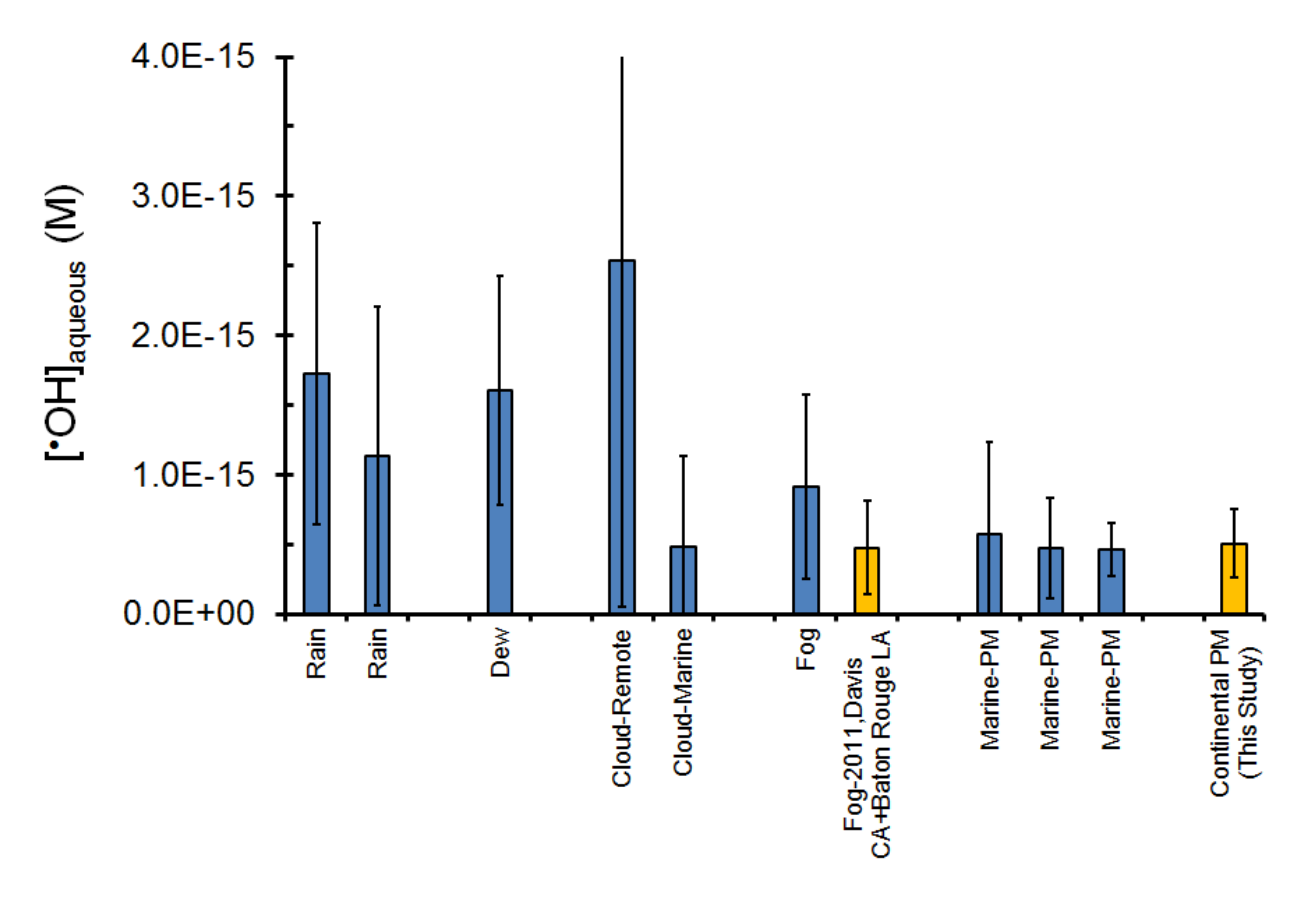


Figure S7. Comparison of hydroxyl radical steady-state concentrations formed *in situ* (i.e., not including mass transport of ${}^{\bullet}$ OH from the gas phase) measured in various atmospheric waters, as summarized in Arakaki et al. (2013) (blue bars) and including (in yellow bars) our recent data for fog (Kaur and Anastasio, 2017) and current data for PM. Error bars are $\pm 1\sigma$, calculated from the variability in values used to calculate the mean for a given study.

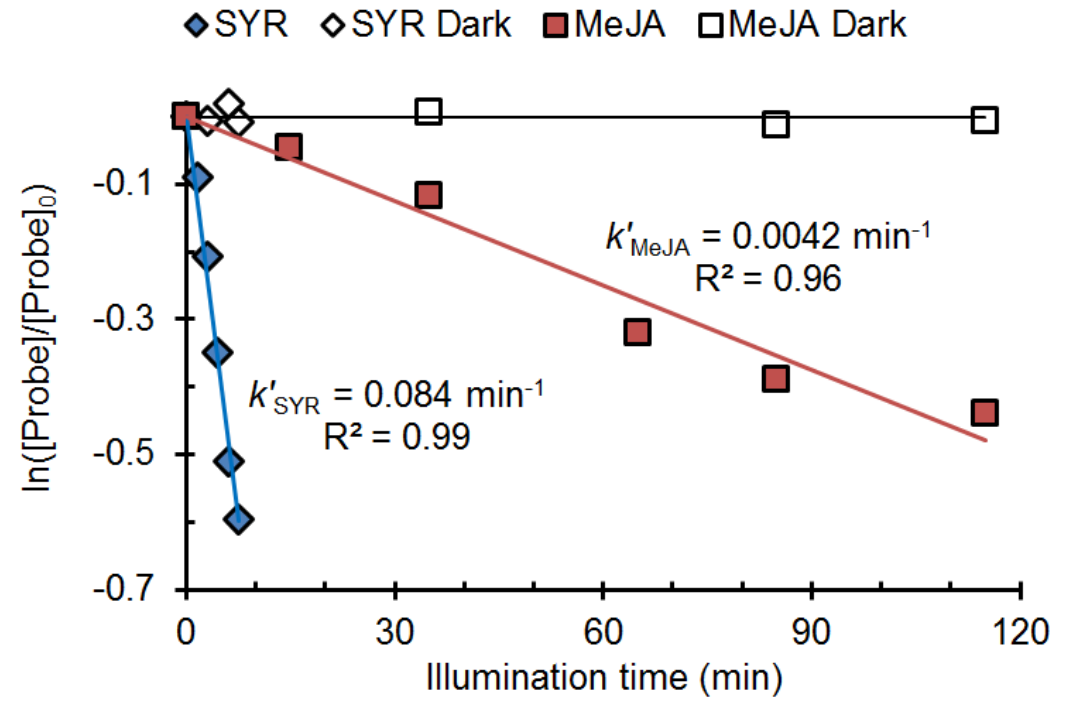


Figure S8. Loss of probes for measuring triplet excited states: syringol (SYR) and methyl jasmonate (MeJA) in extract PME5. Closed symbols are illuminated samples while open symbols represent dark controls.

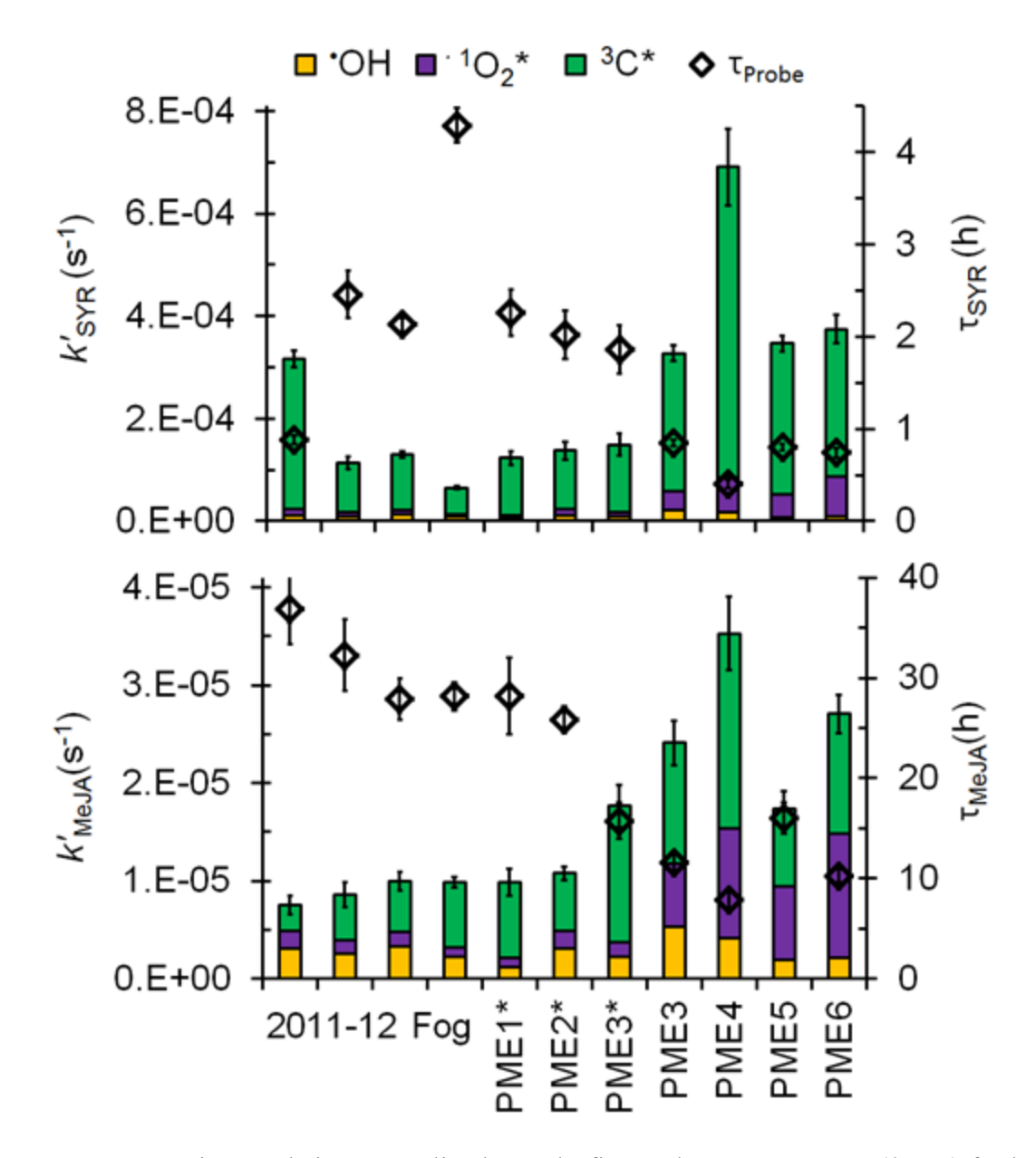


Figure S9. Winter-solstice-normalized pseudo-first-order rate constants (k'_{Probe}) for loss of syringol (top panel) and methyl jasmonate (bottom panel). The bar representing each rate constant is colored to represent the contributions of hydroxyl radical (yellow), singlet molecular oxygen (purple) and triplet excited states (green) to probe loss. The Davis winter-solstice lifetime of each probe (τ_{Probe} , black diamonds) is shown on the right y-axes. The first four bars represent probe data from wintertime fog waters collected in Davis (Kaur and Anastasio, 2018)



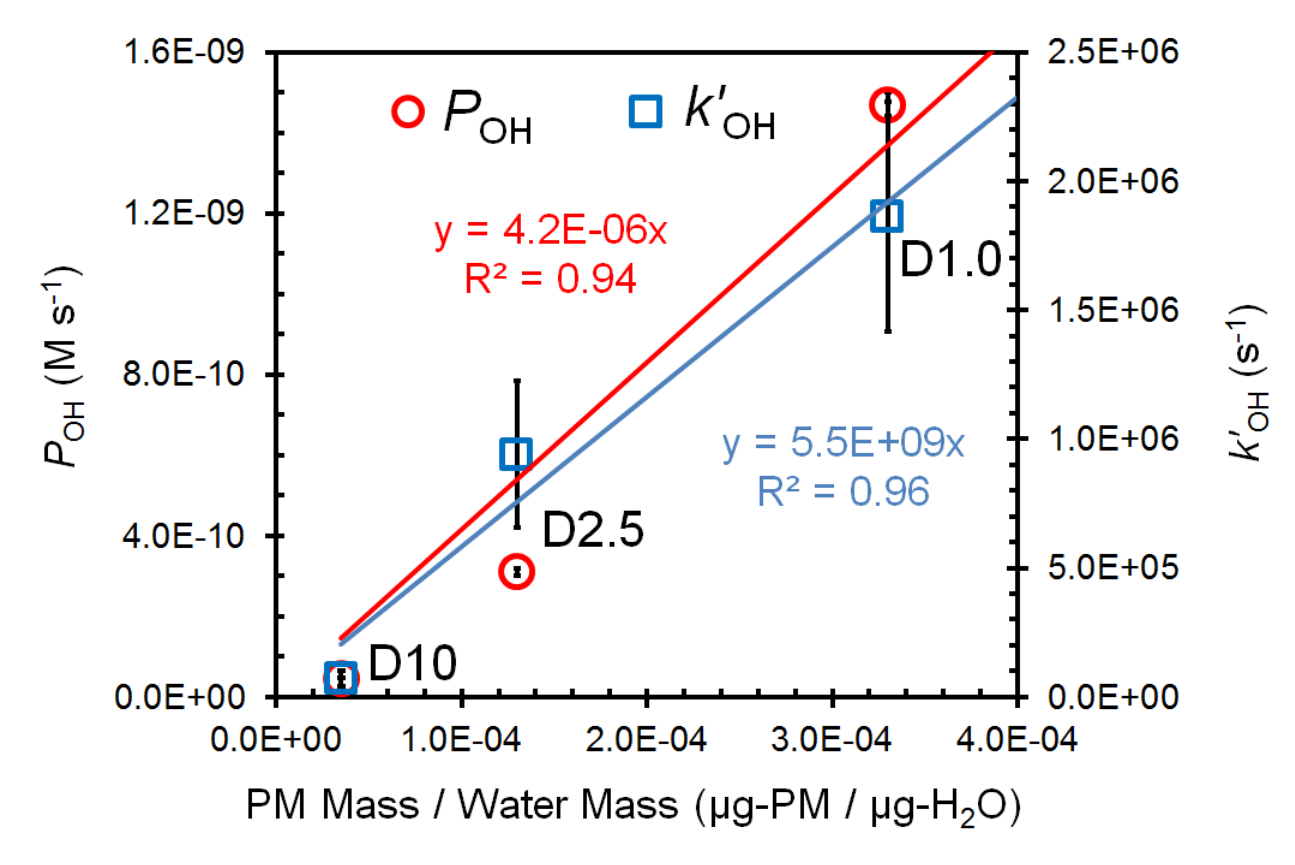


Figure S10. Dependence of rate of 'OH photoproduction (P_{OH} ; red circles, left y-axis) and rate constant for loss of 'OH due to natural sinks (k'_{OH} ; blue squares, right y-axis) with PM mass/water mass ratio in three PME3D samples. ('OH kinetic measurements were not made in the other two PME3D samples.) Measurements of 'OH kinetics in the PME3D samples are discussed in Section S1 and shown in Table S3. Using the slopes of the linear relationships to extrapolate P_{OH} and k'_{OH} to values under ambient particle conditions (1 µg-PM/µg-H₂O) gives $P_{OH} = 4.2 \times 10^{-6} \,\mathrm{M \ s^{-1}}$ and $k'_{OH} = 5.5 \times 10^{9} \,\mathrm{s^{-1}}$. Error bars represent \pm 1 standard error and are too small to be visible for P_{OH} .

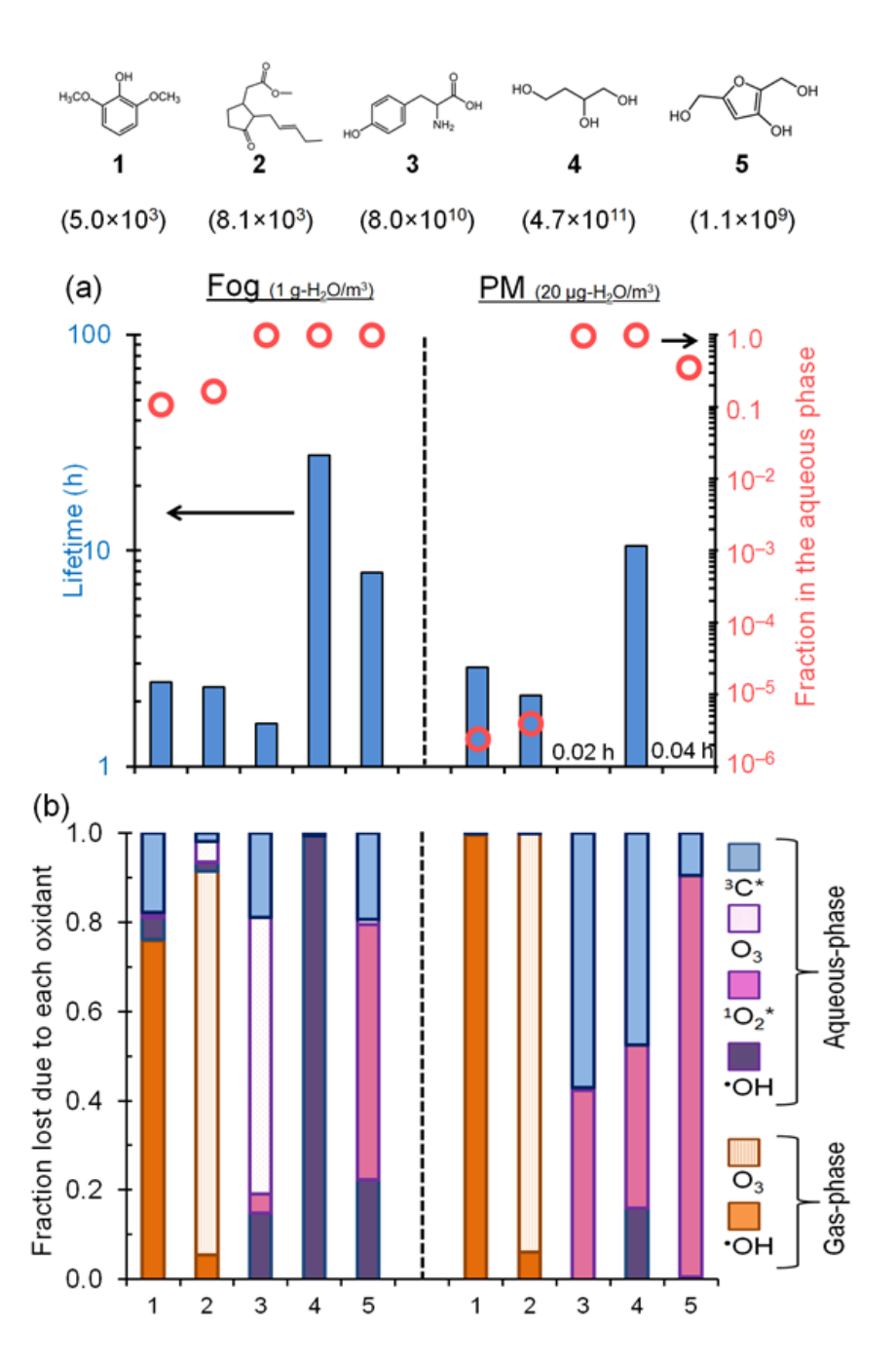


Figure S11. Fate of five model organic compounds – syringol, methyl jasmonate, tyrosine, 1,2,4-butanetriol and 3-hydroxy-2,5-bis(hydroxymethyl)furan – under fog (left of vertical dashed line) and PM (right of dashed line) conditions using an upper-bound estimate for triplet concentrations in PM. Estimated Henry's law constants for the compounds (in units of M atm⁻¹) are in parentheses beneath each structure. Panel (a): the blue columns represent overall lifetimes of the organics via both gas and aqueous-phase loss processes, and the red open circles represent the fractions present in fog or aqueous PM. (b) Fraction of each compound lost via each pathway. The aqueous triplet concentration in PM is 1.5×10^{-10} M (Table S15, Fig. 5, main text). All oxidant concentrations and rate constant data are shown in Tables S16 and S17.

S1. Hydroxyl radical measurements in PME3 and PME3D extracts

S1.1: Determining 'OH steady-state concentrations (['OH])

Typically, for 'OH measurements we used benzene as the probe. Since benzene is volatile, we performed the illumination in 5 mL sealed quartz cuvettes (instead of quartz tubes) fully filled with extract, only withdrawing 100 μL for analysis at each time point to minimize loss of benzene due to volatilization into the headspace. However, for the PME3D extracts, where we had limited sample volume, we could not fully fill the 5 mL cuvettes. Due to this limitation, for the PME3D samples we monitored the loss of 2-methyl-3-buten-2-ol (MBO) to determine 'OH concentrations, then separately measured the production rate of 'OH using benzene (for the three dilutions with sufficient volume), and combined these two measures to determine the 'OH sink.

There are three main reasons we chose MBO as a probe: 1) it is less volatile than benzene in water, 2) its rate constants with the major photooxidants (i.e. 'OH, ¹O₂* and ³C*) are known, and 3) its reaction with 'OH is much faster than with ¹O₂* and ³C* (see below). Fresh MBO stock was made one day prior to each experiment. 1.0 mL of acidified (pH 4.2) PME3D extract was spiked to 75 µM MBO, capped and illuminated with simulated sunlight in a quartz tube of 4 mm pathlength. Unfortunately, we later realized that this relatively high concentration of MBO was sometimes a significant sink for ⁶OH in our PME3 extracts, thus suppressing the apparent steady-state concentration of hydroxyl radical. We are able to approximately correct for this error using an MBO Correction Factor, which is described below.

Throughout the illumination period, MBO loss was measured with HPLC-UV (eluent of 20% acetonitrile: 80% Milli-Q water, flow rate of 0.6 mL/min, detection wavelength of 200 nm and column temperature of 35°C). The pseudo-first-order rate constant for loss of MBO (k'_{MBO} ; s⁻¹) was obtained as the negative of the slope of the plot of ln([MBO]/[MBO]₀) versus time, then normalized to Davis-winter-solstice light using an analog of Eq. (4) in the main text. Because MBO is not a specific probe for 'OH, its loss in each sample is the sum of all its loss pathways:

$$k'_{\text{MBO}} = k_{\text{MBO+OH}} [^{\bullet}\text{OH}] + k_{\text{MBO+1O2}*} [^{1}\text{O}_{2}*] + \sum (k_{\text{MBO+3C}_{i}*} [^{3}\text{C}_{i}*]) + j_{\text{MBO}}$$
 (S1)

where ['OH], [$^{1}O_{2}$ *] and Σ [$^{3}C_{i}$ *] are the steady-state concentrations of the photooxidants. The variables $k_{\text{MBO+OH}}$ (7.4 (± 0.5) × 10 9 M $^{-1}$ s $^{-1}$; (Richards-Henderson et al., 2014b)), $k_{\text{MBO+1O2}}$ * (7.0 (± 1.0) × 10 5 M $^{-1}$ s $^{-1}$; (Richards-Henderson et al., 2014b)) and $k_{\text{MBO+3Ci}}$ * (discussed below) are the

second-order rate constants for reactions of MBO. j_{MBO} is the rate constant for direct

430 photodegradation of the probe and is negligible for our illumination times $(2.7 \times 10^{-7} \text{ s}^{-1})$.

431

- Eq. (S1) has two unknown quantities: 1) [OH] and 2) the loss of MBO due to triplets, i.e.,
- 433 $\Sigma(k_{\text{MBO+3Ci}}^{\dagger}[^{3}C_{i}^{*}])$. To get ['OH], we first estimated MBO loss due to triplets $(\Sigma(k_{\text{MBO+3Ci}}^{\dagger}[^{3}C_{i}^{*}])$
- by using two assumptions about the triplets. Our first assumption is that all loss of the triplet
- probe syringol is due to ${}^{3}C^{*}$ and ${}^{1}O_{2}^{*}$, i.e., ${}^{\bullet}OH$ is a negligible oxidant for SYR, based on our
- measurements in the other samples, PME1-6, where the fraction of SYR lost due to ${}^{3}C^{*}$ and ${}^{1}O_{2}^{*}$
- (combined) is 91 to 98% (Table S8). While we did measure the loss of methyl jasmonate in the
- 438 PME3D samples, we only used syringol loss to determine OH concentrations since our first
- assumption listed above is not valid for MeJA, i.e., we cannot assume that all loss of MeJA is
- due to ${}^{3}C^{*}$ and ${}^{1}O_{2}^{*}$ since ${}^{\bullet}OH$ is a significant sink for MeJA (Table S9).

441

The loss of syringol in the PME3D extracts is the sum of its loss due to 'OH, ${}^{1}O_{2}$ * and ${}^{3}C$ *:

443

444
$$k'_{SYR} = k_{SYR+OH} [^{\bullet}OH] + k_{SYR+1O2*} [^{1}O_{2}*] + \sum (k_{SYR+3C:*} [^{3}C_{i}*])$$
 (S2)

445

- Direct photodegradation of syringol is negligible, and the contributions of other oxidants have
- been previously determined to be small (Section 2.5.3, main text). Based on our first assumption,
- 448 $k_{\text{SYR+OH}}$ [OH] is much smaller than the sum of the other two terms on the right-hand side of Eq.
- 449 (S2) and this equation can be simplified to:

450

451
$$k'_{SYR} \approx k_{SYR+1O2^*}[^{1}O_{2^*}] + \Sigma(k_{SYR+3C.^*}[^{3}C_{i^*}])$$
 (S3)

452

- Our second assumption is that the reactivity of the triplet mixture in the PM extracts most closely
- resembles a binary mixture of the model triplets ³3MAP* and ³DMB*– since these are the best
- 455 triplet matches obtained for majority of the particle extracts (Table S11). For simplicity, we use a
- 1:1 mixture of the two model triplets. Thus, for $k_{SYR+3Ci}$ * we used a triplet-syringol rate constant
- ($\pm \sigma$) of 3.7 (± 0.2) × 10⁹ M⁻¹ s⁻¹, which is the average of $k_{SYR+3MAP}$ * and $k_{SYR+3DMB}$ * (Table S10)
- in Eq. (S3) to obtain the triplet steady-state concentration:

460
$$\Sigma[^{3}C_{i}^{*}] = \frac{k'_{SYR} - (k_{SYR} + 102^{*}[^{1}O_{2}^{*}])}{k_{SYR} + 3C_{i}^{*}}$$
 (S4)

Using the measured singlet oxygen concentration, [$^{1}O_{2}^{*}$], for each PME3 dilution we determine $\Sigma[^{3}C_{i}^{*}]$ in Eq. (S4), which we then plug into Eq. (S1), along with $k_{\text{MBO+3Ci}^{*}} = 3.4 (\pm 0.4) \times 10^{7} \,\text{M}^{-1}$ s⁻¹, the average of $k_{\text{MBO+33MAP}^{*}}$ and $k_{\text{MBO+3DMB}^{*}}$ (Richards-Henderson et al. (2014b)), to obtain the first iteration of [$^{\bullet}$ OH]:

We then remove the first assumption and plug these [*OH] values into Eq. (S2) to get a second set of Σ[³C_i*] values, which we use in Eq. (S1) to obtain the second iteration of [*OH]. We continue this iterative process until the [*OH] values change by less than 0.01% (Table S18).

Table S18. Determination of hydroxyl radical steady-state concentrations, [*OH], from results of the MBO experiments

	[(OH] from Iter	rations, 10^{-16}				
Sample ID	Iteration 1	Iteration 2	Iteration 3	Iteration 4	MBO Correction Factor	$1/S_{\lambda}$	Final [*OH] 10 ⁻¹⁶ M
PME3D0.5	5.54 (1.87)	5.72 (1.93)	5.73 (1.93)	5.73 (1.39)	1.10	1.15	7.3 (1.8)
PME3D1	5.74 (1.91)	5.93 (1.97)	5.94 (1.97)	5.94 (1.40)	1.24	1.07	7.9 (1.9)
PME3D1.3	2.23 (0.76)	2.31 (0.77)	2.31 (0.79)	2.31 (0.57)	1.27	1.05	3.0 (0.8)
PME3D2.5*	2.19 (0.75)	2.26 (0.77)	2.26 (0.77)	2.26 (0.57)	1.43	1.03	3.3 (1.0)
PME3D10	1.89 (0.68)	1.95 (0.70)	1.95 (0.70)	1.95 (0.54)	3.31	1.01	6.6 (2.8)

Uncertainties in parentheses are ± 1 standard error.

478 We then made two corrections to the fourth (and final) iteration values. The first, and largest, 479

correction was to account for the scavenging of OH by MBO by multiplying by an MBO

Correction Factor". This correction factor is the sum of the pseudo-first-order rate constants for 480

MBO and natural scavengers divided by the pseudo-first-order rate constant for natural

scavengers. As shown in Table S18, this correction increases as the sample gets more dilute: 482

483 values range from a modest 1.10 in the most concentrated extract to a very large 3.31 in the most

dilute extract. The second correction was to divide by the light screening factor, S_{λ} (Table S1 and

Sect. 2.5.1 of main text) to account for light absorption in our container; since the light screening

factors are close to 1 (i.e., 0.87 - 0.99), these corrections are relatively small. The standard errors

on the final OH concentrations account for both the experimental uncertainty as well as the

488 uncertainty associated with the MBO correction factor.

S1.2: Rate of 'OH photoproduction (P_{OH})

490 Similar to the other extracts, in the PME3 samples we used benzene as the probe measure 'OH

photoformation (Kaur and Anastasio, 2017; Anastasio and McGregor, 2001; Zhou and Mopper, 491

492 1990). A 5.0 mL aliquot of extract was acidified to pH 4.2 (\pm 0.2) and spiked with 1500 μ M

benzene, which should scavenge essentially all OH. The solution was illuminated in a capped, 493

sealed quartz cuvette with a 1 cm pathlength (Sect. 2.5.1 in main text). In all cases, phenol 494

495 concentration increased linearly with time, and the rate of phenol formation (R_P) was obtained as

the slope of the plot of phenol concentration versus time. We then plotted $1/R_p$ versus 496

497 1/[Benzene] and the intercept of that plot gave the experimentally measured rate of 'OH

photoproduction (P_{OH EXP}) (Zhou and Mopper, 1990). Measured rates of OH formation were 498

normalized to the rate expected under midday Davis, CA winter-solstice sunlight (P_{OH}) based on

2-nitrobenzaldehyde (2NB) actinometry: 500

$$P_{\text{OH}} = P_{\text{OH,EXP}} \times \frac{j2\text{NB,WIN}}{j2\text{NB,EXP}}$$
 (S6)

where $j_{2NB,WIN}$ is the rate constant for loss of 2NB measured at midday near the winter solstice in 502

Davis (0.0070 s⁻¹; Anastasio and McGregor, (2001)), and $j_{2NB,EXP}$ is the measured rate constant 503

for loss of 2NB on the day of the experiment. Due to the volume requirements of this technique, 504

we were only able to measure $P_{\rm OH}$ in three extracts – PME3, PME3D2.5* and PME3D10. 505

506

499

481

484

485

486

487

S1.3 Rate constant for loss of 'OH due to natural sinks (k'_{OH})

- In the PME3 samples we calculated the pseudo-first-order rate constant for loss of 'OH due to
- natural sinks by dividing the measured rate of 'OH photoproduction determined with benzene
- (Sect. S1.2) by the measured 'OH steady-state concentration determined with MBO (Sect. S1.1):

$$511 k'_{\text{OH}} = \frac{P_{\text{OH}}}{[\bullet \text{OH}]} (S7)$$

512 S2. OH sink measurements (k'_{OH}) in field blanks FB1 and FB2

- We also measured the rate constant for loss of OH due to natural sinks (k'_{OH}) in field blank FB1,
- which was extracted under the "dilute conditions", i.e. each 2×2 cm filter square was extracted
- 515 in 2.5 mL Milli-Q.

516

507

- In the early stages of this project, we used benzoate as an 'OH probe (Anastasio and McGregor,
- 518 2001), which reacts with 'OH to form m-hydroxybenzoic acid, m-HBA (and other products),
- which was quantified using UV-HPLC. Four 5.0 mL aliquots of extract were spiked with 100–
- 520 1500 μM of sodium benzoate/benzoic acid solution (20 mM) at pH 4.2. Since P_{OH} in FB1 was
- below our detection limit (Table S3), we added 200 µM hydrogen peroxide as an OH source to
- each aliquot in order to measure the OH sinks. Aliquots were illuminated in capped quartz tubes
- with a 0.4 cm pathlength (Sect. 2.3 main text). The formation of m-HBA was linear in all cases,
- and the slope of the plot of [m-HBA] versus time in each aliquot is the rate of m-HBA formation
- 525 $(R_P, \mu \text{M min}^{-1})$. Similar to the benzene technique, we then plotted $1/R_P$ versus 1/[benzoate], used
- the slope and y-intercept of the inverse plot to obtain P_{OH} , k'_{OH} and [OH], which were
- normalized to Davis midday solstice sunlight conditions. k'_{OH} measured using benzoate was 4.4
- 528 $(\pm 0.5) \times 10^5 \,\mathrm{s}^{-1}$, and represented 56% of the dilute sample average (PME1*, PME2*,
- PME3D2.5). Because this is high, we ran a number of tests to identify the source of the
- background OH sinks in FB1, starting with measuring k'_{OH} in two Milli-Q solutions containing
- only HOOH and probe stocks to identify whether these were the source of contamination. k'_{OH} in
- Milli-Q was nearly as high as in FB1: even after rigorously cleaning the quartz tubes using a
- 533 UV+HOOH treatment (Chen et al., 2016), k'OH was not lowered appreciably (Fig. S12). Since at
- this point, it appeared that the probe chemicals (sodium benzoate and benzoic acid) could be
- contaminated, we decided to switch to benzene as the 'OH probe.

The experimental procedure for the benzene technique is very similar to the benzoate technique, except that the aliquots of FB1 were acidified to pH 4.2 (\pm 0.2) using 10 mM sulfuric acid. While the k'_{OH} value using benzene was slightly lower than the benzoate case ($3.4 \pm 0.4 \times 10^5 \, \mathrm{s}^{-1}$), it still represented 43% of the PM sample average. We then performed the benzene technique in Milli-Q water: the resulting k'_{OH} of 1.2 (\pm 0.1) \times 10⁴ s⁻¹ was more than 10 times lower than the other measurements, typical of solutions without any background organic contamination (Chen et al., 2016). This was the lowest k'_{OH} measured in our trials so, we chose to proceed with benzene as the probe for measuring 'OH in the particle extracts.

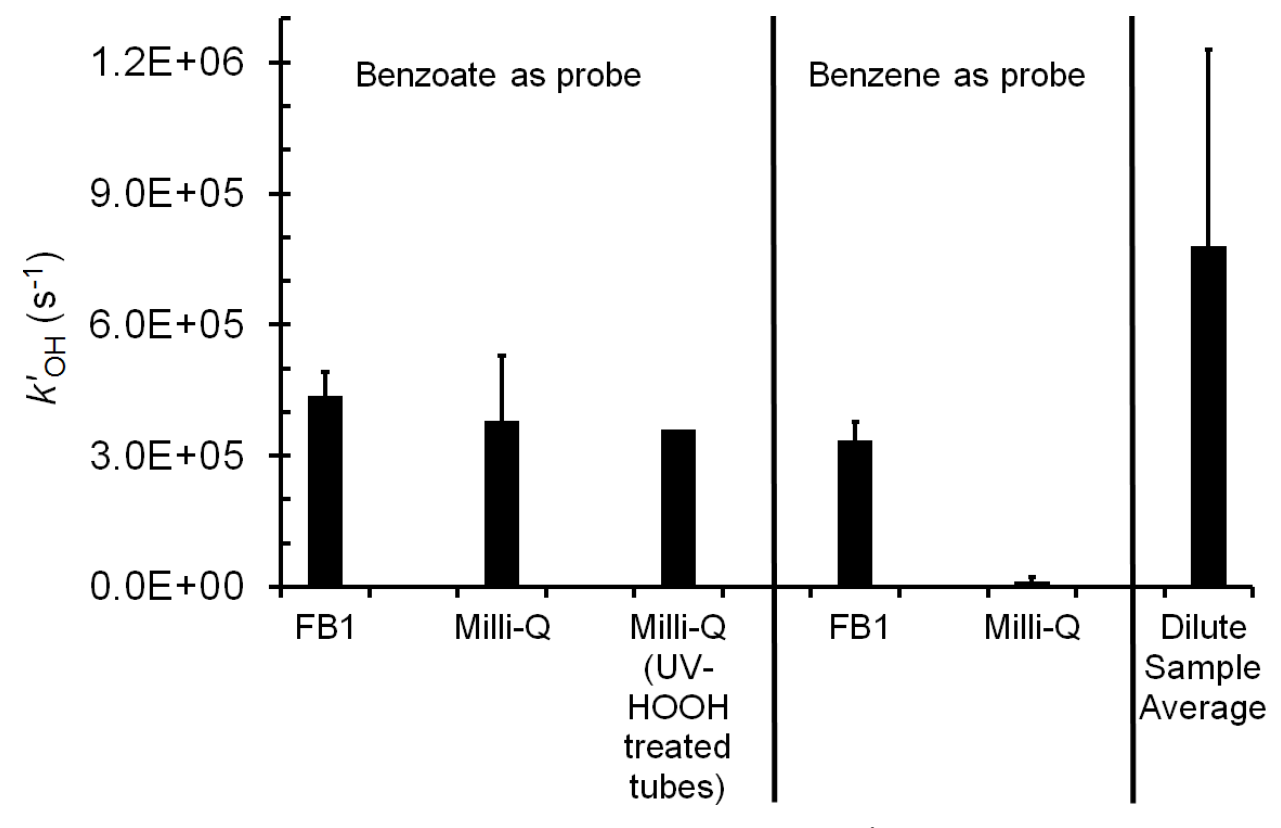


Figure S12. Measured pseudo-first-order rate constant for loss of 'OH due to natural sinks (k'_{OH}) in various solutions using sodium benzoate/benzoic acid and benzene as 'OH probes. Samples labeled "Milli-Q" contain only probe and HOOH. Samples labeled "FB1" are measurements in the extract solution of Field Blank 1. "Dilute Sample Average" is the average of the k'_{OH} measurements in PME1*, PME2* and PME3D2.5* (Table S3).

We next determined k'_{OH} in FB2 with benzene under standard extract conditions (1 mL Milli-Q per filter square). However, the resulting value of 2.7 (± 0.1) × 10⁵ s⁻¹ is not much lower than the value in (more dilute) FB1 determined with benzoate and is 20 times higher than the Milli-Q value. But because the k'_{OH} value in the standard extracts (PME3D1-PME6) is high (Table S3),

556	the corresponding FB2 value is only 11% of the standard sample average. One plausible
557	contributing factor to the high k ' $_{\mathrm{OH}}$ in the field blanks is that organic matter is coming off the
558	filter material during extraction; we see this in the DOC measurements for both field blanks
559	(Table S2). For future studies, we recommend first evaluating a few different types of particle
560	filters by making background k'_{OH} measurements and then picking the filters that introduce the
561	least contamination.
562	We did not adjust values of k'_{OH} measured in the particle extracts for the field blank rate
563	constants. If we had adjusted them, *OH concentrations would have increased by 50% in the
564	"dilute" extracts and by 10% in the standard extracts. However, the concentrations would still be
565	similar to fog. Additionally, this adjustment would have no effect on the extrapolation to ambient
566	PM conditions, since [*OH] in all PME3D extracts would go up equally.

S3. Other oxidants in PM extracts

567

- Since the probes we use for triplet determination do not react with only triplets (Eq. (5), main
- text), we account for the contributions of ${}^{1}O_{2}^{*}$ and ${}^{\bullet}OH$ to probe loss. However, it is also
- possible that other oxidants (that we do not measure) are also contributing to triplet probe loss.
- Here we examine this possibility for triplet probe loss in the PM extracts. In our previous
- 572 measurements of photooxidants in fog water (Kaur and Anastasio, 2018), we estimated the
- importance of hydroperoxyl radical/superoxide radical anion (HO₂*/*O₂¯), ozone (O₃), carbonate
- radical (°CO₃) and hydrogen ion/hydrated electron (H° (aq)/e⁻(aq)) and found that these species
- in total contributed less than 7 % to the average measured syringol loss. To do this calculation
- for our PM extracts, we estimate the steady-state concentrations of these oxidants in the
- 577 illuminated extracts and, using reaction rate constants available in literature, calculate a pseudo-
- first-order rate constant for their reaction with syringol. We then compare that to the average (\pm
- 579 σ) measured syringol loss in the standard extracts, $k'_{SYR} = 3.9 (\pm 1.3) \times 10^{-4} \text{ s}^{-1}$. As we noted in
- our previous paper, there are insufficient rate constants in the literature for reactions of methyl
- jasmonate in order to estimate its potential loss to other oxidants.

Hydroperoxyl Radical / Superoxide Radical Anion (O₂ (-I))

- Hydroperoxyl radical and superoxide radical anion (i.e., O₂(-I)) are a conjugate acid-base pair;
- the p K_a of HO₂ is 4.75 ± 0.08 (Bielski et al., 1985). Since the pH of our extracts was adjusted to
- ambient particle pH of 4.2 (Parworth et al., 2017), the mole fractions of HO_2^{\bullet} and $^{\bullet}O_2^{-}$ in the
- extracts are 0.78 and 0.22, respectively. There are no rate constants available for reaction of
- either species with syringol (2,6-dimethoxyphenol) so we use the fastest reported rate constants
- for reactions of similar compounds with ${}^{\bullet}O_2^-$ and HO_2^{\bullet} . For substituted phenols, the rate
- constant for reaction of ${}^{\bullet}O_2^-$ with guaiacol (2-methoxyphenol) is $2.5 \times 10^3 \text{ M}^{-1}\text{s}^{-1}$ (Yasuhisa et
- al., 1993); for HO_2^{\bullet} , the rate constant with catechol (1,2-benzenediol) is $4.7 \times 10^4 \text{ M}^{-1} \text{ s}^{-1}$
- 591 (Bielski, 1983). At pH 4.2, the mole-fraction weighted rate constant, used as the proxy for
- 592 $k_{\text{SYR}+\text{O2}(-1)}$, is $3.7 \times 10^4 \,\text{M}^{-1} \text{s}^{-1}$.
- To estimate $O_2(-1)$ concentrations in the extracts, we use previously measured rates of HOOH
- formation in illuminated fog waters from California's Central Valley since these two oxidants
- are intimately connected (Deguillaume et al., 2004; Anastasio, 1994):

596 $O_2(-I) + Cu(I) \rightarrow HOOH + Cu(II)$ (S8)

The maximum measured production rate of HOOH, P_{HOOH} , in illuminated Central Valley fogs is

3 μM h⁻¹ (8.3 × 10⁻¹⁰ M s⁻¹; Anastasio (1994)) . We expect that P_{HOOH} in particle extracts will be

599 higher than fog, so we use an enhancement factor based on the observed increase in singlet

oxygen concentrations in the standard extracts, which is a factor of seven higher than Davis fog

average (Table S7). The reaction rate constants for ${}^{\bullet}O_2^-$ and HO_2^{\bullet} reacting with Cu(I) are 9.4 ×

602 $10^9 \,\mathrm{M}^{-1} \,\mathrm{s}^{-1}$ (Piechowski et al., 1993) and $3.5 \times 10^9 \,\mathrm{M}^{-1} \,\mathrm{s}^{-1}$ (Berdnikov, 1973), respectively,

which gives an overall, mole-fraction-weighted reaction rate constant, $k_{O2(-D+Cu(D)}$, of 4.8×10^9 M⁻

604 1 s⁻¹. We assume that the Cu(I) concentration is similar to that of O₂(-I) (e.g., [Cu(I)] ≈ 1 nM in

the daytime urban cloud scenario of Deguillaume et al. (2004)). Solving the rate equation for S8

with these inputs gives an $O_2(-I)$ steady-state concentration of 1.1×10^{-9} M. At this

concentration, the estimated loss rate constant for syringol due to $O_2(-I)$, $k'_{SYR,O2(-I)}$ is 4.1×10^{-5}

s⁻¹, which would account for 11 % of the average observed syringol loss. This suggests that

superoxide is a minor sink for syringol in our samples, although it does appear to be more

significant in particle extracts than fog.

611 **Ozone** (O₃)

609

622

- Based on the Henry's law constant for ozone at 25°C ($K_H = 1.1 \times 10^{-2} \text{ M atm}^{-1}$ (Seinfeld and
- Pandis, 2012) and assuming a gas-phase mixing ratio for O₃ of 30 ppbv, gives an initial aqueous-
- phase concentration of ozone in our samples of 3.3×10^{-10} M. The actual concentration is likely
- lower since our samples are capped during illumination. The bimolecular rate constant for
- reaction of ozone with syringol is not available in the literature, so we estimate the rate constant
- by using the value for phenol ($k_{\text{PhOH+O}_3} = 1.3 \times 10^3 \text{ M}^{-1} \text{ s}^{-1}$) (Hoigné and Bader, 1983)with an
- enhancement factor of 10 based on the measured ratio of phenol and syringol rate constants for
- reaction with ³DMB* (Smith et al., 2015). Under these assumptions, ozone is a very minor sink
- for syringol in the fog samples ($k'_{SYR,O_3} = 4.3 \times 10^{-6} \text{ s}^{-1}$), accounting for 1% of the average
- 621 measured syringol loss.

Carbonate Radical (*CO₃⁻)

- The carbonate radical is formed mainly from the reactions of bicarbonate (HCO₃⁻) and carbonate
- 624 (CO₃²⁻) ions with *OH and triplet CDOM species. Although DOM components are likely

- important sinks for 'CO₃, this quenching is poorly understood (Canonica et al., 2005; Vione et
- al., 2014; Huang and Mabury, 2000). There are no published measurements of CO₃ in
- atmospheric waters, so we use the typical steady-state concentration measured in surface waters
- of 2×10^{-14} M determined using N,N-dimethylaniline as a probe (Huang and Mabury, 2000;
- Zeng and Arnold, 2012). There are concerns that aniline probes overestimate CO₃ since they
- also react rapidly with triplets (Rosario-Ortiz and Canonica, 2016), so we treat this as an upper-
- bound estimate. We do not apply an enhancement factor in this case since DOM appears to play
- the dual role of source and sink. While 'CO₃' reacts rapidly with electron-rich phenolates (i.e., a
- deprotonated phenol), at pH 4.2 syringol is in the neutral, less reactive form. There are no rate
- constants available for 'CO₃ reacting with methoxyphenols, so we assume the value with SYR
- is 10 times higher than that with phenol $(4.9 \times 10^6 \,\mathrm{M}^{-1}\mathrm{s}^{-1};$ Chen et al. (1975)). This results in a
- pseudo-first-order rate constant for loss of SYR due to carbonate radical of 1×10^{-6} s⁻¹, which
- represents a negligible 0.3% of the average measured syringol loss rate constant in our standard
- 638 PM extracts.

639 Hydrogen Ion / Aquated Electron (H^{*}_(aq)/e⁻_(aq))

- 640 Hydrogen ion (H*) and aquated electron (e⁻_(aq)) can be formed during irradiation or illumination
- of dissolved organic matter in natural waters; these exist as a conjugate acid-base pair with a p K_a
- of 9.6 (Kozmér et al., 2014; Buxton et al., 1988a). In our extracts at pH 4.2, the predominant
- species would be H[•] (aq). Zepp et al. (1987) determined an average steady-state concentration of
- 644 $e^{-}_{(aq)}$ in sunlight-illuminated lake waters to be 1.2×10^{-17} M. Similar to ${}^{1}O_{2}$ *, since DOM is the
- main source of e (aq), we assume an enhancement factor of seven in the steady-state
- concentration of $e^{-}_{(aq)}$. As an upper bound, we assume the H^{\bullet} concentration to be equal to this.
- The rate constant for syringol reacting with H is not known. Using the average rate constant for
- methoxyphenol, $2.1 \times 10^9 \,\mathrm{M}^{-1}\mathrm{s}^{-1}$ (O'Neill et al., 1975; Neta and Schuler, 1972), the pseudo-
- first-order rate constant for loss of SYR due to hydrogen ion is 1.7×10^{-7} s⁻¹, which would
- account for only 0.04% of the average observed syringol loss.

Combined Contributions from Other Oxidants

- Based on our upper-bound estimates, the total rate constant for loss of syringol due to $HO_2^{\bullet}/^{\bullet}O_2^{-}$,
- 653 O_3 , ${}^{\bullet}CO_3^-$ and H^{\bullet} (aq)/e-(aq) is $\sim 4.6 \times 10^{-5} \text{ s}^{-1}$, which is only 12% of the average measured

654 syringol loss rate constant. Since this is small, our assumption that the loss of syringol is mainly

due to ${}^{\bullet}OH$, ${}^{1}O_{2}*$ and ${}^{3}C*(Eq. (6), main text)$ seems valid.

S4. Impacts of mass transport and increasing organic concentration on estimates of aqueous photooxidant concentrations in ambient particles

- The steady-state concentration of an oxidant reflects the balance between its rate of formation
- 659 (P_{OX}) and first-order rate constant for loss ($k'_{OX} = 1 / \tau_{OX}$):

660

656

657

661 $[OX] = P_{OX} / k'_{OX}$ (S9)

662663

664

665

666

667

668

669

670

- where $k'_{\rm OX}$ is the sum of all the pseudo-first-order sinks of the oxidant. We can use our oxidant measurements for the dilution series of sample PME3 to estimate how the aqueous formation rate and rate constant for loss vary with solute concentration. But extrapolating these results to particle liquid water conditions requires accounting for additional factors, such as mass transport. Here we combine our aqueous measurements with estimates of these other factors to better estimate oxidant concentrations from dilute fog or cloud drop conditions (i.e., a PM solute mass/water mass ratio of $3 \times 10^{-5} \,\mu \text{g}$ -PM/ μg -H₂O) to a particle liquid water condition (1 μg -PM/ μg -H₂O). We roughly estimate the gas-phase influence using a simplified case assuming a
- temperature of 298 K, total pressure of 1 atm, an aqueous particle radius (R_p) of 0.5 μ m at a PM
- mass/water mass ratio of 1 μ g-PM/ μ g-H₂O, and a constant particle/drop density of 1 g cm⁻³.

- In the case of hydroxyl radical, based on our current measurements and previous work (Arakaki
- et al., 2013; Anastasio and Newberg, 2007), the concentrations of the major aqueous sources
- 676 (nitrate, nitrite, and unknown species) and sinks (organic compounds) both scale linearly with
- PM aqueous mass concentration, indicating that [OH] should be independent of dilution.
- However, this does not consider the influence of the gas phase. The extremely short lifetime of
- 679 'OH in the particles $(1/k'_{OH} \sim 2 \times 10^{-10} \text{ s})$ indicates that this oxidant will not be at Henry's law
- equilibrium and that the gas phase will be a source of OH. We estimate the rate of this gas-phase
- mass transport to the particles $(P_{\rm MT})$ using the Fuchs-Sutugin transition regime formula (Seinfeld
- and Pandis, 2012) with an estimated gas-phase OH concentration of 1×10^6 molecules cm⁻³ and
- a mass accommodation coefficient of 1. Under these conditions the drop-volume-normalized
- rate of OH gas-to-particle transport increases from $7.7 \times 10^{-10} \,\mathrm{M \ s^{-1}}$ in dilute drops $(3 \times 10^{-5} \,\mathrm{\mu g^{-1}})$
- PM/ μ g-H₂O) to 4.2 × 10⁻⁷ M s⁻¹ under particle conditions (1 μ g-PM/ μ g-H₂O). Over this same
- range, the aqueous photoformation of ${}^{\bullet}$ OH increases even more strongly, from $1.3 \times 10^{-10} \, \mathrm{M \ s^{-1}}$
- to $4.2 \times 10^{-6} \,\mathrm{M \ s^{-1}}$, respectively. Thus the contribution of gas-phase mass transport to the overall

'OH formation rate decreases as the drops become more concentrated, dropping from 86% in the dilute drops to 9% in the particle condition. Considering both the aqueous- and gas-phase sources of 'OH to the particles, we estimate the steady-state concentration at any dilution using

690 691

688

689

692
$$[{}^{\bullet}OH(aq)] = (P_{OH} + P_{MT})/k'_{OH}$$
 (S10)

693

These overall steady-state concentrations range from 5.4×10^{-15} M in the dilute drop condition to 8.4×10^{-16} M in the particle condition, as shown by the solid orange line in Figure 5.

696

In the case of singlet molecular oxygen, there is little gas-phase data, but past estimates suggested concentrations on the order of 1×10^8 molecules cm⁻³ (Demerjian, 1974). At Henry's law equilibrium, this gas-phase concentration corresponds to an aqueous concentration of $5 \times 10^-$ M (using the Henry's law constant for ground state O_2 , 1.3×10^{-3} M atm⁻¹ at 298 K; Seinfeld and Pandis (2012)). This estimated aqueous concentration is somewhat smaller than our measured concentrations in dilute extracts (Table S7), which are approximately as concentrated

as fog/cloud drops, and many orders of magnitude lower than our extrapolated particle

- concentrations. Thus the net effect of mass transport will be to move ${}^{1}O_{2}^{*}$ from the particles to
- 705 the gas phase. As an upper bound, the fastest step in evaporation of ${}^{1}O_{2}$ * is likely liquid-phase
- diffusion, which has a characteristic time (Seinfeld and Pandis, 2012) of

707

704

708
$$\tau_{LD} = R_p^2 / (\pi^2 \times D_{aq})$$
 (S11)

709

- where $D_{\rm aq}$ is the aqueous diffusion coefficient, approximately $1 \times 10^{-5}~{\rm cm}^2~{\rm s}^{-1}$ if we assume an
- aqueous particle. Calculated liquid-phase diffusion lifetimes range from 3×10^{-5} s for particles
- 712 (1 μg -PM/ μg -H₂O and an assumed radius of 0.5 μm) to 0.02 s for dilute drops (3 \times 10⁻⁵ μg -
- 713 PM/ μ g-H₂O, which corresponds to a radius of 13 μ m). The inverse of τ_{LD} is the approximate
- first-order rate constant for liquid-phase diffusion, k'_{LD} ; values range from 60 s in dilute drops to
- $4 \times 10^4 \text{ s}^{-1}$ in particles. These values are low compared to the first-order rate constant for
- deactivation of ${}^{1}O_{2}$ * in water ($k'_{H2O} = 2.2 \times 10^{5} \text{ s}^{-1}$; Bilski et al. (1997)), indicating that
- 717 evaporation is a minor sink.

Under cloud and fog drop conditions (and in our PM extracts) deactivation by water is the major sink for singlet oxygen, but under the more concentrated conditions of aqueous particles, organic compounds might also be important. To very roughly estimate this organic sink, we multiply our average DOC concentration in PM extracts (3.4 mM-C; Table S2) by a factor of 1000 to extrapolate to ambient PM conditions and assume all of this material is soluble, resulting in an aqueous concentration of particulate organics of 3.4 M-C. If each organic molecule has an average of 6 C atoms (i.e., the average is the same as levoglucosan), this corresponds to a watersoluble organic molecule concentration of 0.56 mol-compounds L^{-1} . We apportion this total concentration based on the emissions measurements of Jen et al. (2019), where water-soluble organics in biomass burning emissions are roughly 50% sugars, 25% phenols, and 25% organic nitrogen. Table S19 below shows the resulting estimated particle concentrations, along with an estimated average rate constant for each class based on the compilation by Wilkinson et al. (1995). Summing the contributions from each compound class we estimate a total pseudo-first order rate constant for loss of ${}^{1}O_{2}$ * by soluble organics in the particles (at 1 µg-PM/µg-H₂O) of $2.8 \times 10^6 \text{ s}^{-1}$. We linearly scale this sink, k'_{ORG} , by the PM mass/water mass ratio of the drops and particles to address dilution effects; e.g., for particles with 0.1 μ g-PM/ μ g-H₂O, $k'_{ORG} = 2.8 \times$ $10^5 \, \mathrm{s}^{-1}$.

Table S 19. Estimates of the organic sink of ${}^{1}O_{2}^{*}$ in aqueous particles at 1 μ g-PM/ μ g-H₂O

Compound Class	Dissolved Concentration (M)	2^{nd} -order Rate Constant Range $(M^{-1} \text{ s}^{-1})$	Assumed 2^{nd} - order $k (M^{-1} s^{-1})$	$k'_{\mathrm{ORG}}(\mathrm{s}^{-1})$
Sugars	0.28	10^{4}	10^{4}	2800
Phenols	0.14	$10^6 - 10^7$	10 ⁷	1.4×10^{6}
Organic Nitrogen	0.14	$10^3 - 10^9$	107	1.4×10^6

737

738

719

720

721

722

723

724

725

726

727

728

729

730

731

732

733

734

735

736

The resulting estimate for the steady-state concentration of ${}^{1}O_{2}^{*}$ in drops and particles is

739740

$$[^{1}O_{2}^{*}] = P_{1O2^{*}} / (k'_{H2O} + k'_{LD} + k'_{ORG})$$
 (S12)

741742

743

where the numerator, i.e., the rate of ${}^{1}O_{2}$ * photoformation increases with increasing solute concentration according to the linear regression of our PME3D values (with the y-intercept fixed

at zero): $P_{102*} = 5.0 \times 10^{-4} \,\mathrm{M \ s}^{-1} / (\mu \mathrm{g-PM/\mu g-water})$. This gives rates of singlet oxygen formation 744 that range from $1.5 \times 10^{-8} \,\mathrm{M \ s^{-1}}$ in dilute drops to $5.0 \times 10^{-4} \,\mathrm{M \ s^{-1}}$ for our standard particle 745 condition. The denominator of Eq. S12 is 2.2×10^5 s⁻¹ in dilute drops and remains at this value 746 until the particle concentration reaches 10^{-3} µg-PM/µg-water, at which point it increases because 747 748 of the increasingly concentrated organic sinks. At the particle condition of 1 µg-PM/µg-H₂O, the denominator is 3.1×10^6 s⁻¹ and organic sinks account for 92% of $^{1}\text{O}_{2}$ * loss. Calculated values of 749 $[^{1}O_{2}^{*}]$ range from 6.7×10^{-14} M in dilute drops to 1.6×10^{-10} M for the particle liquid water 750 condition. 751

752

For triplet excited states we fit our experimental data to a hyperbolic fit:

754
$$[^{3}C^{*}] = \frac{a \left[m_{PM}/m_{H2O}\right]}{1+b \left[m_{PM}/m_{H2O}\right]}$$
 (S13)

where $m_{\rm PM}/m_{\rm H2O}$ is the PM mass/water mass ratio, the numerator represents the formation of 755 triplets and the denominator represents the sinks. We fit our experimental data to this equation in 756 757 Excel in two ways: (1) a best fit, where the hyperbolic equation parameters were tuned to minimize the regression error, and (2) a high estimate fit, where the parameters were tuned so 758 that the regression line passed near the top of the error bar for the most concentrated sample 759 extract (PME3D0.5). The parameters for these two fits are: (1) $a = 3.08 \times 10^{-10}$ M and $b = 1.31 \times 10^{-10}$ M 760 10^{3} , and (2) $a = 2.26 \times 10^{-10}$ M and b = 17.0. We did not include the data point for PME3D10 761 when determining the regression fits (but do show it in the plots) because of the larger 762 763 uncertainty in its triplet concentration, a result of the significant 'OH perturbation by MBO in this most dilute sample. Our interpretation of the curvature in these regression fits (Figure 5) is 764 765 that as the solutions get more concentrated, organics become the major triplet sink, causing [3C*] to plateau at higher PM mass/water mass ratios; we estimate the size of this organic sink in 766 the next section. Thus, these fits should account for the organic sinks that will be important under 767 768 particle conditions.

769770

771

772

773

774

To a first approximation, we expect that mass transport will have no significant impact on the concentrations of triplets. Since most of the BrC precursors for ${}^{3}C^{*}$ are likely in the particle phase (rather than the gas phase) we expect that gas-phase concentrations of triplets are relatively small and that the gas phase is not a significant source of triplets to the particles. We also expect that evaporation of triplets is minor since their lifetimes are relatively short (1 µs based just on

775 O₂ as a sink) and their gas-particle partitioning (like that of their BrC precursors) is strongly tilted toward the particle phase. Thus we assume that the particle concentration of triplets is 776 777 relatively unaffected by mass transport.

778

779

S5. Estimating triplet characteristics in particle extract PME3

- We can use our measurements of triplet steady-state concentrations in the PME3 dilution series 780 to derive the first-order rate constant for triplet formation and the overall rate constant for triplet 781 reaction and quenching by DOC. The rate of triplet formation (P_{3C^*}) from the photoexcitation of 782
- chromophores 'C' in the extracts can be expressed as: 783

784

785
$$P_{3C^*} = j_{abs} \times \Phi_{ISC} \times [C]$$
 (S14)

786

- where j_{abs} is the rate constant for light absorption (s⁻¹) by C and Φ_{ISC} is the intersystem crossing 787 quantum yield, i.e., the fraction of the first excited single state, S₁, that forms the lowest triplet 788 excited state, T_1 . Assuming the chromophore concentration is a fraction f (mole-chromophore 789 mole-C⁻¹) of the DOC concentration (mole-C L⁻¹), the rate of triplet formation can be expressed
- 790
 - 791 as

792

793
$$P_{3C^*} = j_{abs} \times \Phi_{ISC} \times f \times [DOC]$$
 (S15)

794

The rate constant for loss of the triplet $(k'_{3C^*}; s^{-1})$ in an extract is the sum of all its loss pathways: 795

796

797
$$k'_{3C^*} = k_{3C^*+O2} [O_2] + k_{rxn} [DOC] + k_O [DOC]$$
 (S16)

- where k_{3C^*+O2} is the bimolecular rate constant for O_2 quenching (we use the average value for the 799
- three model triplets with measurements, 2.8 (\pm 0.4) \times 10⁹ M⁻¹s⁻¹; Table S11); [O₂] is the 800
- dissolved oxygen concentration (284 μ M at 20 °C) (USGS, 2018); k_{rxn} (M⁻¹s⁻¹) is the rate 801
- constant for reaction of triplet with dissolved organics; and k_0 (M⁻¹s⁻¹) is the rate constant for 802
- the non-reactive quenching of triplet by DOC (Smith et al., 2014). 803
- 804 Assuming steady state, the triplet concentration is the ratio of its rate of photoproduction and its
- 805 rate constant for loss:

806
$$[^{3}C^{*}] = \frac{P3C^{*}}{k'3C^{*}} = \frac{jabs \times \Phi ISC \times f \times [DOC]}{k3C^{*} + O2[O2] + (krxn + kQ)[DOC]}$$
 (S17)

This can be re-written as

808
$$[^{3}C^{*}] = \frac{\left(\frac{jabs \times \Phi ISC \times f}{k3C* + O_{2}[O_{2}]}\right) \times [DOC]}{1 + \left(\frac{krxn + kQ}{k3C* + O_{2}[O_{2}]}\right) \times [DOC]}$$
 (S18)

- We then fit our triplet steady-state concentration measurements in the PME3D extracts to the
- 810 following two-parameter equation:

811
$$[{}^{3}C^{*}] = \frac{c [DOC]}{1+d [DOC]}$$
 (S19)

- The regression fit is shown in Fig. S13; the parameters for the fit obtained using Excel are c =
- 813 2.9×10^{-11} and $d = 117 \text{ M}^{-1}$; we did not include the data point for PME3D10 in determining the
- 814 regression fit because of the larger uncertainty in its triplet concentration, a result of the
- significant probe perturbation in this most dilute sample. Using the regression parameters, we
- calculate that the rate constant for triplet formation, i.e., $j_{abs} \times \Phi_{ISC} \times f$, is 2.3 (± 0.3) × 10⁻⁵ s⁻¹
- and the sum of the reaction and quenching rate constants for the triplets by DOC, i.e., $k_{\text{rxn}} + k_{\text{O}}$, is
- 818 $9.3 (\pm 1.3) \times 10^7 \,\mathrm{L \ mol \cdot C^{-1} \ s^{-1}}.$



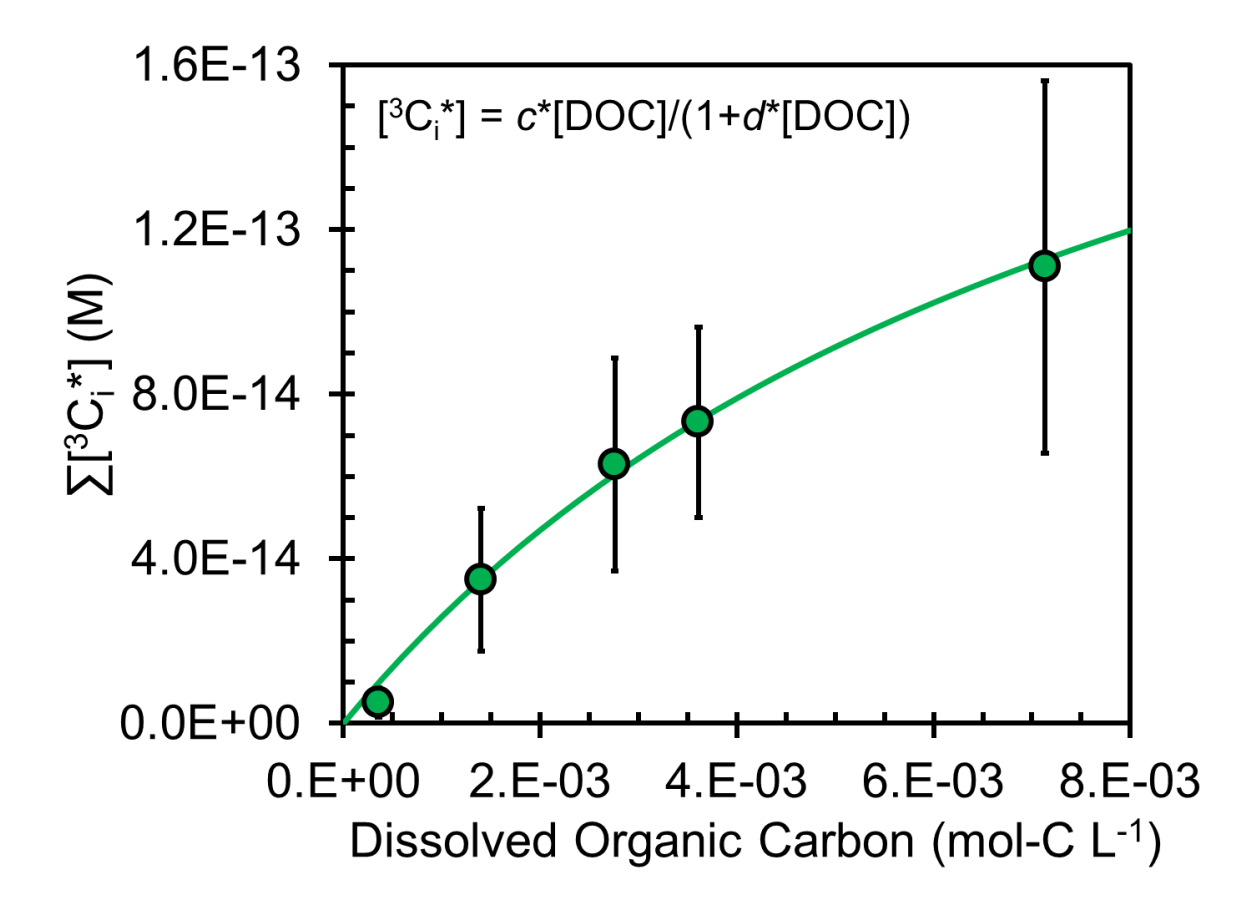


Figure S13. Change in triplet steady-state concentration with dissolved organic carbon concentration in the PME3D extracts. Error bars represent \pm 1 standard error in measured triplet concentrations (Table S13). The regression line is a fit of Equation S19 to the experimental data in Excel, yielding parameter estimates of $c = 2.90 \times 10^{-11}$ and d = 117 M⁻¹. The PME3D10 point was not included in the regression fit (although is shown on the plot) because of issues with too-high probe concentrations in the OH determination. The DOC value for sample PME3D0.5 (which had very limited volume) is estimated based on results for the other four dilutions and given in Table S2.

S6. References

- Anastasio, C.: Aqueous phase photochemical formation of hydrogen peroxide in authentic atmospheric waters and model compound solutions, Ph.D. Dissertation, Duke University, 1994.
- Anastasio, C., and McGregor, K. G.: Chemistry of fog waters in California's central valley: 1. In situ photoformation of hydroxyl radical and singlet molecular oxygen, Atmospheric Environment, 35, 1079-1089, 2001.
- Anastasio, C., and Newberg, J. T.: Sources and sinks of hydroxyl radical in sea-salt particles, J. Geophys. Res., 112, D10306, 2007.
- Anbar, M., Meyerstein, D., and Neta, P.: Reactivity of aliphatic compounds towards hydroxyl radicals, Journal of the Chemical Society B: Physical Organic, 742-747, 1966.
- Andreev, P. Y.: Reaction of ozone with five-membered hetarenes in a liquid phase, Russ. J. Appl. Chem., 85, 1395-1398, 2012.
- Arakaki, T., Anastasio, C., Kuroki, Y., Nakajima, H., Okada, K., Kotani, Y., Handa, D., Azechi, S., Kimura, T., Tsuhako, A., and Miyagi, Y.: A general scavenging rate constant for reaction of hydroxyl radical with organic carbon in atmospheric waters, Environ. Sci. Technol., 47, 8196-8203, 2013.
- Atkinson, R., Aschmann, S. M., Fitz, D. R., Winer, A. M., and Pitts, J. N.: Rate constants for the gas-phase reactions of O3 with selected organics at 296 K, Int. J. Chem. Kinet., 14, 13-18, 1982.
- Atkinson, R., Aschmann, S. M., and Carter, W. P.: Kinetics of the reactions of O3 and OH radicals with furan and thiophene at 298±2 K, Int. J. Chem. Kinet., 15, 51-61, 1983.
- Atkinson, R., Baulch, D., Cox, R., Crowley, J., Hampson, R., Hynes, R., Jenkin, M., Rossi, M.,
 Troe, J., and Subcommittee, I.: Evaluated kinetic and photochemical data for atmospheric chemistry: Volume II–gas phase reactions of organic species, Atmos. Chem. Phys., 6,
 3625-4055, 2006.
- Barker, G., Fowles, P., and Stringer, B.: Pulse radiolytic induced transient electrical conductance in liquid solutions. Part 2.—radiolysis of aqueous solutions of NO₃⁻, NO₂⁻ and Fe(CN)₆³⁻, J. Chem. Soc. Faraday Trans., 66, 1509-1519, 1970.
- Berdnikov, V.: Catalytic activity of the hydrated copper ion in the decomposition of hydrogen peroxide, Russ. J. Phys. Chem., 47, 1060-1062, 1973.
- Bertolotti, S. G., García, N. A., and Argüello, G. A.: Effect of the peptide bond on the singletmolecular-oxygen-mediated sensitized photo-oxidation of tyrosine and tryptophan dipeptides. A kinetic study, Journal of Photochemistry and Photobiology B: Biology, 10, 57-70, 1991.
- Bielski, B.: Evaluation of the reactivities of HO2/O2 with compounds of biological interest, Oxy Radicals and Their Scavenger Systems. G. Cohen and RA Greenwald (Editors), 1, 1-7, 1983.
- Bielski, B. H. J., Cabelli, D. E., Arudi, R. L., and Ross, A. B.: Reactivity of HO₂/O₂⁻ radicals in aqueous solution, Journal of Physical and Chemical Reference Data, 14, 1041-1100, 1985.
- Bilski, P., Holt, R. N., and Chignell, C. F.: Properties of singlet molecular oxygen O2 (1Δg) in binary solvent mixtures of different polarity and proticity, Journal of Photochemistry and Photobiology A: Chemistry, 109, 243-249, 1997.

- Buxton, G. V., Greenstock, C. L., Helman, W. P., and Ross, A. B.: Critical review of rate constants for reactions of hydrated electrons, hydrogen atoms and hydroxyl radicals ('OH/'O⁻) in aqueous solution, J. Phys. Chem. Ref. Data, 17, 513-886, 1988a.
- Buxton, G. V., Wood, N. D., and Dyster, S.: Ionisation Constants of 'OH And HO'₂ in Aqueous Solution up to 200°C. A Pulse Radiolysis Study, J. Chem. Soc., Faraday Trans., 84, 1113-1121, 1988b.
- California Air Resources Board, iADAM database: Air Quality Data Statistics: https://www.arb.ca.gov/adam, access: June 6, 2018.

887

888

889

890

891 892

893

894 895

896

899

900

901

902

903

904

- Canonica, S., Hellrung, B., and Wirz, J.: Oxidation of phenols by triplet aromatic ketones in aqueous solution, J. Phys. Chem. A, 104, 1226-1232, 2000.
 - Canonica, S., Kohn, T., Mac, M., Real, F. J., Wirz, J., and von Gunten, U.: Photosensitizer method to determine rate constants for the reaction of carbonate radical with organic compounds, Environmental science & technology, 39, 9182-9188, 2005.
 - Chen, S.-N., Hoffman, M. Z., and Parsons Jr, G. H.: Reactivity of the carbonate radical toward aromatic compounds in aqueous solution, J. Phys. Chem., 79, 1911-1912, 1975.
 - Chen, Z., Chu, L., Galbavy, E. S., Ram, K., and Anastasio, C.: Hydroxyl radical in/on illuminated polar snow: Formation rates, lifetimes, and steady-state concentrations, Atmos. Chem. Phys., 16, 9579-9590, 2016.
 - Deguillaume, L., Leriche, M., Monod, A., and Chaumerliac, N.: The role of transition metal ions on HO_x radicals in clouds: a numerical evaluation of its impact on multiphase chemistry, Atmos Chem Phys, 4, 95-110, 2004.
- Demerjian, K. L.: The mechanism of photochemical smog formation, Adv. Environ. Sci. Technol., 4, 1-262, 1974.
 - Hess, M., Koepke, P., and Schult, I.: Optical properties of aerosols and clouds: The software package OPAC, Bulletin of the American meteorological society, 79, 831-844, 1998.
 - Hoigné, J., and Bader, H.: Rate constants of reactions of ozone with organic and inorganic compounds in water—II: dissociating organic compounds, Water Res., 17, 185-194, 1983.
 - Huang, J., and Mabury, S. A.: Steady-state concentrations of carbonate radicals in field waters, Environmental Toxicology and Chemistry, 19, 2181-2188, 2000.
- Hunter, T.: Radiationless transition T 1→ S 0 in aromatic ketones, Transactions of the Faraday
 Society, 66, 300-309, 1970.
- Jen, C. N., Hatch, L. E., Selimovic, V., Yokelson, R. J., Weber, R., Fernandez, A. E., Kreisberg,
 N. M., Barsanti, K. C., and Goldstein, A. H.: Speciated and total emission factors of
 particulate organics from burning western US wildland fuels and their dependence on
 combustion efficiency, Atmos. Chem. Phys., 19, 1013-1026, 2019.
- Kaur, R., and Anastasio, C.: Light absorption and the photoformation of hydroxyl radical and singlet oxygen in fog waters, Atmos. Environ., 164, 387-397, 2017.
- Kaur, R., and Anastasio, C.: First measurements of organic triplet excited states in atmospheric waters, Environ. Sci. Technol., 52, 5218-5226, 2018.
- Kozmér, Z., Arany, E., Alapi, T., Takács, E., Wojnárovits, L., and Dombi, A.: Determination of the rate constant of hydroperoxyl radical reaction with phenol, Radiat. Phys. Chem., 102, 135-138, 2014.
- Lauraguais, A., Coeur-Tourneur, C., Cassez, A., and Seydi, A.: Rate constant and secondary organic aerosol yields for the gas-phase reaction of hydroxyl radicals with syringol (2, 6-dimethoxyphenol), Atmos. Environ., 55, 43-48, 2012.

- Lilie, J.: Pulsradiolytische untersuchung der oxydativen ringöffnung von furan, thiophen und pyrrol/pulsradiolytic investigations of the oxydativ ring scission of furan, thiophen and pyrrol, Zeitschrift für Naturforschung B, 26, 197-202, 1971.
- 925 McGregor, K. G., and Anastasio, C.: Chemistry of fog waters in California's Central Valley: 2. 926 Photochemical transformations of amino acids and alkyl amines, Atmos. Environ., 35, 927 1091-1104, 2001.
- Meylan, W. M., and Howard, P. H.: Computer estimation of the atmospheric gas-phase reaction rate of organic compounds with hydroxyl radicals and ozone, Chemosphere, 26, 2293-2299, 1993.
- Neta, P., and Schuler, R. H.: Rate constants for reaction of hydrogen atoms with aromatic and heterocyclic compounds. Electrophilic nature of hydrogen atoms, Journal of the American Chemical Society, 94, 1056-1059, 1972.

935

936 937

938

939

940

941

942

943

944

945

946

947

948

949

950

951

952

953 954

955

- O'Neill, P., Steenken, S., and Schulte-Frohlinde, D.: Formation of radical cations of methoxylated benzenes by reaction with OH radicals, Ti 2+, Ag 2+, and SO 4.-in aqueous solution. An optical and conductometric pulse radiolysis and in situ radiolysis electron spin resonance study, Journal of Physical Chemistry, 79, 2773-2779, 1975.
- O'Neill, P., and Steenken, S.: Pulse radiolysis and electron spin resonance studies on the formation of phenoxyl radicals by reaction of OH radicals with methoxylated phenols and hydroxybenzoic acids, Ber. Bunsenges. Phys. Chem., 81, 550-556, 1977.
- Parworth, C. L., Young, D. E., Kim, H., Zhang, X., Cappa, C. D., Collier, S., and Zhang, Q.: Wintertime water-soluble aerosol composition and particle water content in Fresno, California, J. Geophys. Res. Atmos., 122, 3155-3170, 2017.
- Piechowski, M. V., Nauser, T., Hoignè, J., and Bühler, R. E.: O-2 decay catalyzed by Cu2+ and Cu+ ions in aqueous solutions: a pulse radiolysis study for atmospheric chemistry, Berichte der Bunsengesellschaft für physikalische Chemie, 97, 762-771, 1993.
- Rehorek, D., and Seidel, A.: A. Leifer. The kinetics of environmental aquatic photochemistry. ACS professional and reference book. American Chemical Society, Washington 1988, 304 S., 41 Abb., 35 Tab., Kart, Preis: US & Canada \$59.95, Export \$71.95, ISBN 0-8412-1464-6, Cryst. Res. Technol., 24, 732-732, 1989.
- Richards-Henderson, N. K., Hansel, A. K., Valsaraj, K. T., and Anastasio, C.: Aqueous oxidation of green leaf volatiles by hydroxyl radical as a source of SOA: Kinetics and SOA yields, Atmos. Environ., 95, 105-112, 2014a.
 - Richards-Henderson, N. K., Pham, A. T., Kirk, B. B., and Anastasio, C.: Secondary organic aerosol from aqueous reactions of green leaf volatiles with organic triplet excited states and singlet molecular oxygen, Environ. Sci. Technol., 49, 268-276, 2014b.
- Rinke, M., and Zetzsch, C.: Rate Constants for the Reactions of OH Radicals with Aromatics:
 Benzene, Phenol, Aniline, and 1, 2, 4-Trichlorobenzene, Ber. Bunsenges. Phys. Chem.,
 88, 55-62, 1984.
- Rosario-Ortiz, F. L., and Canonica, S.: Probe compounds to assess the photochemical activity of dissolved organic matter, Environ. Sci. Technol., 50, 12532-12547, 2016.
- Seinfeld, J. H., and Pandis, S. N.: Atmospheric chemistry and physics: From air pollution to climate change, John Wiley & Sons, 2012.
- 964 Smith, J. D., Sio, V., Yu, L., Zhang, Q., and Anastasio, C.: Secondary organic aerosol production 965 from aqueous reactions of atmospheric phenols with an organic triplet excited state, 966 Environ. Sci. Technol., 48, 1049-1057, 2014.

- 967 Smith, J. D., Kinney, H., and Anastasio, C.: Aqueous benzene-diols react with an organic triplet 968 excited state and hydroxyl radical to form secondary organic aerosol, Phys. Chem. Chem. 969 Phys., 17, 10227-10237, 2015.
- 970 Solar, S., Solar, W., and Getoff, N.: Reactivity of hydroxyl with tyrosine in aqueous solution 971 studied by pulse radiolysis, J. Phys. Chem., 88, 2091-2095, 1984.
- Tetreau, C., Lavalette, D., Land, E., and Peradejordi, F.: Sensitized triplet-triplet absorption of biphenylene, Chem. Phys. Lett., 17, 245-247, 1972.
- Tratnyek, P. G., and Hoigne, J.: Oxidation of substituted phenols in the environment: A QSAR analysis of rate constants for reaction with singlet oxygen, Environ. Sci. Technol., 25, 1596-1604, 1991a.
 - Tratnyek, P. G., and Hoigne, J.: Oxidation of substituted phenols in the environment: a QSAR analysis of rate constants for reaction with singlet oxygen, Environmental science & technology, 25, 1596-1604, 1991b.
 - USEPA: Estimation Programs Interface Suite™ for Microsoft® Windows, v 4.11, United States Environmental Protection Agency, Washington, DC, USA, 2012.
 - USGS: U.S. Geological Survey. Water Properties Dissolved Oxygen. Available at https://water.usgs.gov/edu/dissolvedoxygen.html [last accessed: January 23, 2018], 2018.
 - Vempati, H. S.: Physico-chemical properties of green leaf volatiles, 2014.

978 979

980

981 982

983

984

985

986

987

988 989

990

991

992

993

996

997 998

999

- Vione, D., Minella, M., Maurino, V., and Minero, C.: Indirect photochemistry in sunlit surface waters: photoinduced production of reactive transient species, Chemistry-A European Journal, 20, 10590-10606, 2014.
 - Wilkinson, F., Helman, W. P., and Ross, A. B.: Quantum yields for the photosensitized formation of the lowest electronically excited singlet state of molecular oxygen in solution, J. Phys. Chem. Ref. Data, 22, 113-262, 1993.
 - Wilkinson, F., Helman, W. P., and Ross, A. B.: Rate constants for the decay and reactions of the lowest electronically excited singlet state of molecular oxygen in solution. An expanded and revised compilation, J. Phys. Chem. Ref. Data, 24, 663-677, 1995.
- Yasuhisa, T., Hideki, H., and Muneyoshi, Y.: Superoxide radical scavenging activity of phenolic compounds, International journal of biochemistry, 25, 491-494, 1993.
 - Young, D. E., Kim, H., Parworth, C., Zhou, S., Zhang, X., Cappa, C. D., Seco, R., Kim, S., and Zhang, Q.: Influences of emission sources and meteorology on aerosol chemistry in a polluted urban environment: results from DISCOVER-AQ California, Atmos. Chem. Phys., 16, 5427-5451, 2016.
- Zein, A. E., Coeur, C. c., Obeid, E., Lauraguais, A. l., and Fagniez, T.: Reaction kinetics of
 catechol (1, 2-benzenediol) and guaiacol (2-methoxyphenol) with ozone, The Journal of
 Physical Chemistry A, 119, 6759-6765, 2015.
- Zeng, T., and Arnold, W. A.: Pesticide photolysis in prairie potholes: probing photosensitized processes, Environmental science & technology, 47, 6735-6745, 2012.
- Zepp, R. G., Braun, A. M., Hoigne, J., and Leenheer, J. A.: Photoproduction of hydrated
 electrons from natural organic solutes in aquatic environments, Environmental science &
 technology, 21, 485-490, 1987.
- Zhou, X., and Mopper, K.: Determination of photochemically produced hydroxyl radicals in seawater and freshwater, Mar. Chem., 30, 71-88, 1990.